Numerical Solutions for Two- and Three-Dimensional Non-Reacting Flowfields in an Internal Combustion Engine

by

Michael Douglas Griffin III

Dissertation submitted to the Faculty of the Graduate School
of the University of Maryland in partial fulfillment
of the requirements for the degree of
Doctor of Philosophy
1977

APPROVAL SHEET

Title of Thesis: Numerical Solutions for Two- and Three-Dimensional Non-Reacting Flowfields in an Internal Combustion Engine

Name of Candidate: Michael Douglas Griffin
Doctor of Philosophy, 1977

Thesis and Abstract Approved:

John D. Anderson, Jr.
Dr. John D. Anderson, Jr.
Professor and Chairman
Department of Aerospace Engineering

Everett Jones
Dr. Everett Jones
Associate Professor
Department of Aerospace Engineering

Date Approved: 20 July 1977

ABSTRACT

Title of Dissertation: Numerical Solutions for Two- and Three-Dimensional Non-Reacting Flowfields in an Internal Combustion Engine

Michael Douglas Griffin, Doctor of Philosophy, 1977

Dissertation directed by: Dr. John D. Anderson, Jr.
Professor and Chairman
Department of Aerospace Engineering

Dr. Everett Jones
Associate Professor
Department of Aerospace Engineering

The numerical solution for the flowfield established in a spark-ignition internal combustion engine during the four-stroke (intake, compression, power, exhaust) cycle is considered. Only fluid-dynamic effects are treated with combustion simulated by constant-volume heat addition near top-dead-center on the compression stroke. The working fluid is assumed to be air of constant specific heat, with both viscous and inviscid models considered. Two- and three-dimensional engine models are examined, with the three-dimensional models including both rectangular and cylindrical geometries. The difficulties associated with obtaining numerical solutions in cylindrical coordinates for three-dimensional non-axisymmetric problems when the centerline is included in the region of interest are discussed. A new method which avoids the coordinate-singularity problems associated with such cases is presented and used to obtain the first known four-stroke inviscid-flow solution for a three-dimensional cylindrical engine model. Similar results are presented for a three-dimensional rectangular model, and for the first known two-dimensional four-stroke calculation for a viscous fluid. The inviscid three-dimensional results are compared with each other and with

previously obtained two-dimensional inviscid-flow calculations. The use of two-dimensional models is found to be justified for the non-reacting flowfields considered, since the results obtained from a two-dimensional calculation in the valve plane are apparently not strongly dependent on the flowfield perpendicular to the valve plane. It is found that significant flowfields do exist in all I.C. engine models considered. It is shown that the unit-cell-Reynolds-number criterion limits viscous flow calculations to Reynolds numbers of approximately one ten-thousandth the realistic value, and that this produces flowfields which are strongly piston-dominated. In contrast, inviscid results show marked circulatory patterns, which are more realistic. The velocity patterns which develop in the three-dimensional cylindrical engine model are shown to exhibit a marked swirl in planes parallel and perpendicular to the cylinder axis.

Acknowledgements

The author has received much help during his progress toward the Ph.D., and is happy to have this opportunity to acknowledge the debts he has incurred.

The author's co-advisors, Dr. John D. Anderson, Jr., and Dr. Everett Jones, deserve special mention. Dr. Anderson is responsible for the original offer of financial assistance that allowed the author to attend graduate school on a full-time basis, and for providing the opportunity for additional support through a Faculty Research Assistantship in the University of Maryland Wind Tunnel laboratory when the need arose. Dr. Anderson's technical guidance has at all times been of the highest order, as has the quality of his teaching. He is in the author's opinion one of the few who has clearly attained the academic goal of excellence in both teaching and research.

Dr. Jones has consistently demonstrated the ability to understand the day-to-day problems his students encounter in their research, and to provide suggestions useful in circumventing them. He possesses one of the quickest minds the author has encountered, yet assists in such a way as to make his students feel more like his colleagues.

Also deserving of special mention is R. W. MacCormack of NASA - Ames Research Center. His technical suggestions have been extremely helpful to the author, as has his unfailing courtesy and friendliness during several visits and telephone conversations.

The author's fellow graduate students, Messr. Ajay Kothari, R. Diwakar, and K. N. Parthasarathy deserve thanks both for their companionship during three years of graduate work and for the genuinely useful suggestions that each has at times provided.

Miss Susan Osborn and Mr. Peter Cheung are responsible for the excellent typing and artwork found in this dissertation.

The University of Maryland Computer Science Center has very kindly donated the computer time used throughout this study.

Finally, the author wishes to thank his wife, Denise, for her patient support over the last three years. Without it, this work could not have been completed.

Table of Contents

List of Symbols

a	speed of sound
$A(z)$	area function for quasi-one-dimensional duct flow
c	damping constant for artificial viscosity term, Chapter 5
C_p	specific heat at constant pressure
C_v	specific heat at constant volume
e	specific internal energy
e_t	specific total energy
E	x_1 component of conserved vector in conservation form of equations
F	x_2 component of conserved vector in conservation form of equations
$\underline{F}_c$	vector of centrifugal terms used in cylindrical coordinate equations
g	symbol for generalized flowfield variable when identity is unimportant
G	x_3 component of conserved vector in conservation form of equations
h	specific static enthalpy
h_i	metric scale factors for generalized coordinate systems
H	vector of centrifugal terms in conservation form of equations
H	total enthalpy, used in Chapter 5
$H(t)$	non-dimensional piston position function in inertial coordinate system
$\hat{i}$	unit vector in x-direction for cartesian coordinates
$\hat{j}$	unit vector in y-direction for cartesian coordinates

J_0 zeroth-order Bessel function of first kind

$\hat{k}$ unit vector in z-direction for cartesian coordinates

L reference length

p pressure

P pressure times radial coordinate, equal to (rp), used in special formulation of governing equations in Chapter 2

Pr Prandtl number

$\underline{Q}$ vector of (U,V,W) velocities, see below

r radial coordinate in cylindrical coordinate system

$\hat{r}$ unit vector for radial coordinate

R specific gas constant

Re Reynolds number

t time

T temperature

T_{01} temperature constant used in Sutherland's Law for viscosity

T_{02} temperature constant used in Sutherland's Law for thermal conductivity

u x_1 component of velocity in all coordinates; e.g., x-component of velocity for cartesian systems, r-component for cylindrical systems

U vector of dependent variables used in various systems of governing equations developed in Chapter 2

U component of $\underline{Q}$, equal to (ru), for use in special system of Chapter 2

U x-component of velocity obtained by resolving cylindrical coordinate flowfield, used in Chapter 5

U_{avg} average x-velocity used in Chapter 5

U_i	i^{th} component of U-vector of dependent variables
v	x_2 component of velocity in all coordinates; e.g., y-component of velocity for cartesian systems, ϕ-component for cylindrical systems
V	component of $\underline{Q}$, equal to (rv), for use in special system of Chapter 2
V	y-component of velocity obtained by resolving cylindrical coordinate flowfield, used in Chapter 5
$\underline{V}$	velocity vector equal to (u,v,w) in any system
V_i	i^{th} component of velocity for use in indicial (tensor) forms of governing equations in Chapter 2
V_p	non-dimensional piston velocity
w	x_3 component of velocity in all coordinates; e.g., z-component of velocity for both cartesian and cylindrical systems
W	component of $\underline{Q}$, equal to (rw), for use in special system of Chapter 2
x	x_1 coordinate for cartesian systems
x_i	generalized coordinate, or i^{th} cartesian coordinate when used in indicial forms of governing equations
X_p	non-dimensional value of piston location, equal to H(t) for a specific time, always with a total range of one to nine in this work, used in Chapter 4
y	x_2 coordinate for cartesian systems
Y_o	zeroth-order Bessel function of second kind
z	x_3 coordinate for both cartesian and cylindrical systems
$\hat{z}$	unit vector for z-direction for cylindrical coordinates

z' transformed z-coordinate equal to (z/H(t)), used in section 2.7

Z_p non-dimensional value of piston location, equal to H(t) for a specific time, always with a total range of one to nine in this work, used in Chapter 5

Greek Symbols

γ ratio of specific heats, C_p/C_v

δ_{ij} Kronecker delta symbol

Δ generalized grid spacing

ϕ x_2 coordinate in cylindrical systems

$\hat{\phi}$ unit vector in ϕ-direction for cylindrical systems

Φ viscous dissipation function, Chapter 2

Φ dummy variable, Chapter 5

ρ fluid density

Ψ acoustic pressure field, Chapter 5

τ temperature times radial coordinate, equal to (rT), used in special formulation of governing equations in Chapter 2

ω dummy variable, Chapter 5

List of Figures

CHAPTER 1

INTRODUCTION

1.1 Preliminary remarks

This dissertation is concerned with a body of work that has attempted to bring to bear some of the techniques of computational fluid dynamics to the analysis of a problem that is of relatively recent interest, the problem of obtaining detailed solutions for the flow-field inside a standard spark-ignition reciprocating internal combustion engine. Interest in I.C. engines is of course not new. For many years a course dealing with them has been a standard part of the undergraduate mechanical engineering curriculum. But until rather recently, the main feature of I.C. engine analysis was its empiricism, as exemplified by Obert's classic book [1], or Lichty's work [2]. No disparagement of of such work is intended. It has been, is, and will continue to be of use in practical I.C. engine design for many years before being supplanted by more detailed analyses. Certainly the current effort amounts to only a small step in the direction of obtaining such analyses. Only with the advent of extremely large, fast computers could one hope to produce a detailed, accurate analysis of the flow processes in an internal combustion engine, and until very recently there seemed little incentive to attempt such a task. The concern of the last few years over oil price levels and energy conservation in general, as well as the desire to understand and control the air polluting effect of the automobile, has encouraged renewed interest in the study of the internal combustion engine, and particularly in the possibility of advanced computer modeling and simulation of I.C. engine processes. So recent has this increased

interest been that in late 1974 when the current work was begun, a moderately detailed literature search failed to reveal any work more sophisticated than zero-dimensional or one-dimensional analyses. Other investigators were active at this time, however, as the survey of currently available literature included here will show. It is thus apparent that the time is ripe to take some of the advanced aerospace technology that has been built up in the analysis of complex aerodynamic flowfields and transfer it to the analysis of the I.C. engine. That, in broad outline, is the main thrust of this dissertation.

1.2 The physical problem

The detailed analysis of the internal combustion engine as it exists in its operating environment is a task of incredible complexity. The power obtained depends on the integrated pressure distribution of the working fluid in the cylinder over the piston surface, which depends on the energy released during combustion. The efficiency of the combustion process is coupled to the fluid mechanics in a complicated, highly non-linear fashion. Factors to be considered include the exact mechanism for the mixing of the fuel and air, the two-phase flow problems involved in spray and droplet modeling, the role of turbulence in the flow, the actual process by which the spark ignites the fuel-air mixture, the effects due to the valve geometry on the inflowing or exhausting fluid, coupling between intake and exhaust manifolds and the combustion chamber, and the role of finite-rate chemical processes in producing undesired products of combustion. There is no hope of obtaining a closed-form, analytical solution for any mathematical model which even faintly resembles such a system, so the approach must be numerical. Even here, as this work will show, the detailed study of the full problem such as

outlined above cannot be accomplished at present; its achievement will be the result of an evolutionary process over a long period of time.

This being the case, the steps that can be taken at the present time are necessarily small ones. Simplistic models must be constructed, and the methods of analysis of them well understood, before advanced work is begun. Thus, since the study of turbulence has itself been a lifetime work for several generations of investigators without a complete understanding of it yet having been achieved, it seems logical to omit, or to employ very simple models of, turbulent effects in current I.C. engine analyses. The complicated geometry associated with an intake or exhaust valve would require enormous storage in a computer to be properly defined and to have its fluid dynamic effects modeled. It therefore seems best at this time to treat valves as unobstructed ports which are either open or closed. The study of two-phase flows is an entire field in itself, so an acceptable approximation for the present could be to model the fuel-air mixture as a mixture of gases. The full problem is three-dimensional in nature, due to the offset position of the valves in a real engine, but since the computer simulation of three--dimensional flows is in its infancy, it is logical to attempt to do as much as possible with geometrically and computationally simpler one- and two-dimensional models. The list of such approximations could be made virtually endless; the necessity for making them is a fact which must be faced by an investigator who wishes to study a problem too complex for detailed analysis by available techniques. Even when appropriately simple model problems are set up, there are many questions which must be answered before the model may be said to be understood. Roache [3] gives a very good example of some of these questions concerning I.C. engine models

"1. Do the outflow conditions (exhaust back pressure) represent any special difficulties? Are inflow conditions well specifiable? Is it necessary or worthwhile to calculate the non-burning portions of the cycle?

2. How many reacting species must be included in the calculation? For coarse studies? for refined studies? for performance calculations? for pollutant calculations? What is the utility of systematic sensitivity studies using variational techniques?

3. Are radiation effects significant? If so, can a grey gas approximation be used? Can a radiation diffusion approximation be used?

4. Are discontinuities (shocks, contact surfaces, flame fronts) present and important enough to warrant shock-fitting techniques. In what dimensionality?

5. What additional requirements are imposed by the introduction of fuel droplets? Can or should droplet breakup be calculated from first principles, or should droplet characteristics be an empirical input? Is strong or weak coupling of the droplets to the fluid dynamics required?

6. Can the incompressibility assumption be used to advantage in the expansion phase? If so, can the geometry be simplified enough to use the fast Poisson solvers to advantage? What other simplifications (e.g., constant viscosity, constant conductivity, weak compressibility) should be considered?

7a. What dimensionality is useful? Are fully 3D + time calculations absolutely necessary? Are 1D calculations meaningful? Are they really an improvement over lumped-parameter models

(control volume or 0-dimensional models)? Are axisymmetric and pseudo-3D calculations likely to be meaningful? Is a multi--level approach appropriate, or should a single "best code" be used?

7b. What is the utility of boundary-layer methods and parabolic marching equations?

8. What are the computer requirements and realistic computation times for 1D, 2D pseudo-3D and fully 3D calculations? How sensitive are estimates of computer time to estimates of resolution requirements? of steady-state criteria? Are there special problems associated with the attainment of a cyclic steady-state? Should one try to calculate early transients, i.e., engine warm-up, with accuracy.

9. Which classes of numerical techniques appear to be most suited for automotive applications? Eulerian, Lagrangian, or mixed? Explicit, implicit, or mixed? Parabolic, elliptic, or hyperbolic equations? Higher-order or lower-order methods?

10. What are the best algorithms for integrating stiff differential equations typical of reacting flows? Are they adequate? Are there special numerical difficulties associated with calculating the distinction between deflagration and detonation?

11. What are the best techniques for describing boundary layers (viscous and thermal)? Are "one-cell" resolutions adequate or of value?

12. What special computational problems arise from the more complicated turbulence theories? Is it worthwhile to calculate the laminar viscous stress terms?

13. Can something of value be learned from $O(\Delta x)$ differencing? Is $O(\Delta t)$ differencing adequate? is $O(\Delta x^4)$ or higher worthwhile? What computational techniques exist to minimize numerical diffusion and dispersion?

14a. Does the finite element methodology offer any real advantages over finite difference methods for automotive applications?

14b. What is the utility of grid-free methods (vortex filament, etc.)?

15. What additional development of numerical methods (rather than specific codes) needs to be accomplished?"

This work will address some of the above topics, the companion work of Diwakar [4].will treat others, and still more remain unanswered. There is a need at this stage of work on the analysis of I.C. engines to begin with models simple enough that the questions and problems they pose may be treated with present methods, yet complex enough so that those questions are important to answer. As the answers are obtained, the level of subsequent questions may increase.

1.3 Literature survey

As has been remarked, in the past few years there has been a tremendous increase in the literature in the same general subject area as this dissertation, the numerical analysis and simulation of flowfields associated with internal combustion engines. In order to properly judge the state of the art in this field and the relation of the work presented here to it, this section will be devoted to surveying the available literature. The work will be covered in approximately chronological order according to its appearance in print, except that on occasion it may be useful to consider a sequence of publications by the same author and dealing with closely related topics. Since this dissertation is not

concerned with the detailed treatment of combustion phenomena, but rather with the problems associated with the basic fluid-mechanical simulation of an I.C. engine, the work of others will be considered with a view toward

1. the geometrical model used in the analysis
2. the numerical method used to obtain solutions
3. the fluid mechanical assumptions made; i.e., viscous or inviscid, laminar or turbulent flow, reacting or non-reacting, etc.

but no detailed examination of the combustion models assumed will be made. A survey of the available literature with a view toward combustion phenomena will be found in the work of Diwakar [4].

The relatively early work of Lavoie, Heywood and Keck [5] is an example of the type of work which can be done with so-called zero-dimensional modeling. In this approach, the only independent variable is time, and all spatially varying quantities must be replaced by averaged values. Properties like burning rate which are intrinsically spatially determined must be obtained by including either experimental results or an ad-hoc set of additional equations. The authors claim that experimental results confirm the main features of the model.

The next level of sophistication is represented by the time-dependent, one-dimensional models. Examples are the work of Sirignano [6], and the successive papers which extend the original work, such as those due to Bracco and Sirignano [7] and Bellan and Sirignano [8,9]. Reference [6] sets the tone of the work which follows. In this paper a theory based on a concept of a turbulent flame front model was developed and resulted in predictions of pressure and temperature as functions of crank angle and the one spatial variable, taken to be either a radial line

outward from the center of the cylinder, or a vertical line down the center of the cylinder. A turbulent eddy diffusivity model is developed which is time-dependent and spatially constant; the model is applied to both heat and mass transfer. A constant specific heat fluid is assumed. The numerical method used is the method of quasi-linearization, which is an implicit, iterative finite-difference scheme [10,11]. Reference [7] applies basically the same model to the analysis of Wankel engine combustion, while [8,9] deal with a stratified charge engine, again with the same approach as in Reference [6]. Reference [8] avoids the assumption of constant specific heats by using a fifth-degree polynomial fit for C_p vs. temperature, and also adds another term to the turbulence model that was used in the original work. In [9], a two--equation, time- and space-dependent turbulence model is introduced, although the authors claim that without experimental comparisons it is difficult to see whether or not it is superior to earlier work. Finally, Bracco [12] applies the same time-dependent, one-dimensional model of Reference [6] to the analysis of a stratified-charge Wankel engine, and includes a treatment of two-phase flow in the fuel-injection process.

At this point in the developmental sequence being summarized here, results for the first two-dimensional unsteady calculations begin to appear in the literature. The well-timed survey paper of Bracco [13], contains an excellent discussion of the state of the art at that time, and also of the implications of various levels of simplifying assumptions which are brought to bear in reducing the complex original problem to a tractable model problem.

The work of Boni, et. al. [14,15] constitutes the first new approach insofar as the numerical method of solution is concerned. Reference

[14] is an unsteady one-dimensional solution, while [15] is a two-dimensional (axisymmetric) unsteady solution. Both are for viscous flow with chemical reactions to model combustion, although methane is substituted for gasoline in order to simplify the chemistry. Both sets of results include an attempt to model turbulent effects by setting the coefficients of viscosity, thermal conductivity, and diffusivity to high constant values. The numerical method employed is the Arbitrary Lagrangian--Eulerian (ALE) method due to Hirt, Amsden, and Cook [16]. Because of the axisymmetric model employed by Boni, only the compression and power strokes may be simulated.

Bracco, et al. [17,18] have recently published the results of two--dimensional unsteady calculations involving two-phase flow with two types of model geometry; i.e., fuel injection vertically into the cylinder with solutions obtained in a plane of constant azimuth, and tangential injection with solutions obtained in a plane of constant vertical location. The numerical solutions are obtained via the RICE code [19]. As Bracco states, there were some limitations on the method as of the time that results were obtained. In particular, the curvilinear boundaries desired by Bracco had to be approximated by a sequence of small straight-line segments. Also, the RICE code contains no physical modeling of the transport processes, but rather sets the transport coefficients to relatively high valves to obtain numerical stability.

As far as is known, the work of Griffin, Anderson, and Diwakar [20], and Diwakar, Anderson, Griffin, and Jones [21] represents the first two--dimensional, unsteady, four-stroke solutions, although for very simple working fluids and no modeling of combustion except for constant-volume heat addition near the top of the compression stroke. Reference [20]

contains calculations for viscous, laminar flow in a two-dimensional rectangular engine in a plane normal to the piston and running through the centerline between the intake and exhaust valves. Reference [21] employs the same geometrical model and numerical method as in [20], but for the case of inviscid flow. The use of the inviscid flow model permits the four-stroke computation to be run in a sufficiently short time to allow the inclusion of a detailed finite-rate chemical reaction model for combustion. Progress in this area is reported in Reference [4].

Gosman [22] also has results for a four-stroke calculation which were obtained for a two-dimensional axisymmetric model. The fluid-mechanical model, while not involving reacting flows as in the axisymmetric calculations of Boni [15], is considerably more advanced that that used in References [20,21]. A two-equation turbulence model is employed, and the valve is treated as an open port of time-varying area and having a prescribed constant discharge coefficient. Gosman attempted some comparison of his results with the experimental work of Witze [28,29], and claims qualitative agreement. The numerical method used by Gosman is an implicit finite-difference method, with the resulting difference equations solved iteratively. Details are not given.

The work of Dwyer and Sanders [23,24] returns to the one-dimensional unsteady case to demonstrate the application of a new numerical approach to the solution of reacting flows in which widely varying chemical, acoustic, and differential time scales are present [26,27]. Reference [23] concentrates on the unsteady ignition process and its interaction with the flame front propagation. Reference [24] examines two cases in more detail, an overdriven detonation wave and the propagation of a flame front in open and closed ducts. In both bases turbulent flow is assumed,

engine modeling have chosen to attack the problem in such a way that the emphasis is on solving combustion modeling problems first, using only the simplest geometrical descriptions to begin with. When an investigator has been sufficiently active to have produced several papers, it has been the case that he has used any increased sophistication and/or computer power to strive for a more sophisticated combustion model, rather than increasing the sophistication of the geometrical model.

This is a perfectly acceptable plan of attack. It is quite clear that at the present time the entire problem of interest cannot be handled adequately, so simplifications must be made. The particular choices of which simplifications to make and which complexities to attempt to treat often depend on the researcher's personal bias quite as much as on any a priori necessity that things be done a certain way. Many of those now working in the field of internal combustion engine research had experience of long standing in combustion research in general, so that their choices as outlined above were perfectly reasonable.

The present work is part of an effort which, from its inception, was oriented toward a different plan of attack. It was felt that the purely fluid mechanical and geometrical modeling difficulties were as challenging as those associated with combustion. Accordingly, the work reported here has sought to deal with the problems presented by the intake and exhaust valve boundary conditions, Reynolds number problems, coordinate system singularities, the particular choice of dependent variables in the governing equations, numerical instability, required grid resolution, etc.; in effect, everything not included under the heading of combustion modeling. In this sense, this work is complementary to, rather than in

the same area as, most of the work discussed in section 1.2. The eventual goal, of course, is for both lines of development to converge in the future to a capability to numerically solve the full problem, with all known effects included.

Because detailed consideration of the heat release due to the combustion process is not of interest in this work, a convention concerning its inclusion in the algorithms used has been adopted, and will be noted at this point. All "combustion modeling" in this work takes the form of spatially-uniform constant-volume heat addition which is added instantaneously at a given time on the compression stroke. It is recognized that this is unrealistic; it has as its only purpose the deliberate stressing of the numerical algorithms used, to demonstrate that they will remain stable following sudden changes such as are more rigorously computed when chemically-reacting flows are treated. Since the heat-addition process as implemented here is a delta-function process, the term (often denoted by $\dot{Q}$) normally required in the governing equations for diabatic flows has been omitted. Instead, the view has been taken that the I.C. engine flow process is adiabatic both before and after heat addition, with the effect of heat addition being merely to change the working fluid to another with a higher heat content.

In accordance with the objectives as stated above, this dissertation will include:

1. Two-dimensional viscous flow solutions for the full four-stroke cycle, in cartesian coordinates.
2. Some three-dimensional viscous flow solutions for inflow and exhaust test cases in cartesian coordinates.

3. A variety of three-dimensional inviscid flow solutions obtained in cartesian and cylindrical coordinates, using different formulations of the governing fluid dynamic equations, and for various test cases which have proven useful.
4. A four-stroke three-dimensional inviscid flow calculation at 3000 RPM in cartesian coordinates with constant-volume heat addition used to simulate combustion.
5. A case similar to (4) but with a three-dimensional calculation in cylindrical coordinates.
6. Detailed discussion of the numerical technique used to obtain the results in (5), since this technique is original with this work and provides a capability in computational fluid dynamic analysis that had not previously existed.

The governing equations of the fluid-dynamical systems considered here will be developed in Chapter 2. The numerical method and associated considerations by which the solutions were obtained is described in Chapter 3. Results for viscous flow cases are given in Chapter 4, for inviscid flow analyses in Chapter 5, and the final conclusions and discussion will be found in Chapter 6. A listing of the cylindrical engine program, together with a sample input data set and the resulting output, are given in the Appendix.

Chapter 2

GOVERNING EQUATIONS

The scope and purpose of this dissertation have necessitated the use of several geometrical models and various formulations of the governing fluid mechanical equations during the course of the work. It would seem to be simpler to present all of the relevant sets of equations in one place. It is hoped that this will result in a degree of brevity and clarity that would be lacking if the text were interrupted frequently for the development of a particular set of equations needed at a given point.

As has been mentioned, this work serves mainly to examine and resolve some of the difficulties inherent in the numerical analysis and modeling of the flowfield in an internal combustion engine, but from the purely fluid-dynamic point of view. Since no chemical reactions are considered, the working fluid (air) is treated as a single-component calorically-perfect (constant specific heats) gas. The governing partial differential equations will thus in all cases considered here consist of a global continuity equation, an energy equation, and a vector momentum equation with the number of components equal to the spatial dimensionality of the particular model under consideration. These equations express the fact that mass, momentum, and energy must be conserved for the system as a whole.

2.1 Navier-Stokes equations

2.1.1 Equations for variable viscosity and thermal conductivity

The introductory work in this investigation was, perhaps surprisingly, carried out with the most complex set of equations. The fluid

was assumed to be compressible and viscous, with varying viscosity and thermal conductivity. The appropriate equations are then the complete Navier-Stokes equations, which may be written in indicial form as [30]:

Continuity

$$\frac{\partial \rho}{\partial t} + \frac{\partial(\rho V_i)}{\partial x_i} = 0 \tag{2-1}$$

Momentum

$$\frac{\partial V_i}{\partial t} = -V_j \frac{\partial V_i}{\partial x_j} - \frac{1}{\rho}\frac{\partial p}{\partial x_i}$$

$$+ \frac{1}{\rho}\frac{\partial}{\partial x_j}\left[\mu\left(\frac{\partial V_i}{\partial x_j} + \frac{\partial V_j}{\partial x_i} - \frac{2}{3}\frac{\partial V_k}{\partial x_k}\delta_{ij}\right)\right] \tag{2-2}$$

Energy

$$\frac{\partial h}{\partial t} = -V_j \frac{\partial h}{\partial x_j} + \frac{1}{\rho}\left[\frac{\partial}{\partial x_j}\left(k \frac{\partial T}{\partial x_j}\right) + \frac{\partial p}{\partial t} + V_j \frac{\partial p}{\partial x_j} + \Phi\right] \tag{2-3}$$

where

p = static pressure

ρ = static density

T = static temperature

h = static enthalpy

V_i = i^{th} component of velocity; $i = 1,2,3$

μ = dynamic viscosity coefficient

k = coefficient of thermal conductivity

δ_{ij} = Kronecker delta

Φ = viscous dissipation function

The summation convention is assumed. The dissipation function is given by

$$\Phi = \mu\left[\left(\frac{\partial V_i}{\partial x_j} + \frac{\partial V_j}{\partial x_i}\right)\frac{\partial V_i}{\partial x_j} - \frac{2}{3}\frac{\partial V_i}{\partial x_i}\frac{\partial V_j}{\partial x_j}\right] \tag{2-4}$$

and the relations among the state variables are the ideal gas equation

$$p = \rho RT \tag{2-5}$$

and

$$dh = C_p dT \tag{2-6}$$

It was felt that the most appropriate choice for primary variables in the above set was velocity, pressure, and temperature. This choice was retained in all subsequent work involving the non-conservation forms of the governing equations, of which the above set is an example. The main reason for this early initial choice was the feeling that the required valve boundary conditions (to be discussed later) could most reasonably be formulated in terms of temperature and pressure. No reason to alter this decision was ever found. The following reference variables were used to non-dimensionalize the system:

p_r = reference pressure = 101325 Nt./m^2

T_r = reference temperature = 273.16^oK

V_r = reference velocity = $(\gamma RT_r)^{1/2}$

γ = ratio of specific heats = $\frac{C_p}{C_v} = \frac{C_p}{C_p - R}$

L = reference length

t_r = reference time = L/V_r

μ_r = reference viscosity = $\mu(T_r)$ = $1.708 \times 10^{-5} \frac{kg}{m\text{-}sec}$

k_r = reference conductivity = $k(T_r)$ = $2.414 \times 10^{-2} \frac{kg\text{-}m}{sec\ ^oK}$

With this choice, we obtain

Continuity

$$\frac{\partial p}{\partial t} = \frac{\gamma}{PrRe}\left(k \frac{\partial^2 T}{\partial x_i \partial x_i} + \frac{\partial T}{\partial x_i}\frac{\partial T}{\partial x_i}\frac{dk}{dT}\right) + \frac{\gamma(\gamma-1)}{Re}\Phi - \gamma p \frac{\partial V_i}{\partial x_i} - V_i \frac{\partial p}{\partial x_i} \tag{2-7}$$

Momentum

$$\frac{\partial V_i}{\partial t} = -V_j \frac{\partial V_i}{\partial x_j} - \frac{T}{\gamma p} \frac{\partial p}{\partial x_i} + \frac{1}{Re} \frac{T}{p} \left[\left(\frac{\partial V_i}{\partial x_j} + \frac{\partial V_j}{\partial x_i} \right) \frac{\partial T}{\partial x_j} \frac{d\mu}{dT} \right.$$

$$\left. - \frac{2}{3} \frac{\partial V_j}{\partial x_j} \frac{\partial T}{\partial x_i} \frac{d\mu}{dT} + \mu \left(\frac{\partial^2 V_i}{\partial x_j \partial x_j} + \frac{1}{3} \frac{\partial^2 V_j}{\partial x_j \partial x_i} \right) \right] \qquad (2\text{-}8)$$

Energy

$$\frac{\partial T}{\partial t} = \frac{\gamma T}{p} \left[\frac{1}{PrRe} \left(k \frac{\partial^2 T}{\partial x_i \partial x_i} + \frac{\partial T}{\partial x_i} \frac{\partial T}{\partial x_i} \frac{dk}{dT} \right) + \frac{(\gamma-1)}{Re} \Phi \right]$$

$$- (\gamma-1) T \frac{\partial V_i}{\partial x_i} - V_i \frac{\partial T}{\partial x_i} \qquad (2\text{-}9)$$

as the corresponding non-dimensional forms of equations (1-3), expressed only in terms of the prime variable vector

$$(v_1, v_2, v_3, p, T)^t = (u, v, w, p, T)^t$$

The non-dimensional parameters are

$$Re = \frac{\rho_r V_r L}{r} = \text{Reynolds number}$$

$$Pr = \frac{\mu_r C_p}{k_r} = \text{Prandtl number}$$

After choosing the reference pressure and temperature, the equation of state yields

$$\rho_r = \frac{p_r}{R T_r} \qquad (2\text{-}10)$$

hence the non-dimensional state equation

$$p = \rho T \qquad (2\text{-}11)$$

which will be of use later.

It should be noted that the reference pressure is given by

$$p_r = \rho_r RT_r = \frac{1}{\gamma}\rho_r(\gamma RT_r) = \frac{1}{\gamma}\rho_r V_r^2$$

hence the reference pressure is not in this particular formulation equal to the reference dynamic pressure. This produces stray factors of $(1/\gamma)$ in various places in the non-dimensional equations. Such a formulation yields non-dimensional velocity data upon output that closely approximates the local Mach number for many of the cases examined. In later work it sometimes became convenient to use

$$V_r = (RT_r)^{1/2}$$

which is an energy-based reference velocity, so as to eliminate the factor $(1/\gamma)$ in certain terms.

The terms $\frac{d\mu}{dT}$ and $\frac{dk}{dT}$ in equations (7-9) result from Sutherland's Laws for viscosity and thermal conductivity. In non-dimensional form, these are [31]:

$$\mu = \mu(T) = \left(\frac{1+T_{01}}{T+T_{01}}\right) T^{3/2} \qquad (2\text{-}12)$$

$$k = k(T) = \left(\frac{1+T_{02}}{T+T_{02}}\right) T^{3/2} \qquad (2\text{-}13)$$

where

$$T_{01} = \frac{110.33\ ^oK}{T_r}$$

$$T_{02} = \frac{194.44\ ^oK}{T_r}$$

2.1.2 Equations for constant viscosity and thermal conductivity

The above equations, while completely defining the fully-viscous problem for a single-component fluid of constant specific heat, are

perhaps unnecessarily complex for the type of investigations being discussed here. The inclusion of variable μ and k in particular results in the generation of terms which greatly complicate the system, while yielding little useful sophistication at this time. Dropping those terms containing $\frac{d\mu}{dT}$ and $\frac{dk}{dT}$ results in

Continuity

$$\frac{\partial p}{\partial t} = \frac{\gamma}{PrRe} \frac{\partial^2 T}{\partial x_i \partial x_i} + \frac{\gamma(\gamma-1)}{Re} \Phi - \gamma p \frac{\partial V_i}{\partial x_i} - V_i \frac{\partial p}{\partial x_i} \qquad (2\text{-}14)$$

Momentum

$$\frac{\partial V_i}{\partial t} = -V_j \frac{\partial V_i}{\partial x_j} - \frac{T}{\gamma p} \frac{\partial p}{\partial x_i} + \frac{1}{Re} \frac{T}{p} \left(\frac{\partial^2 V_i}{\partial x_j \partial x_j} + \frac{1}{3} \frac{\partial^2 V_j}{\partial x_i \partial x_j} \right) \qquad (2\text{-}15)$$

Energy

$$\frac{\partial T}{\partial t} = \frac{\gamma T}{p} \left[\frac{1}{PrRe} \frac{\partial^2 T}{\partial x_i \partial x_i} + \frac{(\gamma-1)\Phi}{Re} \right] - (\gamma-1) T \frac{\partial V_i}{\partial x_i} - V_i \frac{\partial T}{\partial x_i} \qquad (2\text{-}16)$$

The non-dimensional coefficients μ and k of equations (7-9) are absent above, since if taken equal to μ_r and k_r they assume a non-dimensional value of one.

The above equations with constant viscosity and thermal conductivity have the advantage of possessing an easily-recognizable vector form. Thus, we obtain

Continuity

$$\frac{\partial p}{\partial t} = -\underline{V} \cdot \underline{\nabla} p - \gamma p \, \underline{\nabla} \cdot \underline{V} + \frac{\gamma}{Re} \left[\frac{\nabla^2 T}{Pr} + (\gamma-1) \Phi \right] \qquad (2\text{-}17)$$

Momentum

$$\frac{\partial \underline{V}}{\partial t} = -\underline{V} \cdot \underline{\underline{\nabla V}} - \frac{T}{\gamma p} \underline{\nabla} p + \frac{1}{Re} \frac{T}{p} \left[\nabla^2 \underline{V} + \frac{1}{3} \underline{\nabla} (\underline{\nabla} \cdot \underline{V}) \right] \qquad (2\text{-}18)$$

Energy

$$\frac{\partial T}{\partial t} = -\underline{V} \cdot \nabla T - (\gamma-1)\, T\, \nabla \cdot \underline{V} + \frac{\gamma}{Re}\frac{T}{p}\left[\frac{\nabla^2 T}{Pr} + (\gamma-1)\,\Phi\right] \qquad (2\text{-}19)$$

Again, the reader is reminded that unless specifically stated otherwise, all equations are in non-dimensional form.

2.2 Governing equations for inviscid flow - non-conservation form

As subsequent results will show, the use of viscous flow models in the analysis of I.C. engine flowfields has severe practical limitations. In many ways an inviscid fluid flow model makes more sense and has greater potential for providing useful results, particularly if the realism of a true three-dimensional geometrical model is desired. The non-dimensional, vector non-conservative forms of the governing equations for inviscid flow may be obtained directly from equations (17-19) by dropping the viscous and heat conduction terms. The result is the following set:

Continuity

$$\frac{\partial p}{\partial t} = -\underline{V} \cdot \nabla p - \gamma p\, \nabla \cdot \underline{V} \qquad (2\text{-}20)$$

Momentum

$$\frac{\partial \underline{V}}{\partial t} = -\underline{V} \cdot \underline{\underline{\nabla V}} - \frac{T}{\gamma p}\nabla p \qquad (2\text{-}21)$$

Energy

$$\frac{\partial T}{\partial t} = -\underline{V} \cdot \nabla T - (\gamma-1)\, T\, \nabla \cdot \underline{V} \qquad (2\text{-}22)$$

These equations are often referred to as Euler's equations.

2.2.1 Cartesian component forms

In three-dimensional Cartesian space, with

$$\underline{V} = u\hat{i} + v\hat{j} + w\hat{k} \qquad (2\text{-}23)$$

and

$$\nabla \cdot \underline{V} = \frac{\partial u}{\partial x} + \frac{\partial v}{\partial y} + \frac{\partial w}{\partial z} \tag{2-24}$$

$$(\underline{V} \cdot \nabla) = (u \frac{\partial}{\partial x} + v \frac{\partial}{\partial y} + w \frac{\partial}{\partial z}) \tag{2-25}$$

$$\nabla = \hat{i} \frac{\partial}{\partial x} + \hat{j} \frac{\partial}{\partial y} + \hat{k} \frac{\partial}{\partial z} \tag{2-26}$$

we may expand the above set to yield the five component equations

$$\frac{\partial u}{\partial t} = -(u \frac{\partial u}{\partial x} + v \frac{\partial u}{\partial y} + w \frac{\partial u}{\partial z}) - \frac{T}{\gamma p} \frac{\partial p}{\partial x} \tag{2-27}$$

$$\frac{\partial v}{\partial t} = -(u \frac{\partial v}{\partial x} + v \frac{\partial v}{\partial y} + w \frac{\partial v}{\partial z}) - \frac{T}{\gamma p} \frac{\partial p}{\partial y} \tag{2-28}$$

$$\frac{\partial w}{\partial t} = -(u \frac{\partial w}{\partial x} + v \frac{\partial w}{\partial y} + w \frac{\partial w}{\partial z}) - \frac{T}{\gamma p} \frac{\partial p}{\partial z} \tag{2-29}$$

$$\frac{\partial p}{\partial t} = -(u \frac{\partial p}{\partial x} + v \frac{\partial p}{\partial y} + w \frac{\partial p}{\partial z}) - \gamma p \, (\frac{\partial u}{\partial x} + \frac{\partial v}{\partial y} + \frac{\partial w}{\partial z}) \tag{2-30}$$

$$\frac{\partial T}{\partial t} = -(u \frac{\partial T}{\partial x} + v \frac{\partial T}{\partial y} + w \frac{\partial T}{\partial z}) - (\gamma-1)T \, (\frac{\partial u}{\partial x} + \frac{\partial v}{\partial y} + \frac{\partial w}{\partial z}) \tag{2-31}$$

2.2.2 Cylindrical component forms

Although the analysis of three-dimensional inviscid flows in I.C. engines which are approximated by rectangular models constitutes an important portion of the present work, there is little doubt that a more suitable geometrical model can be obtained in cylindrical coordinates, where the flow boundaries of a true piston and cylinder combination lie along surfaces defined by constant values of the coordinates z and r. In this system, the velocity vector is

$$\underline{V} = u\hat{r} + v\hat{\phi} + w\hat{z} \tag{2-32}$$

and the required vector identities are

$$\underline{\nabla} = \left(\hat{r}\,\frac{\partial}{\partial r} + \frac{\hat{\phi}}{r}\,\frac{\partial}{\partial \phi} + \hat{z}\,\frac{\partial}{\partial z}\right) \tag{2-33}$$

$$\nabla \cdot \underline{V} = \frac{1}{r}\,\frac{\partial (ru)}{\partial r} + \frac{1}{r}\,\frac{\partial v}{\partial \phi} + \frac{\partial w}{\partial z} \tag{2-34a}$$

$$= \frac{\partial u}{\partial r} + \frac{u}{r} + \frac{1}{r}\,\frac{\partial v}{\partial \phi} + \frac{\partial w}{\partial z} \tag{2-34b}$$

$$\underline{V} \cdot \underline{\nabla} = \left(u\,\frac{\partial}{\partial r} + \frac{v}{r}\,\frac{\partial}{\partial \phi} + w\,\frac{\partial}{\partial z}\right) \tag{2-35}$$

Also, the unit vectors are functions of position and hence the time-derivatives of the velocity vector in equation (21) produce extra terms. Thus

$$\frac{\partial (u\hat{r})}{\partial t} = \frac{\partial u}{\partial t}\,\hat{r} + \frac{\partial \hat{r}}{\partial t}\,u$$

$$\frac{\partial (v\hat{\phi})}{\partial t} = \frac{\partial v}{\partial t}\,\hat{\phi} + \frac{\partial \hat{\phi}}{\partial t}\,v$$

and from the kinematic relations among the unit vectors [32]

$$\frac{\partial \hat{r}}{\partial t} = \hat{\phi}\,\frac{v}{r} \quad , \quad \frac{\partial \hat{\phi}}{\partial t} = -\hat{r}\,\frac{v}{r}$$

hence

$$\frac{\partial (u\hat{r})}{\partial t} = \frac{\partial u}{\partial t}\,\hat{r} + \frac{uv}{r}\,\hat{\phi}$$

$$\frac{\partial (v\hat{\phi})}{\partial t} = \frac{\partial v}{\partial t}\,\hat{\phi} - \frac{v^2}{r}\,\hat{r}$$

The component equations in cylindrical coordinates then become

$$\frac{\partial u}{\partial t} = \frac{v^2}{r} - \left(u\,\frac{\partial u}{\partial r} + \frac{v}{r}\,\frac{\partial u}{\partial \phi} + w\,\frac{\partial u}{\partial z}\right) - \frac{T}{\gamma p}\,\frac{\partial p}{\partial r} \tag{2-36}$$

$$\frac{\partial v}{\partial t} = -\frac{uv}{r} - \left(u\,\frac{\partial v}{\partial r} + \frac{v}{r}\,\frac{\partial v}{\partial \phi} + w\,\frac{\partial v}{\partial z}\right) - \frac{T}{\gamma p}\,\frac{1}{r}\,\frac{\partial p}{\partial \phi} \tag{2-37}$$

$$\frac{\partial w}{\partial t} = -\left(u\,\frac{\partial w}{\partial r} + \frac{v}{r}\,\frac{\partial w}{\partial \phi} + w\,\frac{\partial w}{\partial z}\right) - \frac{T}{\gamma p}\,\frac{\partial p}{\partial z} \tag{2-38}$$

$$\frac{\partial p}{\partial t} = -(u \frac{\partial p}{\partial r} + \frac{v}{r} \frac{\partial p}{\partial \phi} + w \frac{\partial p}{\partial z}) - \gamma p \, (\frac{\partial u}{\partial r} + \frac{u}{r} + \frac{1}{r} \frac{\partial v}{\partial \phi} + \frac{\partial w}{\partial z}) \qquad (2\text{-}39)$$

$$\frac{\partial T}{\partial t} = -(u \frac{\partial T}{\partial r} + \frac{v}{r} \frac{\partial T}{\partial \phi} + w \frac{\partial T}{\partial z}) - (\gamma-1)T \, (\frac{\partial u}{\partial r} + \frac{u}{r} + \frac{1}{r} \frac{\partial v}{\partial \phi} + \frac{\partial w}{\partial z}) \qquad (2\text{-}40)$$

2.3 Governing equations for inviscid flow, conservation form

The equations of sections 2.1 and 2.2 are in what is called a non--conservative form. These forms result from the application of the basic physical principles of conservation of mass, momentum, and energy to an infinitesimal control volume that is allowed to move with the fluid. If the control volume to which the governing physical principles are applied is instead fixed in space, a set of equations in what is called the conservation form results. These two representations are of course equivalent. Some moderately involved algebraic rearrangement will suffice to reduce one form to the other.

As far as the technique of computational fluid dynamics is concerned, it is not obvious which particular mathematical formulation of the given physical laws will results in a set of equations posing the fewest numerical difficulties. There probably is no single approach that is suitable for all problems. Nevertheless, certain schools of thought on the matter do exist. Moretti and his co-workers [33,34,35] have been among the most ardent proponents of the use of non-conservation systems, while workers at NASA - Ames Research Center have generally favored the use of conservation forms [36,37,38,39].

It is not the intention of this work to attempt to resolve such questions. The conservation forms to be discussed have certain properties which suggested great utility in the work presented here, and so considerable use was made of them. It will be shown later that the best

results were obtained with the non-conservation forms, but it is stated in advance that this may well be due to nothing more than the particular algorithm implemented.

The conservation - law formulation of Euler's equations in generalized coordinates is [40]

$$\frac{\partial U}{\partial t} = - \frac{\partial E}{\partial x_1} - \frac{\partial F}{\partial x_2} - \frac{\partial G}{\partial x_3} - H \tag{2-41}$$

where

$$U = h_1 h_2 h_3 \begin{pmatrix} \rho \\ \rho u \\ \rho v \\ \rho w \\ \rho e_t \end{pmatrix} \tag{2-42}$$

$$E = h_2 h_3 \begin{pmatrix} \rho u \\ p+\rho u^2 \\ \rho uv \\ \rho uw \\ (p+\rho e_t)u \end{pmatrix} \tag{2-43}$$

$$F = h_1 h_3 \begin{pmatrix} \rho v \\ \rho uv \\ p+\rho v^2 \\ \rho vw \\ (p+\rho e_t)v \end{pmatrix} \tag{2-44}$$

$$G = h_1 h_2 \begin{pmatrix} \rho w \\ \rho uw \\ \rho vw \\ p+\rho w^2 \\ (p+\rho e_t)w \end{pmatrix} \tag{2-45}$$

$$H = \begin{bmatrix} 0 \\ \rho uvh_3 \frac{\partial h_1}{\partial x_2} + \rho uwh_2 \frac{\partial h_1}{\partial x_3} - (p+\rho v^2)h_3 \frac{\partial h_2}{\partial x_1} - (p+\rho w^2)h_2 \frac{\partial h_3}{\partial x_1} \\ \rho vwh_1 \frac{\partial h_2}{\partial x_3} + \rho uvh_3 \frac{\partial h_2}{\partial x_1} - (p+\rho w^2)h_1 \frac{\partial h_3}{\partial x_2} - (p+\rho u^2)h_3 \frac{\partial h_1}{\partial x_2} \\ \rho uwh_2 \frac{\partial h_3}{\partial x_1} + \rho vwh_1 \frac{\partial h_3}{\partial x_2} - (p+\rho u^2)h_2 \frac{\partial h_1}{\partial x_3} - (p+\rho v^2)h_1 \frac{\partial h_2}{\partial x_3} \\ 0 \end{bmatrix} \qquad (2\text{-}46)$$

The velocity components u, v, w are in the x_1, x_2, and x_3 directions, respectively, and the h_i are the metric coefficients for the chosen (orthogonal) coordinate system. The above equations are in dimensional form, but can easily be non-dimensionalized to have exactly the same form as equations (41-46), provided that a consistent set of reference values is chosen. In terms of the previous non-dimensionalizing procedure used, this means only that the reference velocity must be taken as

$$V_r = (RT_r)^{1/2} \qquad (2\text{-}47)$$

to avoid introducing stray factors of γ into the E, F, and G vectors. As pointed out earlier, this choice results in a reference pressure equal to the reference dynamic pressure, $\rho_r V_r^2$. Is is then easily verified that equations (41-46) are in fact non-dimensional.

Some additional relations are necessary to connect the state variables in the above system. Note that

$$e_t \triangleq e(p,T) + \frac{u^2 + v^2 + w^2}{2} \qquad (2\text{-}48)$$

but for a calorically perfect gas such as we have assumed

$$e(p,T) = e(T) = C_v T = \frac{RT}{\gamma - 1} = \frac{1}{\gamma - 1}\frac{p}{\rho} \qquad (2\text{-}49)$$

hence equation (48) becomes

$$e_t = \frac{1}{\gamma-1}\frac{p}{\rho} + \frac{u^2 + v^2 + w^2}{2} \tag{2-50}$$

It is then easy to obtain

$$\rho e_t = \frac{p}{\gamma-1} + \frac{(\rho u)^2 + (\rho v)^2 + (\rho w)^2}{2\rho} \tag{2-51a}$$

and

$$p = (\gamma-1)\left[\rho e_t - \frac{(\rho u)^2 + (\rho v)^2 + (\rho w)^2}{2\rho}\right] \tag{2-51b}$$

which gives the state relations entirely in terms of the components of the U-vector.

2.3.1 Conservation law form in cartesian coordinates

Again, the two coordinate systems of interest in this work are cartesian and cylindrical. For the cartesian system all scale factors are unity, hence

$$H = \begin{pmatrix} 0 \\ 0 \\ 0 \\ 0 \\ 0 \end{pmatrix}$$

and we use

$$\frac{\partial U}{\partial t} = -\frac{\partial E}{\partial x} - \frac{\partial F}{\partial y} - \frac{\partial G}{\partial z} \tag{2-52}$$

$$U = \begin{pmatrix} \rho \\ \rho u \\ \rho v \\ \rho w \\ \rho e_t \end{pmatrix} \tag{2-53}$$

$$E = \begin{pmatrix} \rho u \\ p+\rho u^2 \\ \rho uv \\ \rho uw \\ (p+\rho e_t)u \end{pmatrix} \tag{2-54}$$

$$F = \begin{pmatrix} \rho v \\ \rho u v_2 \\ p+\rho v^2 \\ \rho u w \\ (p+\rho e_t)v \end{pmatrix} \tag{2-55}$$

$$G = \begin{pmatrix} \rho w \\ \rho u w \\ \rho v w_2 \\ p+\rho w^2 \\ (p+\rho e_t)w \end{pmatrix} \tag{2-56}$$

and the state relations are exactly as in equations (51a and 51b).

2.3.2 Conservation law form in cylindrical coordinates

The metric coefficients for cylindrical coordinates (r, ϕ, z) are

$$\begin{pmatrix} h_1 \\ h_2 \\ h_3 \end{pmatrix} = \begin{pmatrix} h_r \\ h_\phi \\ h_z \end{pmatrix} = \begin{pmatrix} 1 \\ r \\ 1 \end{pmatrix}$$

so that

$$H = \begin{pmatrix} 0 \\ -(p+\rho v^2) \\ \rho u v \\ 0 \\ 0 \end{pmatrix} \tag{2-57}$$

$$U = \begin{pmatrix} \rho r \\ \rho u r \\ \rho v r \\ \rho w r \\ \rho e_t r \end{pmatrix} \tag{2-58}$$

$$E = \begin{pmatrix} \rho u r_2 \\ (p+\rho u^2)r \\ \rho u v r \\ \rho u w r \\ (p+\rho e_t)u r \end{pmatrix} \tag{2-59}$$

$$F = \begin{pmatrix} \rho v \\ \rho u v_2 \\ p+\rho v^2 \\ \rho v w \\ (p+\rho e_t)v \end{pmatrix} \tag{2-60}$$

$$G = \begin{pmatrix} \rho w r \\ \rho u w r \\ \rho v w r \\ (p+\rho w^2)r \\ (p+\rho e_t)wr \end{pmatrix} \tag{2-61}$$

It is convenient to restate equations (51a and 51b) in terms of primary variables for this system. Algebraic rearrangement yields

$$\rho e_t r = \frac{pr}{\gamma-1} + \frac{(\rho u r)^2 + (\rho v r)^2 + (\rho w r)^2}{2\rho r} \tag{2-62a}$$

$$pr = (\gamma-1)\left[\rho e_t r - \frac{(\rho u r)^2 + (\rho v r)^2 + (\rho w r)^2}{2\rho r}\right] \tag{2-62b}$$

2.4 Special non-conservation form of inviscid equations

It will be seen in Chapter 3 that the numerical solution of governing systems of equations such as have been presented so far requires the computation of finite-difference approximations to the spatial derivatives appearing in the equations. For example,

$$\frac{\partial u}{\partial r} \cong \frac{u(r,\phi,z) - u(r-\Delta r,\phi,z)}{\Delta r} \tag{2-63}$$

is a first-order backward-difference approximation for the r-derivative in cylindrical coordinates. When $r = \Delta r$, a value of u at $r = 0$ is required, and the finite-difference scheme breaks down because $r = 0$ is a singular point of the coordinate system; the expressions for the flow-field variables in cylindrical coordinates are multivalued at that point. This is the major stumbling block in attempting to obtain a three-dimensional

solution in cylindrical coordinates. Work on this problem constitutes a major portion of this dissertation and will be dealt with in detail later, but for now it is sufficient to note that it is possible to recast equations (36-40) in a form where values on the centerline are trivially zero, thus eliminating the difficulty in equation (63) where $r = \Delta r$.

It was suggested by Professor Everett Jones that an attempt be made to reformulate the governing equations (36-40) in terms of the prime variable vector

$$U \triangleq \begin{pmatrix} ru \\ rv \\ rw \\ rp \\ rT \end{pmatrix} \triangleq \begin{pmatrix} U \\ V \\ W \\ P \\ \tau \end{pmatrix} \tag{2-64}$$

so that $U|_{r=0} = 0$. The derivation of such a system follows most easily if (36-40) are put in vector form and then multiplied by r, the radial coordinate. This yields

$$\frac{\partial \underline{Q}}{\partial t} = \underline{F}_c - r\,\underline{V} \cdot \underline{\underline{\nabla V}} - \frac{T}{\gamma p}\, r\, \nabla \underline{p} \tag{2-65}$$

$$\frac{\partial P}{\partial t} = - r\,\underline{V} \cdot \underline{\nabla p} - r\,\gamma\, p\, \underline{\nabla} \cdot \underline{V} \tag{2-66}$$

$$\frac{\partial \tau}{\partial t} = - r\,\underline{V} \cdot \nabla T - r\,(\gamma-1)T\, \underline{\nabla} \cdot \underline{V} \tag{2-67}$$

where, for convenience, we use

$$\underline{Q} \triangleq U\,\hat{r} + V\,\hat{\phi} + W\,\hat{z} \tag{2-68}$$

and

$$\underline{F}_c = r \begin{pmatrix} v^2/r \\ -uv/r \\ 0 \end{pmatrix} = \frac{1}{r^2} \begin{pmatrix} V^2 \\ -UV \\ 0 \end{pmatrix} \tag{2-69}$$

It is emphasized that although $\underline{F}_c$ looks like a body-force term, its use is meant only as a notational convenience, as a vector representing the centrifugal terms due to the non-constant unit vectors of the cylindrical coordinate system. With this convenience, the time derivatives on the left may be treated as in equations (36-40); i.e., they apply only to the flowfield variables U and V in vector $\underline{Q}$. All the effect of the unit vectors is in $\underline{F}_c$.

Some new vector identities are needed. Note that for any scalar g,

$$\underline{\nabla} \cdot (g\underline{V}) = g\, \underline{\nabla} \cdot \underline{V} + \underline{V} \cdot \underline{\nabla g}$$

or

$$g\, \underline{\nabla} \cdot \underline{V} = \underline{\nabla} \cdot (g\underline{V}) - \underline{V} \cdot \underline{\nabla g}$$

and in cylindrical coordinates for the special case g = r,

$$r\, \underline{\nabla} \cdot \underline{V} = \underline{\nabla} \cdot (r\underline{V}) - u$$

or

$$r\, \underline{\nabla} \cdot \underline{V} = \underline{\nabla} \cdot \underline{Q} - \frac{U}{r} \tag{2-70}$$

For any scalar g and vector $\underline{h}$,

$$\underline{\underline{\nabla(gh)}} = g\, \underline{\underline{\nabla h}} + \underline{h}\, \underline{\nabla g} \tag{2-71}$$

Also, in cylindrical coordinates with g = r and h = p (a scalar),

$$\underline{\nabla}(rp) = r\, \underline{\nabla p} + p\, \underline{\nabla r} = r\, \underline{\nabla p} + p\, \hat{r}$$

or

$$r\, \underline{\nabla p} = \underline{\nabla P} - \frac{P}{r} \hat{r} \tag{2-72}$$

Finally, from (2-71) it is apparent that

$$\underline{V} \cdot \underline{\underline{\nabla(gh)}} = g\,\underline{V} \cdot \underline{\underline{\nabla h}} + \underline{h}\,(\underline{V} \cdot \underline{\nabla g})$$

and again in cylindrical coordinates with g = r,

$$r\,\underline{V} \cdot \underline{\underline{\nabla h}} = V \cdot \underline{\underline{\nabla(rh)}} - u\,\underline{h}$$

or

$$r\,\underline{V} \cdot \underline{\underline{\nabla h}} = \frac{1}{r}\,\underline{Q} \cdot \underline{\underline{\nabla(rh)}} - \frac{U}{r}\,\underline{h} \tag{2-73}$$

Using equations (70), (72), and (73) with $\underline{h} = \underline{V}$, p, or T allows equations (65-67) to be written as

$$\frac{\partial \underline{Q}}{\partial t} = \underline{F}_c - \frac{1}{r}\,\underline{Q} \cdot \underline{\underline{\nabla(r\underline{V})}} + \left(\frac{U}{r}\right)\underline{V} - \frac{T}{\gamma p}\left[\underline{\nabla P} - \frac{P}{r}\,\hat{r}\right] \tag{2-74}$$

$$\frac{\partial P}{\partial t} = -\frac{1}{r}\,\underline{Q} \cdot \underline{\nabla}(rp) + \frac{pU}{r} - \gamma p\,\left(\nabla \cdot \underline{Q} - \frac{U}{r}\right) \tag{2-75}$$

$$\frac{\partial \tau}{\partial t} = -\frac{1}{r}\,\underline{Q} \cdot \underline{\nabla}(rT) + \frac{UT}{r} - (\gamma-1)\,T\,\left(\nabla \cdot \underline{Q} - \frac{U}{r}\right) \tag{2-76}$$

It is now easy to eliminate the vector $(u,v,w,p,T)^t$ in favor of $(U,V,W,P,\tau)^t$ to obtain:

$$\frac{\partial \underline{Q}}{\partial t} = \underline{F}_c - \frac{\underline{Q}}{r} \cdot \underline{\underline{\nabla Q}} + \frac{UQ}{r^2} - \frac{\tau}{\gamma P}\left[\underline{\nabla P} - \frac{P}{r}\,r\right] \tag{2-77}$$

$$\frac{\partial P}{\partial t} = -\frac{1}{r}\,\underline{Q} \cdot \underline{\nabla P} + \frac{(\gamma+1)UP}{r^2} - \frac{\gamma P}{r}\,\nabla \cdot Q \tag{2-78}$$

$$\frac{\partial \tau}{\partial t} = -\frac{1}{r}\,\underline{Q} \cdot \nabla\tau + \frac{\gamma U\tau}{r^2} - \frac{(\gamma-1)\tau}{r}\,\nabla \cdot \underline{Q} \tag{2-79}$$

Finally, (2-77) may be expanded to obtain the five scalar equations:

$$\frac{\partial U}{\partial t} = \frac{U^2 + V^2}{r^2} - \frac{1}{r}\underline{Q}\cdot\underline{\nabla U} - \frac{\tau}{\gamma P}\left(\frac{\partial P}{\partial r} - \frac{P}{r}\right) \tag{2-80}$$

$$\frac{\partial V}{\partial t} = -\frac{1}{r}\underline{Q}\cdot\underline{\nabla V} - \frac{\tau}{\gamma P}\frac{1}{r}\frac{\partial P}{\partial \phi} \tag{2-81}$$

$$\frac{\partial W}{\partial t} = \frac{UW}{r^2} - \frac{1}{r}\underline{Q}\cdot\underline{\nabla W} - \frac{\tau}{\gamma P}\frac{\partial P}{\partial z} \tag{2-82}$$

$$\frac{\partial P}{\partial t} = -\frac{1}{r}\underline{Q}\cdot\underline{\nabla P} + \frac{(\gamma+1)UP}{r^2} - \frac{\gamma P}{r}\underline{\nabla}\cdot\underline{Q} \tag{2-83}$$

$$\frac{\partial \tau}{\partial t} = -\frac{1}{r}\underline{Q}\cdot\underline{\nabla \tau} + \frac{\gamma U\tau}{r^2} - \frac{(\gamma-1)\tau}{r}\underline{\nabla}\cdot\underline{Q} \tag{2-84}$$

2.5 Equations at the centerline in cylindrical coordinates from L'Hospital's rule

The equations developed in section 2.4 were, as mentioned, derived as part of a continuing effort in this work to develop methods for obtaining solutions in cylindrical coordinates. Another, and eventually more fruitful, technique was developed which involved the solution of a completely separate set of equations on the centerline where r = 0. These equations were obtained by applying L'Hospital's rule to equations (36-40) to obtain a set containing no (1/r) terms and valid in the limit as r approaches zero. To do this, limits are required for the following terms:

$$\lim_{r=0}\frac{v^2}{r} = \lim_{r=0} 2v\frac{\partial v}{\partial r} \tag{2-85}$$

$$\lim_{r=0}\frac{-uv}{r} = \lim_{r=0}\left(-u\frac{\partial v}{\partial r} - v\frac{\partial u}{\partial r}\right) \tag{2-86}$$

$$\lim_{r=0} \frac{v}{r}\frac{\partial}{\partial\phi}\begin{pmatrix} u \\ v \\ w \\ p \\ T \end{pmatrix} = \lim_{r=0} \left[v \frac{\partial^2}{\partial r \partial\phi} + \frac{\partial v}{\partial r}\frac{\partial}{\partial\phi} \right] \begin{pmatrix} u \\ v \\ w \\ p \\ T \end{pmatrix} \tag{2-87}$$

$$\lim_{r=0} \frac{1}{r}\frac{\partial p}{\partial\phi} = \lim_{r=0} \frac{\partial^2 p}{\partial r \partial\phi} \tag{2-88}$$

$$\lim_{r=0} \frac{u}{r} = \lim_{r=0} \frac{\partial u}{\partial r} \tag{2-89}$$

$$\lim_{r=0} \frac{1}{r}\frac{\partial v}{\partial\phi} = \lim_{r=0} \frac{\partial^2 v}{\partial r \partial\phi} \tag{2-90}$$

As stated above, L'Hospital's Rule is applied to equations (36-40), with the terms from equations (85-90) applied where needed, to obtain

$$\frac{\partial u}{\partial t} = \lim_{r=0} \left(2v \frac{\partial v}{\partial r}\right) - u\frac{\partial u}{\partial r} - \lim_{r=0} \left(v \frac{\partial^2 u}{\partial r \partial\phi} + \frac{\partial v}{\partial r}\frac{\partial u}{\partial\phi}\right) - w\frac{\partial u}{\partial z} - \frac{T}{\gamma p}\frac{\partial p}{\partial r} \tag{2-91}$$

$$\frac{\partial v}{\partial t} = -\lim_{r=0} \left(u\frac{\partial v}{\partial r} + v\frac{\partial u}{\partial r}\right) - u\frac{\partial v}{\partial r} - \lim_{r=0} \left(v \frac{\partial^2 v}{\partial r \partial\phi} + \frac{\partial v}{\partial r}\frac{\partial v}{\partial\phi}\right) - w\frac{\partial v}{\partial z} - \frac{T}{\gamma p} \lim_{r=0} \frac{\partial^2 p}{\partial r \partial\phi} \tag{2-92}$$

$$\frac{\partial w}{\partial t} = -u\frac{\partial w}{\partial r} - \lim_{r=0} \left(v \frac{\partial^2 w}{\partial r \partial\phi} + \frac{\partial v}{\partial r}\frac{\partial w}{\partial\phi}\right) - w\frac{\partial w}{\partial z} - \frac{T}{\gamma p}\frac{\partial p}{\partial z} \tag{2-93}$$

$$\frac{\partial p}{\partial t} = -u\frac{\partial p}{\partial r} - \lim_{r=0} \left(v \frac{\partial^2 p}{\partial r \partial\phi} + \frac{\partial v}{\partial r}\frac{\partial p}{\partial\phi}\right) - w\frac{\partial p}{\partial z} - \gamma p \left[\lim_{r=0} \left(2\frac{\partial u}{\partial r} + \frac{\partial^2 v}{\partial r \partial\phi}\right) + \frac{\partial w}{\partial z}\right] \tag{2-94}$$

$$\frac{\partial T}{\partial t} = - u \frac{\partial T}{\partial r} - \lim_{r=0} \left(v \frac{\partial^2 T}{\partial r \partial \phi} + \frac{\partial v}{\partial r} \frac{\partial T}{\partial \phi}\right) - w \frac{\partial T}{\partial z}$$

$$- (\gamma-1)T \left[\lim_{r=0} \left(2 \frac{\partial u}{\partial r} + \frac{\partial^2 v}{\partial r \partial \phi}\right) + \frac{\partial w}{\partial z}\right] \qquad (2\text{-}95)$$

It is emphasized that equations (91-95) apply only at r = 0. The appropriate limits are not known in all cases, so the equations have been left in the above form until their actual implementation is discussed in a later, more appropriate, section.

2.6 Quasi-one-dimensional equations for inviscid flow

It will be of interest in a later section to examine the effect of adding to the basic piston/cylinder model of the I.C. engine a computational region intended to model an intake manifold. Since such a manifold is nothing more than a duct connecting the engine to the carburetor, it would seem logical to use the same quasi-one-dimensional assumptions as are frequently used in the analysis of fluid flows in rocket engines, gasdynamic lasers, and similar situations where the primary interest is in the streamwise variation of the flow properties [41,42,43]. The relevant equations in dimensional form are [44]

Continuity

$$\frac{\partial \rho}{\partial t} = - \frac{1}{A(z)} \frac{\partial (\rho w A)}{\partial z} \qquad (2\text{-}96)$$

Momentum

$$\frac{\partial w}{\partial t} = - w \frac{\partial w}{\partial z} - \frac{1}{\rho} \frac{\partial p}{\partial z} \qquad (2\text{-}97)$$

Energy

$$\frac{\partial h}{\partial t} = - w \frac{\partial h}{\partial z} - \frac{1}{\rho} \left(\frac{\partial p}{\partial t} + w \frac{\partial p}{\partial z}\right) \qquad (2\text{-}98)$$

where

$A = A(z)$ = duct area as a function of length.

Non-dimensionalizing as in section 2.1 and eliminating density in favor of pressure and temperature yields

$$\frac{\partial p}{\partial t} = - \gamma p \left(\frac{\partial w}{\partial z} + \frac{w}{A} \frac{\partial A}{\partial z}\right) - w \frac{\partial p}{\partial z} \tag{2-99}$$

$$\frac{\partial w}{\partial t} = - w \frac{\partial w}{\partial z} - \frac{T}{\gamma p} \frac{\partial p}{\partial z} \tag{2-100}$$

$$\frac{\partial T}{\partial t} = - w \frac{\partial T}{\partial z} - (\gamma-1)T \left(\frac{\partial w}{\partial z} + \frac{w}{A} \frac{\partial A}{\partial z}\right) \tag{2-101}$$

2.7 Moving-grid transformation

So far, all equations have been given in a form that is correct only for an inertial coordinate system. In an internal combustion engine the flowfield is of varying size because of the motion of the piston up and down in the cylinder. A glance at Figure 1 will show that as the piston moves the grid points at which the solution is obtained must either move with it or be eliminated from the calculation as the piston passes them. The former situation implies an accelerated coordinate system which compresses or expands as the piston moves. The latter choice would seem to waste grid points and hence computer storage, and so was not considered. The computational mesh for the non-inertial system is laid out so that it will always have the appearance of Figure 1 in the transformed space. The same number of equally-spaced points will always lie in the space between the top of the cylinder and the piston. Let z be the non-dimensional coordinate normal to the piston, with $z = 0$ at the top of the cylinder and $z = z_{max}$ at the piston surface. Let H(t)

be the time-dependent non-dimensional value of z_{max}, i.e., the total length of the available flowfield at time t. Then for any dependent variable g, it must be true that

$$g = g(x,y,z',t) \tag{2-102}$$

where

$$z' = \frac{z}{H(t)} \, . \tag{2-103}$$

This is simply a statement that all dependent variables are functions only of the available space within the cylinder. Note that the range of z' is (0,1).

The z-derivatives will transform as

$$\frac{\partial}{\partial z} = \frac{\partial z'}{\partial z} \frac{\partial}{\partial z'} = \frac{1}{H(t)} \frac{\partial}{\partial z'} \tag{2-104}$$

hence the finite-difference transformation is

$$\Delta z = H(t) \, \Delta z' = \frac{H(t)}{(N_z - 1)} \tag{2-105}$$

where N_z is the number of z-points used in the calculation. Similarly, the time derivatives transform as

$$\left(\frac{\partial}{\partial t}\right)_{moving} = \left(\frac{\partial}{\partial t}\right)_{fixed} + \frac{\partial z'}{\partial t} \frac{\partial}{\partial z'}$$

or

$$\left(\frac{\partial}{\partial t}\right)_{moving} = \left(\frac{\partial}{\partial t}\right)_{fixed} - \frac{z}{H^2} \frac{dH}{dt} \frac{\partial}{\partial z'}$$

$$= \left(\frac{\partial}{\partial t}\right)_{fixed} - \frac{z' V_p(t)}{H(t)} \frac{\partial}{\partial z'}$$

where $V_p(t) = \frac{dH(t)}{dt}$ is the non-dimensional piston velocity. H(t) is sinusoidal for all work presented here. From equation (104) and the

result above, the required transformation from the non-inertial system to an inertial one is obtained,

$$\left(\frac{\partial}{\partial t}\right)_{moving} = \left(\frac{\partial}{\partial t}\right)_{fixed} - z'V_p \frac{\partial}{\partial z} \qquad (2\text{-}106)$$

In practice, equation (105) is applied at the beginning of each time step, while the extra term of equation (106) is added to the right-hand-side of all equations given so far. With this procedure, no further thought need be given to the treatment of the non-inertial system.

It should be noted that in the two-dimensional analyses reported in Chapter 4, the piston motion is actually in the x-direction (see Figure 1). Therefore, all of the above transformation equations actually have "z" replaced by "x" when used in the two-dimensional equations.

Chapter 3

THE NUMERICAL METHOD

The equations necessary to describe the flowfields of interest have been developed in Chapter 2. The type of problem to which they are being applied was discussed in Chapter 1. Boundary conditions which are required to obtain solutions for a specific problem will vary somewhat in this work because of the range of problems considered, and so will be dealt with on an individual basis where appropriate. The remaining topic to be discussed before proceeding to the results is the method by which results are obtained.

The same numerical algorithm, equations (1-5) below, was used in all work presented here. The algorithm is a second-order, explicit, time-dependent finite-difference scheme due to MacCormack [45]. The basic approach has been refined by MacCormack and his co-workers [38,39,46], but the refinements seem not to be applicable to the current problem, so only the basic algorithm will be discussed here.

3.1 MacCormack's method

Suppose that all flowfield variables are known or specified at some time t. Let g(x,y,z,t) represent any such dependent variable. The basic idea of MacCormack's method is to advance the known solution in time by means of the first-order Taylor series

$$g(x,y,z,t+\Delta t) = g(x,y,z,t) + \left(\frac{\partial g}{\partial t}\right)_{avg} (\Delta t) \qquad (3\text{-}1)$$

where

$$\left(\frac{\partial g}{\partial t}\right)_{avg} = \frac{1}{2}\left[\frac{\partial g}{\partial t}\Big|_{x,y,z,t} + \frac{\partial \bar{g}}{\partial t}\Big|_{x,y,z,t+\Delta t}\right] \qquad (3\text{-}2)$$

and

$$\bar{g}(x,y,z,t+\Delta t) = g(x,y,z,t) + \left(\frac{\partial g}{\partial t}\right)_{x,y,z,t} (\Delta t) \qquad (3\text{-}3)$$

The algorithm is thus a two-step procedure. To illustrate, consider equations (2-26 to 2-31). If the flowfield is known at time t, then all spatial derivatives on the right-hand-sides may be computed (actually, approximated by finite differences). This in turn allows the computation of a number for the time derivatives on the left-hand-side, represented above by the term $\left(\frac{\partial g}{\partial t}\right)_{x,y,z,t}$. These time derivatives are then in turn used in equation (3) to yield $\bar{g}(x,y,z,t+\Delta t)$. This completes the first, or predictor, step. The predicted values are then spatially differenced, as before, which again allows the computation of the corresponding time derivatives, given above by the term $\left(\frac{\partial \bar{g}}{\partial t}\right)_{x,y,z,t+\Delta t}$. Equation 2 is then employed to average the time derivaties, followed by application of equation (1), which gives the corrected value for $g(x,y,z,t+\Delta t)$. MacCormack [45] has shown that the combined scheme results in 2nd-order accuracy in both space and time. The method has the advantage of being simple to apply while still yielding good accuracy, and can be used with virtually any formulation of the governing equations or coordinate system. On the other hand, the application to a particular situation can be somewhat ambigous. For example, in the original algorithm MacCormack demonstrates 2nd-order accuracy for a scheme in which forward spatial differences, i.e.,

$$\frac{\partial g}{\partial x} \cong \frac{g(x+\Delta x,y,z,t) - g(x,y,z,t)}{\Delta x} \qquad (3\text{-}4)$$

are used on the predictor step and backward differences,

$$\frac{\partial g}{\partial x} \cong \frac{g(x,y,z,t) - g(x-\Delta x,y,z,t)}{\Delta x} \qquad (3\text{-}5)$$

are employed for the corrector. Other permutations are possible, especially when second derivatives are present, and MacCormack suggests [38] that the best procedure is to cycle among them during the computation. Evidence that this might be helpful is provided quite graphically in work by Kothari and Anderson [47]. In their work, it was shown that repeated application of certain differencing patterns could lead to severe instability, while others gave excellent results. The problem is that the investigator may not know in advance which technique will work best.

The integration step size, or time step, can be estimated by application of the Courant-Friedrichs-Lewy (CFL) criterion,

$$\Delta t \leq \frac{\Delta}{|\underline{V}| + a} \tag{3-6}$$

where

Δ = local grid spacing

$|\underline{V}|$ = magnitude of local flow velocity

a = local speed of sound

This linearized stability criterion states that the computational cell must at least include the region of acoustic influence at a point. In practice, equation (6) was applied at all grid points in the flowfield and some multiple (usually .7) of the smallest time step thus obtained was used as the actual step size.

Note that the CFL condition is not the only possible stability criterion. For problems involving chemical reactions, the relaxation times associated with finite-rate processes will often be substantially more restrictive than the CFL criterion. For parabolic or nearly parabolic problems, the characteristic time scale of the diffusion-type terms will be important. In this work, the CFL condition was found to provide the limiting time-step.

MacCormack's method and time-dependent methods in general see widespread application to problems where the desired result is actually a steady-state solution. In such cases, a rough, qualitatively correct initial guess for the solution is used to initialize the algorithm. This rough solution then relaxes to the steady-state as it is advanced in time. The transient results in such a case are of doubtful interest, but this is irrelevant if the steady-state solution is sought. However, in a transient problem such as the one at hand there will never be a steady-state, so that the question of convergence of the algorithm to a time-varying solution becomes important. This was found not to be a problem in the present work. The results showed that convergence to the quasi-steady solution is both quick and readily apparent, with little or no "lagging" of the calculation. Two explanations of this fact can be made:

1. When the calculations are initiated, the piston is at the top of the intake stroke, with the intake valve open and ambient conditions inside and out. The initial dynamic state is in effect a trivial steady-state solution; there is no fluid or piston motion. Further, the piston motion is sinusoidal, so the velocity is initially zero and increases smoothly. The results showed that the piston motion has a time scale that is very large relative to the limiting CFL step. Many integrations are thus performed over any physically significant time interval, and there is no reason not to expect the algorithm to be able to cope with such modest requirements.
2. Even in cases where truly transient events occur (such as opening and closing of valves), the results settle down in a few time

steps. This is in direct contrast to the behavior when a steady-state solution is sought, where on the order of a thousand time steps are generally required to relax the initial guess to the final result. The explanation for this would seem to lie in the presence of the driving term for the flow, the piston motion. The behavior of the results makes it appear that a driving transient term will smother smaller effects, thus helping to produce a good solution.

3.2 Spatial differencing techniques

In section 3.1 it was mentioned that the selection of spatial differencing schemes can be important in obtaining good results from MacCormack's method. It is therefore of interest to discuss in detail the particular approach to setting up the difference equations that was used in this work.

For inviscid flow, whether in conservation-law form or otherwise, the equations contain only first derivatives (unless damping terms are explicitly added, a point for later discussion). Thus, on the predictor/corrector steps, one uses forward/backward or backward/forward differences. Both were tried, and when no difference in the results were obtained for a sample calculation, the forward/backward difference scheme for the predictor/corrector steps was chosen since that was the original choice in MacCormack's work [45].

For viscous flow, the treatment of the first derivatives follows the same logic as above in terms of the choices available, and the same scheme was selected. The treatment of second derivatives can depend, however, on whether the governing equations are in conservation form or not. If they are, then shear-stress and heat conduction terms which

themselves involve first derivatives must be included inside the E, F, and G vectors of equations (2-41 to 2-45). The second derivatives in the full Navier-Stokes equations then appear implicitly as first derivatives of first derivatives. It was with systems of this type that Kothari and Anderson [47] pointed out the need for care, particularly in avoiding situations where the "inner" first derivatives were differenced in the same direction as the "outer" derivatives.

The only viscous flow results obtained by the present author were with the non-conservation forms developed in Chapter 2. Here, more of a conscious decision as to how the second-derivative differencing (particularly on cross-derivatives) should be performed is required, since one cannot set up the 2nd-derivative computation to occur automatically. For second derivatives of the type $\frac{\partial}{\partial x^2}$, $\frac{\partial}{\partial y^2}$, and $\frac{\partial}{\partial z^2}$ the only choice ever considered or used in this investigation was the well-known central second-difference formula,

$$\frac{\partial^2 g}{\partial x^2} \cong \frac{g(x+\Delta x) - 2g(x) + g(x-\Delta x)}{(\Delta x)^2} \qquad (3\text{-}7)$$

which is accurate to the second order in Δx. For cross-derivatives, such as $\frac{\partial^2}{\partial x \partial y}$, the initial choice was to take the central difference of a central difference, for the reason that the symmetry involved was thought desirable. Thus the equation used was

$$\frac{\partial^2 g}{\partial x \partial y} = [g(x+\Delta x,y+\Delta y) - g(x+\Delta x,y-\Delta y) - g(x-\Delta x,y+\Delta y) + g(x-\Delta x,y-\Delta y)]/4(\Delta x)(\Delta y) \qquad (3\text{-}8)$$

This turned out to be a poor choice. When the results of Kothari and Anderson's experiences became known [47], a switch was made to the following procedure:

1. On the predictor step, all cross-derivatives were obtained as backward differences of forward differences. Thus,

$$\frac{\partial^2 g}{\partial x \partial y} = [g(x,y+\Delta y) - g(x,y) - g(x-\Delta x,y+\Delta y) + g(x-\Delta x,y)]/(\Delta x)(\Delta y) \qquad (3\text{-}9)$$

2. On the corrector step, all cross-derivatives were obtained as forward differences of backward differences. Thus,

$$\frac{\partial^2 g}{\partial x \partial y} = [g(x+\Delta x,y) - g(x+\Delta x,y-\Delta y) - g(x,y) + g(x,y-\Delta y)]/(\Delta x)(\Delta y) \qquad (3\text{-}10)$$

Analogous formulas are used for $\frac{\partial^2 g}{\partial x \partial y}$, $\frac{\partial^2 g}{\partial x \partial z}$, etc. The use of this procedure made an immediate difference in the solutions then being obtained. For the first time, stable results were achieved.

It will be noted that all of the above-described differencing procedures are suitable only for interior flowfield points. That is, it is obvious that a backward x-difference cannot be obtained at the first x-point in the grid, and similarly for the other mesh boundaries. This difficulty was touched on in section 2.4 in connection with coordinate--singularity problems at r = 0 in cylindrical systems. In the more easily treated case where the mesh boundary is an actual flowfield boundary (i.e., wall point or valve point, in the I.C. engine problem), several alternatives are available:

1. The simplest approach is to use one-sided differences on both predictor and corrector steps, setting the boundary conditions on each step, and accept the fact that the solution at these points will in general lack the overall accuracy usually

obtainable from the algorithm and the mesh spacing.

2. One may add sophistication to the above technique through the use, at such special points, of additional information that is outside the numerical method. An important example is the use of method-of-characteristics schemes to provide wall-boundary information. Abbett's simple wave corrector [48] is an example of such a technique that provides excellent results for supersonic flow. An analogous technique utilizing the x-t plane method of characteristics results for one-dimensional unsteady flow was adapted from the work of Rudinger [49] and applied to the present problem. The technique and the results obtained will be discussed more fully in the section where they were applied.
3. One may avoid specifying any grid points that are actually on a wall boundary, by beginning the grid layout at a distance of $(\Delta x)/2$ from the boundary at $x = 0$, for example. Then one may employ a reflection technique [50], possibly combined with some additional technique as in (2) above.

In the present work, alternatives (1) and (2) were used. Again, it is felt that detailed discussion of results is best deferred until those sections which deal with the particular cases run and results obtained.

There is one variation on method (1) that should be discussed here, since it yields a difference formula that proved to be of some value. Note that since the usual second-order forward/backward MacCormack algorithm fails at a mesh boundary, it is logical to think of correcting the situation by using a second-order one-sided difference at such points. An example of such a formula is

$$\left(\frac{\partial g}{\partial x}\right)_x = \frac{-3g(x) + 4g(x+\Delta x) - g(x+2\Delta x)}{2\Delta x} + O(\Delta x)^3 \qquad (3\text{-}11)$$

which may be derived by writing two Taylor series about the point x,

$$g(x+\Delta x) = g(x) + \left(\frac{\partial g}{\partial x}\right)_x (\Delta x) + \left(\frac{\partial^2 g}{\partial x^2}\right)_x \frac{(\Delta x)^2}{2} + \ldots .$$

$$g(x+2\Delta x) = g(x) + 2\left(\frac{\partial g}{\partial x}\right)_x (\Delta x) + 4\left(\frac{\partial^2 g}{\partial x^2}\right)_x \frac{(\Delta x)^2}{2} + \ldots .$$

and solving for $\left(\frac{\partial g}{\partial x}\right)_x$ by eliminating $\left(\frac{\partial^2 g}{\partial x^2}\right)_x$.

This scheme was used at mesh boundaries in several different solutions, and nearly always resulted in degradation of the solution, or sometimes in outright instability. It seems that in cases where mesh spacing is fine the second-order one-sided difference is useful. However, for the relatively coarse mesh spacing used here, equation (11) produces poor behavior in the solution. There was, however, one situation in which it proved useful in the present work. This is in connection with the computational scheme that was eventually implemented at the centerline (r = 0) in cylindrical coordinates. This application will be described in Chapter 5.

Surprisingly, the computation of second derivatives at the mesh boundaries presents little problem. They occur only for viscous flow, and if the mesh boundary is a wall, velocity and temperature are both specified, so that the use of second-derivative information to compute them is not required. The equation for the time derivative of pressure, equation (2-7), does contain the Laplacian of temperature. The second derivative normal to the wall, at a wall, that can thus occur is obtained

by the usual three-point central-difference formula, equation (7), and making the assumption that the temperature inside the wall is the same as that on the surface of the wall.

More difficulty is apparent in the case where the mesh boundary is a valve. Second derivatives of both velocity and temperature are required here, and will include both Laplacian-type derivatives and cross-derivatives. The Laplacian-type terms are obtained using the same approximation as outlined in the paragraph above. The cross derivatives are handled in a way that is felt to be as consistent as possible with the approach of equations (9) and (10). Thus, the component of the cross-derivative that is normal to the mesh boundary is always treated with a one-sided first-order difference, while the component tangential to the mesh boundary is forward/backward differenced in accordance with the usual MacCormack scheme. These approximations seem to work quite well.

Finally, note that for viscous flow the computation of pressure at a corner becomes a problem. A careful examination of equation (2-7) shows that at a corner all terms which could contribute to the time derivative of pressure are identically zero. Such a point therefore acts as a "pressure source" or a "pressure sink" of a constant value, and so ruins the calculation. The method used to avoid this was to simply specify the pressure at a corner point in viscous flow to be the average of three or four neighboring points. This caused no apparent problems.

Chapter 4

TWO- AND THREE-DIMENSIONAL VISCOUS FLOW ANALYSES

As has been mentioned, the first results during the course of the work leading to this dissertation were those for the case where the engine is assumed to be two-dimensional and the fluid is assumed to be the single-component, non-reacting, viscous, heat-conducting fluid for which the governing equations are (2-7 to 2-9). This is not as paradoxical as it might at first seem. In many ways it is simpler to obtain numerical results for viscous flows. The boundary conditions are less troublesome, little difficulty is encountered with numerical instability (at low Reynolds number), and in general the calculations prove less sensitive than is the case for inviscid flow. There are many disadvantages that eventually became apparent during the early work with viscous flow calculations, but for obtaining a baseline result, the use of the full Navier-Stokes equations was quite helpful.

Much of this early work with two-dimensional viscous flow I.C. engine calculations was reported in Reference [20]. It is included here for the sake of completeness, and because subsequent work has in some cases resulted in new conclusions concerning the earlier results.

4.1 Two-dimensional viscous flow calculations

4.1.1 Details of the problem

Consider the idealized model of the piston-cylinder geometry in an I.C. engine as shown in Figure 1. The flowfield between the top of the cylinder and the piston face is computed as a function of position and time as the piston moves through a conventional four-stroke cycle, with the intake and exhaust valves opening and closing at the proper times

within the cycle. Several simplifying assumptions have been made in the present analysis. The piston motion is assumed to be simple-harmonic in time, and the valves are assumed to open and close instantaneously. These limitations do not at this time appear to be serious, and in any case are easily removed for future work. Of greater importance is the assumption that the valves are open ports; i.e, the usual structure, in which the valve stem extends into the cylinder, is not involved in the present model.

The real physical problem of interest is three-dimensional, because of the off-center positioning of the valves. However, for the first stage of the analysis, it was felt that the increased computer time associated with the use of a three-dinensional model in cylindrical coordinates would be unnecessary. Moreover, there are problems associated with specifying conditions along the line r = 0 in cylindrical coordinates, and in the absence of axial symmetry, it was not clear what conditions were appropriate. For these reasons the initial work assumed the piston--cylinder arrangement of Figure 1 to be two-dimensional (infinite aspect ratio engine). Such 2-D solutions yield valuable information on the qualitative aspects of the real problem, and help to underscore the fact that fluid-flow processes during the four-stroke cycle are important.

Also, for reasons to be discussed later, it seemed desirable to investigate the effect on the internal flowfield of applying the boundary conditions directly to the valve points. For this reason, a simplified "manifold" or plenum chamber was added to the geometry of Figure 1, with the results as shown in Figure 2, and this model was then used in several calculations.

The governing equations and non-dimensionalizing procedure have been

developed in section 2.1.1, and the transformation relating the moving grid system to an inertial system was derived in section 2.7. It remains to discuss the boundary conditions appropriate to this particular case.

The boundary conditions for the Navier-Stokes equations are $V_1 = V_2 = 0$ on the walls, $V_1 = V_p$ and $V_2 = 0$ on the piston, and $T = T_w$ = constant on all walls. At an open valve, pressure and temperature are held constant at ambient conditions and the transverse (V_2) component of velocity set to zero. The imposed cooled-wall boundary condition is an approximation to reality; that is, at some distance from the cylinder, for example in the water jacket, the temperature is relatively constant, but it is clear that on the actual cylinder wall it is not. Therefore, a more sophisticated procedure would be to run a heat-conduction solution for the walls in parallel with the present scheme and thus allow the wall temperature to be a computed, time-dependent quantity. However, it was thought that this would be a relatively straightforward extension to the current work, and hence not worth the extra computer time at this stage.

The handling of the open-valve boundary condition follows a somewhat similar line of reasoning. It is apparent that at some great distance from an open valve, "ambient" values of pressure and temperature are reached; but again, this clearly does <u>not</u> happen exactly at a valve. A rigorous computation would include a manifold solution to allow the valve conditions to be computed as time-dependent values. As mentioned before, it is of interest to see how poor an approximation the constant temperature and pressure valve boundary condition is. Thus, some computations are made with the geometry of Figure 2. Results will be presented later which suggest that the constant p and T boundary condition is somewhat reasonable for the case discussed here.

It turns out that an extermely important criterion for obtaining a useful viscous flow solution is that the Reynolds number based on the grid size (hence the term "cell Reynold's number") be of order unity. This is a well-known fact of life in the field of computational fluid dynamics, and imposes severe limitations on the attainable realism for viscous-flow calculations of I.C. engine flowfields. This fact will be demonstrated in detail by certain results to be presented here.

4.1.2 Discussion of results for 2-D viscous flow

An initial set of results were obtained for a special case in order to verify the consistency and accuracy of the numerical solutions. In this special case, the piston is held stationary with one valve open. The initial conditions specify zero velocity within the cylinder, an internal pressure substantially higher or lower than the external value, and the internal temperature equal to the ambient value. This is simply a pressurized or evacuated rigid tank which, at time zero, is opened to the ambient conditions through a hole in the wall. The ensuing flowfield and equilibration to ambient conditions within the cylinder make an appropriate test case for the present analysis. It also hints at an important effect of Reynolds number on the computations, and allows a convenient study of the effect of different boundary conditions at the valve.

Figure 3 shows a transient velocity distribution from one such test, where the initial internal pressure was five times the ambient value. It must be noted that this and all subsequent velocity distributions are not to scale. The actual velocities vary over two orders of magnitude and a scaled plot is more confusing than revealing. So, in Figure 3 and in others to follow, the larger arrows indicate higher velocities, but not how much higher.

The most striking thing about the velocity distribution of Figure 3 is that it clearly shows that there really is a detailed flowfield inside such a cylinder model. The swirl and convergence of the velocity field to the open valve is clearly evident, and even on this relatively coarse scale there is evidence of recirculation zones in the corners. This has important implications for studies of combustion processes for an I.C. engine, and the behavior of the resulting emission products.

As shown, this test was conducted at a very low pressure. The scale size of the problem is also small (thimble size) to keep the cell Reynolds number small without excesssive computer time. In the interest of examining the effect of the cell Reynolds number of the computations, a series of cases such as described above were run, with the pressure and scale size of the problem varied to produce cell Reynolds numbers between unity and order 10^4 (corresponding to the real physical case). The results of these tests for the two extremes are shown in Figures 4 and 5, where pressure and temperature distributions at constant y (near the middle) and varying x are shown. In Figure 4 there are four pressure distributions, the upper graph depicting a transient and steady-state result for the low cell Reynolds number case and the lower graph the distributions at corresponding scale times for the high cell Re case. Both of the steady-state results are exactly as expected, but the transient case for high cell Re clearly shows excessive and undesirable waves and wiggles. It does not seem likely that these represent reality; rather, they are interpreted to be the result of violating the unit cell Re criterion.

Similar behavior is evident in the corresponding temperature distributions for these cases, as shown in Figure 5. Notice on the upper graph

how a smooth initial expansion cooling is followed by eventual equilibration to ambient conditions, exactly as expected for such a flow. In the high cell Reynolds number case, however, the transient result almost immediately picks up a wiggle pattern which persists thereafter. Notice however that the oscillations, both transient and steady-state, are centered about the isentropic result which would be expected for a nearly inviscid test case such as $Re_{cell} \approx 10{,}000$. This clearly shows how a high cell Reynolds number renders the viscous terms insignificant, so that the calculation resembles that for an inviscid flow. Moreover, close inspection of the numerical results shows the "steady-state" to be actually a very slowly rising distribution. This is expected if the viscous heat conduction terms have been dwarfed, but not totally eliminated, by cell Reynolds number effects. That is in fact the case, as shown by a trunction-error analysis for a non-linear model equation (Burgers' equation) such as is done by Taylor [51]. The analysis brings out the fact that in any numerical solution of the Navier-Stokes equations based on a finite-differencing procedure, there is a trunction-error term that appears in the denominator of the viscous terms and which is proportional to the cell Reynolds number. It is therefore important that the mesh spacing be such that a cell Reynolds number of order unity be maintained if the effect of the viscous terms (including heat conduction and diffusion terms) is to be correctly treated.

As mentioned before, it is apparent from the outset that the specification of valve boundary conditions as being constant temperature and pressure is at best an approximation. In fact, one cannot legitimately specify such "free boundary" conditions anywhere short of an infinite distance from the region of interest. However, the geometry of Figure 2

represents at least a better approximation to infinity, in that the free boundary is removed ten units away from both the valves and the actual interior flowfield of interest, thus allowing conditions at the valve to be computed as time-dependent values. The previously described test case (at low cell Re) was run, but now with the plenum attached, as shown in Figure 2. Initial conditions in the external plenum chamber were specified as ambient pressure and temperature and zero velocity. Figure 6 shows in succession three sets of transient pressure and temperature distributions, this time taken down a line of constant y from the valve point to the rear wall. It is gratifying to note that in general the results with and without the manifold are quite close, within about four percent, except at early times at the valve point itself. Figure 7 shows the results at the valve point alone for all times. It is clear that the constant-pressure stipulation appears to be a reasonable approximation, in close agreement with the more exact case after about 250 time steps (.02 μsec in this case). The temperature takes about three times as long to achieve similar agreement. However, the overall results give a measure of confidence that the constant pressure and temperature boundary condition is adequate for the present low Re solutions, especially in view of the fact that during the actual four stroke engine cycle the internal to external pressure ratio is not nearly as severe as in these test cases.

This question of what constitutes an appropriate way to model the flow in the neighborhood of the intake and exhaust valves will arise again in connection with 3-D inviscid solutions. For that situation, it will be shown that a feasible technique is to attach a duct (for which the flowfield is modeled by the quasi-one-dimensional equations of

section 2.6) at the intake valve and thus allow the actual valve point or points to be computed as with any other interior point. This option is not feasible for viscous flow calculations, since quasi-one-dimensional viscous duct-flow calculations tend toward Fanno-line flows. This means that velocities in the duct tend toward choking values, a situation that causes problems with the programs and is probably unrealistic also.

The results shown in Figures 3-7 serve as a check of the analysis and progamming. The general quality of the transient results as well as the approach to ambient conditions yield some confidence in the extension of this work to the more complex case of the four-stroke cycle, always providing that the cell Reynolds number is of order one. To achieve $Re_{cell} \approx 1$ keeping the same 10 x 9 grid, the "engine model" for the present work is (8 x 9) mm in size and is operating at an ambient pressure of .01 atmosphere. Obviously, these are not full-scale operating conditions for typical I.C. engines. However, the present results for a small--scale engine at low density serve to illustrate the general nature of the Navier-Stokes solution, and illustrate the influence and character of a flowfield in the engine process.

Note that if a turbulence model were employed, one immediate effect would be an increase in the overall viscosity of several orders of magnitude, thus allowing normal-size engines to be treated at reasonable pressures. The author feels that without a correspondingly more realistic treatment of combustion and the mixing processes induced by turbulent flow, such a procedure is of no benefit, and the present laminar flow solutions are acceptable.

Figures 8-15 give results for the velocity, pressure, and temperature distributions at various times throughout the intake, compression, power

and exhaust strokes for the geometry of Figure 1. On each graph is a small schematic diagram of the piston-cylinder geometry showing the piston position and direction of motion at the particular time under consideration. When relevant, as in the pressure and temperature diagrams of Figures 12-15, a small dotted line inside the cylinder shows the line along which the results are plotted.

Figure 8 shows the velocity distribution six degrees past top dead center (about a tenth of the way through the intake stroke; the total non-dimensional range of piston travel is $1.0 < x_p < 9.0$). The compression ratio is therefore nine-to-one. Swirl patterns, as in the stationary piston exhaust test (Fig. 3), can be seen in Figure 8. However in this case it is quite clear that the overall driving force on the flow is the piston motion, not a pressure differential at the valve.

Figure 9 shows the velocity flowfield near the beginning of the compression stroke, when both valves are shut. Note how quickly the flowfield adjusts to the change in direction of the piston, and that the transient solution is indeed responding to the piston motion quite closely. In this connection, it is worthwhile to mention once again that there was some initial concern that several complete cycles might be required to allow the time-dependent computation to converge to the transient solution, i.e., to overcome the built in history introduced by the arbitrary initial conditions at the beginning of the intake stroke. This feeling was based on past experience with the use of time-dependent methods as a means of obtaining solutions to steady-state problems in the limit of large times, starting from fairly crude initial conditions. In fact, these fears turned out to be unjustified. The possible reasons for this were presented in section 3.1. To check on all of this, part

of the intake stroke was re-run, continuing after the exhaust stroke. No significant difference between that and the first intake stroke after a few hundred time steps was observed.

At TDC on the compression stroke, combustion was simulated by artifically introducing constant-volume heat addition. The velocity pattern for the resultant power stroke is shown in Figure 10.

The exhaust stroke velocity distribution, Figure 11, is shown near the time of maximum piston velocity. The upper left-hand corner, near the intake valve, is a region of particular interest. It seems to be a region of recirculation, more or less cut off from the main swirl of the flow.

Plots of pressure and temperature for the complete four-stroke cycle are given in Figures 12-15, and are taken at the same times as the velocity distributions at Figures 8-11. In each case the upper graph shows values at constant y and varying x, while the lower shows values at constant x and varying y.

Figure 12 shows the intake stroke pressure and temperature distributions on expanded scales. There are several interesting features here. The most obvious is the hump in the temperature distribution on the upper graph during what would seem to be an expansion phase of the cycle. An examination of the lower graph shows this peak to be part of a pattern of weak (again, recall that the scale of the plots is expanded) waves in pressure and temperature. These waves persist throughout the intake stroke, hence are standing waves, and seem to be maintained by the addition of energy from the mass flowing into the cylinder as the piston withdraws.

Figure 13 displays the pressure and temperature behavior for the

compression stroke. The temperature shows a beautifully smooth, boundary--layer type behavior, clearly a result of the small scale of the problem and hence relatively greater importance of heat conduction. The pressure is constant to at least five significant digits. This behavior further indicates that the wave patterns shown on the intake stroke are either real, or are introduced by the boundary conditions at an open valve. The results of the tests with the geometry of Figure 2 would tend to support the contention that the waves really exist, since detailed examination of the numerical results shows weak waves in those cases also. However, this cannot be considered conclusive, since the resolution of the flowfield in the neighborhood of an open valve is in both cases relatively coarse. The waves definitely do not seem to be due to the instantaneous opening and closing of the valves. Indeed, there are distributions set up when this occurs, but they are transient, not standing throughout an entire stroke, and as Figure 13 shows, the compression stroke is perfectly smooth shortly after the intake valve has closed. The waves do appear to be related to the flow viscosity, at least insofar as their persistence is concerned. The inviscid, non-reacting intake--stroke solutions of Diwakar [4,21] show that in the 2-D case a definite large-scale circulatory pattern establishes itself at an early time and persists throughout the intake and compression strokes.

The results of the power stroke (Figure 14) show the strong heat--conduction effects in this low Reynolds number problems. The initial temperature distribution immediately after the simulated combustion was strongly peaked (to about $1500^{o}K$, or a non-dimensional temperature of 5.5), but as the graphs show, the small scale size and the constant--temperature wall boundary condition combine to quickly reduce the

temperature gradients. It is apparent that future attempts to produce a realistic engine model must include a heat-conduction solution for the region outside the cylinder walls, for it is doubtful that the temperature really drops so quickly, wall "quench" layers not withstanding.

The results for the exhaust stroke are shown in Figure 15. There is a slight wave pattern evident in the transverse direction, but not as much as on the intake stroke.

The next two graphs, Figures 16 and 17, compare the fully viscous solution at high cell Re (corresponding to a cylinder of realistic scale) with the corresponding inviscid solution by Diwakar. These figures indicate in what way, if any, the high cell Reynolds number solutions may be considered useful.

Figure 16 shows corresponding velocity distributions in the intake stroke for the two cases. It can be seen at once that, except near the walls where viscous effects must always be important, the two cases are remarkably similar. This is not surprising, since at high flow Reynolds numbers the inertia terms dominate the viscous terms in the Navier-Stokes equations. It is even less surprising because of the effect of violating the unit cell Reynolds number criterion is to reduce the effect of viscosity. On the other hand, a comparison of Figures 8 and 16 shows that, again in the core region, the low cell Reynolds number results are virtually identical to the inviscid and high cell Reynolds number cases. The only possible interpretation here is that, away from the walls, the flow is primarily inviscid in character. This suggests the possibility in future work of combining a boundary layer and an inviscid solution to yield an overall improvement in speed, or of using a coordinate system which is relatively dense near the walls and relatively coarse out in the core region.

The pressure and temperature comparisons for the inviscid and high cell Reynolds number cases are shown in Figure 17. As with the velocity distributions, the two sets of results are nearly identical (the upper graph is a highly expanded scale). It is of particular interest to note that, as on Figure 5, the temperature oscillations for the high cell Reynolds number case tends to bracket the inviscid, isentropic value.

4.2 Three-dimensional viscous flow calculations

It was not originally intended that any three-dimensional viscous flow calculations should be done. The limitations on viscous flow solutions imposed by the unit-cell Reynolds-number criterion made the use of inviscid flow models for further developmental work, particularly in three dimensions, seem much more reasonable. However, when even the simplest 3-D inviscid calculations began behaving in a manner that was at that time inexplicable, it began to seem prudent to return to the Navier-Stokes equations and attempt to obtain some sort of three-dimensional result as a piece of baseline information. It was hoped that this would involve little more than adding an additional coordinate loop to the existing program. It was in fact not much more trouble than that, and so the first true 3-D solution obtained was the by-product of failure with what should have been a much simpler system.

The three-dimensional viscous flow problem is not really in the mainstream of this work, and so will not receive as much attention as some other areas. However, certain simple exhaust tests are of interest because they can be compared with the corresponding 2-D tests discussed above, and hence an idea of the usefulness of future 2-D viscous calculations obtained.

4.2.1 The three dimensional rectilinear engine model

The calculations were performed for an engine model such as depicted in Figure 18. Note that the y-coordinate is now the direction normal to the valve plane, and that the x-y plane model of Figure 1 would be the x-z plane in Figure 18. The x-z plane, or valve plane, is necessarily a plane of symmetry, so that only half of the chamber need be treated, with no loss in accuracy. This is true because the "boundary conditions" at a plane of symmetry may be specified exactly, unlike the case for a wall. The correct condition is that all flowfield variables except for the velocity normal to the symmetry plane are even functions of the coordinate normal to the plane, while the normal velocity component is an odd function. This allows image points to be specified across the symmetry plane from the values inside the computational domain, hence the finite differences required on the plane of symmetry present no problem. One can actually go further; because all flowfield variables except normal velocity are even functions across the symmetry plane, their derivatives on that plane, in the direction normal to it, are identically zero. The same is true for the second derivative of the normal component of velocity in the direction perpendicular to the symmetry plane. This information can be used if desired, rather than computing finite differences. On some occasions such use of analytical information that does not come from the differencing scheme itself can lead to trouble. Thus, Anderson reports that in time-dependent nozzle-flow calculations [41,42,43] one should not use the known result that at the throat of a nozzle, $\frac{dA(x)}{dx} = 0$, because this leads to a "bump" in the mass flux. Both approaches were tried in this work, and it seemed that the results on the test cases were slightly better using

the exact values for derivatives normal to the plane of symmetry, so this approach was retained.

All other boundary conditions for the 3-D viscous flow solutions are as described above for the 2-D case. Also, as mentioned in Chapter 2, the assumption of constant viscosity and thermal conductivity was used in the 3-D case, so that equations (2-17 to 2-19) were used. At the temperatures involved, this is expected to make no difference.

4.2.2 Discussion of results for 3-D viscous flow

Two cases were run with the 3-D Navier-Stokes code after it was checked out. The first was a simple inflow case, with the external pressure at .01 atmospheres, and temperature at $273^{o}K$, while inside the chamber the pressure was .008 atmospheres and the temperature equal to .938 of the ambient value. The case is for a cell Reynolds number of order one, as indicated by the low pressure. The piston was held motionless with the intake valve open. The expected behavior is that there will be a sudden inflow of air, followed by equilibration to ambient pressure and temperature inside and out. The calculations produced the expected behavior; the case was of interest because the inviscid flow model had been experiencing difficulty (to be discussed) on an identical test case.

The next case to be run was the reverse of the situation above, and essentially a three-dimensional duplicate of the low cell Reynolds number exhaust test discussed earlier for two dimensions, and for which the results are shown in Figures 3-5. The work "essentially" is used because exact duplication is not possible. In the 2-D solutions, only one point of the relatively coarse grid system was used as the intake valve point. Since the flow is two-dimensional, this point gives the valve an effective

"area" of about one-ninth of the total top surface "area". In the 3-D case, the effective number of points on the top surface is eighty-one, counting the image points which were not actually stored in the machine. One-ninth of these is nine, hence nine points should be, and were, specified as valve points. To do this, more than one must be placed on the symmetry plane (x-axis) and this was done as shown in Figure 19, where it is seen that three of the valve points are necessarily image points. The net effect is that an exact 3-D duplicate the earlier 2-D test cannot be obtained without reducing the effective size of the valve. This is undesirable also, so the same valve area was retained at the expense of modifying the shape.

Figure 20 shows pressure and temperature distributions taken in the valve plane along a line perpendicular to the central axis for the 2-D and 3-D exhaust tests. They are taken at approximately the same time (0.37 msec for 3-D and .041 msec for 2-D. A distinct difference in behavior is evident. The slight variation in the levels of pressure and temperature is unimportant, since the times are different by about ten percent. But notice that the 2-D pressure distribution shows the same standing wave pattern, at the beginning of its formation , that is clearly evident in Figures 12 and 15 for the 2-D tests. The data in both cases is taken in the same locations. Such standing wave patterns are not found in the 3-D cases. This may be due to the altered valve geometry, in line with the earlier conjecture that the 2-D waves were initially caused by the valve boundary condition, or it may be that their absence is due to the "3-D relief" that is not present in the earlier results. This kind of result does not support any extensive conclusions, but still, there is evidence that a pattern clearly visible in a viscous 2-D flow is missing in a 3-D calculation for the corresponding case.

This completes the discussion of 3-D solutions of the Navier-Stokes equations. As mentioned, the main incentive for the work was the demonstration that a three-dimensional solution of some kind could be obtained with the algorithm being used. This goal was achieved.

4.3 Conclusions based on viscous flow analyses

The viscous flow studies discussed above form a subset of this dissertation that merits a summary at this point. As stated, much of this work may be found in Reference [20], and at the time of its preparation certain conclusions were drawn regarding the utility of the results so far obtained and the direction of future work. The benefit of hindsight and additional experience allows some further conclusions to be made, and some earlier ones to be modified.

First, the cell Reynolds number limitation on viscous flow calculations is still a major restriction, and one that appears unlikely to be surmounted in the near future. In this work, the use of a representative laminar flow viscosity necessitated the use of greatly reduced scale size and density to satisfy the unit cell Reynolds number criterion. It would have been as easy to increase the viscosity and other transport coefficients such as thermal conductivity and diffusivity (for multi-component fluids) by several orders of magnitude. This is in fact the first-order effect of turbulence, and as mentioned in the literature survey of Chapter 1, this constitutes the "turbulence model" of several studies. No criticism is intended; it is simply that this author fails to see any fundamental difference between such models and the laminar viscous flow studies discussed here. Similarly, one may question the logic of a code such as RICE [18,19] which sets the transport coefficients as necessary to achieve stability. If such compromises need to be made,

and it appears at this time that they do, then one may also question whether equally valid (that is, incorporating a different set of errors!) inviscid flow models might not serve as well for the next generation of developmental work. This allows 2-D computations, even including reacting chemistry, to be performed without prohibitive amounts of computer time being expended. This is the thrust of a major portion of the companion work of Diwakar [4]. Similarly, for the purpose of extending the geometrical models to the three dimensions in cylindrical coordinates, it certainly makes sense to employ an inviscid flow model.

At the time of publication of Reference [20], it seemed that a promising line of development might be in the area of applying an improved numerical method to the I.C. engine problem. Extensive searching of the recent literature failed to turn up any other approach with the combination of reasonable speed, ease of applicability and history of successful use as the explicit finite difference scheme of MacCormack [45]. Accordingly, work to develop three-dimensional inviscid flow calculations was seen as the next logical step.

Chapter 5

THREE-DIMENSIONAL INVISCID FLOW ANALYSES

5.1 The physical models considered

Since the analyses of Chapter 4 led to the conclusion that further work with inviscid flow models offered the best chance to obtain reasonable solutions within acceptable computer time, the choice of the exact geometrical model became the next step. The geometry for which a solution was most desired is the cylindrical piston/cylinder model depicted in Figure 21. It was thought that the difficult portion of the work would lie in finding an appropriate way to specify conditions at r = 0, the centerline (z-axis) of the cylinder. This was in fact a problem, but not the only one associated with three-dimensional calculations. A few abortive attempts to begin work directly with the 3-D geometry of Figure 21 led to the conclusion that more than one type of difficulty might be involved. Therefore, an inviscid flow model in cartesian coordinates was developed for the analysis of the flowfields in the rectangular engine model of Figures 18 and 19. This proved to be a well-chosen step, as it developed that additional problems unique to the three-dimensional inviscid solution for this type of internal flow were present, and in all probability could not have been successfully analyzed without decoupling them from those associated with the use of cylindrical coordinates. Thus, both rectangular and cylindrical engines were extensively studied. This has proven to be most helpful in analyzing the results eventually obtained from the four-stroke engine cycle calculations for both these models.

All factors involved in specifying the grid layout for the rectangular model were discussed in section 4.2.1, and as they are not unique

to viscous flow, they will not be repeated here. Figure 22 shows the grid layout which was used in the cylindrical coordinate model, including the valve points. Note that considerably more valve points are required to define a valve than in the rectangular case as a result of the coordinate bunching that occurs for small values of r. The pattern of Figure 22 is repeated in all planes defined by z = constant, with the exception that the valves obviously are found only at z = 0. Ten z-planes were used in all three-dimensional work reported here. The physical size is not important since no non-isentropic effects which would "scale" the model are found in the inviscid flow equations used, but a nominal size of nine centimeters in height by eight in width (or diameter) was chosen to simplify comparison with the work of Diwakar [4,21] and so that an ordinary value of engine speed would result in realistic piston velocities.

5.2 Boundary conditions for inviscid flows

5.2.1 Wall boundary conditions

The absence of viscosity in the governing equations used for this work (sections 2.3 through 2.5) obviously eliminates the use of the no-slip condition for the tangential components of velocity at a wall. Another way to view the situation is that the inviscid system is of lower order than the viscous system, so the solution requires fewer boundary conditions. In any case, the neglect of viscosity is consistent with the neglect of thermal conductivity, so that neither a temperature nor a temperature gradient may be specified at a wall. This leaves only the primary kinematic condition that the normal component of velocity at a solid wall must equal the velocity of the wall. In the I.C. engine problem, this value is zero on all interior walls except the piston.

This condition is applied computationally as follows. The MacCormack algorithm is applied at wall points just as at interior points, except that one-sided differencing in the same direction must be used for both predictor and corrector steps. In general, the normal component of velocity will not be computed as zero, and so prior to each predictor or corrector step, it is reset to zero.

The application of this condition alone is sufficient in all cases the author has encountered to at least yield a solution. However, there are refinements available that will improve the solution. One in particular is obtained by noting that resetting the kinematic condition on the normal component of velocity at a wall does nothing to correct the slightly erroneous values of pressure and temperature which were computed consistent with the erroneous value of wall velocity. An excellent scheme for correcting this situation in supersonic flow calculations is Abbett's simple-wave corrector [48]. In this approach, the angle of the velocity vector at a wall is first computed after application of the numerical algorithm for one step. The Prandtl-Meyer formula is then used to compute a weak compression or expansion wave of the appropriate strength to turn the flow back toward the wall through the known angle. The strength of this wave is the pressure correction, and the isentropic formula may be applied to give the corresponding temperature correction.

A scheme similar in concept that is useful for subsonic flows is obtained by assuming that the normal component of fluid flow at a wall is locally one-dimensional. The results of unsteady one-dimensional characteristic theory [44,49] may then be applied to compute the temperature that would have to exist at a wall if the fluid were to be reduced to a stagnant (one-dimensionally) gas. The pressure is then obtained from

the isentropic relation. The working formulae are:

$$T_{wall} = (T^{1/2} \pm \frac{\gamma-1}{2} u)^2 \qquad (5\text{-}1)$$

$$p_{wall} = p \left(\frac{T_{wall}}{T}\right)^{\frac{\gamma}{\gamma-1}} \qquad (5\text{-}2)$$

The positive sign applies if the wall is reached by a right-running characteristic, the negative sign for a left-running wave. Physically this corresponds to saying that if the normal velocity is positive and headed toward a wall, then as the one-dimensional flow is brought to stagnation conditions, the temperature must increase, and vice-versa for the opposite case.

It is interesting to note that, in theory, only one condition may be obtained by applying a characteristics scheme at a wall, since only one wave from the "flowfield", which is actually a wall point, can reach the "wall". Equation (1) shows this clearly. To obtain the pressure, additional information in the form of equation (2) must be introduced. This in theory overspecifies the fluid properties at the wall. An inconsistency is avoided because the additional information (isentropy) is in fact implied by the original inviscid system of equations, hence information obtained from it is not really inconsistent with the original system.

Figure 23 shows the results of applying the wave-reflection scheme outlined above when resetting the wall boundary values. Clearly, the solution is smoother and less oscillatory when the method is used. These results are obtained with the non-conservation forms of the governing equations; the conservation-form algorithm consistently gave poor results if anything other than the simple kinematic boundary condition

was employed. No explanation for this suggests itself at the present time.

5.2.2 Valve boundary conditions

The valve boundary conditions are less susceptible to the kind of analytical treatment above than the wall boundary conditions. Neither the mathematical or physical aspects of the problem are sufficiently well understood to allow a rigorous formulation of conditions for numerical analysis. It is clear that the constant pressure and temperature conditions of the viscous analyses are unacceptable; for one thing, they bear no relation to the isentropic relation which must hold for the inviscid flows under discussion here. All attempts to use such a condition, including variations where the constant-property point is placed outside the chamber and the valve points are treated as regular interior points which "feel" the constant-property point on the backward-difference step, have failed.

Diwakar [21] formulated the first workable valve boundary condition for inviscid flow during the course of adapting an existing viscous flow program to the 2-D inviscid case. Diwakar noted that the isentopic condition

$$p_{valve} = p_{ambient} \left(\frac{T_{valve}}{T_{ambient}}\right)^{\frac{\gamma}{\gamma-1}} \qquad (5\text{-}3)$$

must apply, no matter what else is done. If one then assumes that the intake flow is one-dimensional and steady, conservation of total enthalpy requires

$$\left(h + \frac{w^2}{2}\right)_{valve} = H_{valve} = H_{ambient}$$

or

$$T_{valve} = T_{ambient} - \frac{\gamma-1}{2} w^2_{valve} \qquad (5\text{-}4)$$

The procedure then consists of assuming the velocity as obtained from the algorithm is acceptable, applying equations (4) and (3) in succession, and setting the transverse components of velocity at the valve to zero. This is done for both predictor and corrector on each time step, and seems to work quite well. Success seems to be tied strongly to the requirement that the time derivatives which are neglected in obtaining equation (4) are actually small. That is, the full unsteady quasi-one-dimensional energy equation may be written

$$\frac{\partial H}{\partial t} = -w \frac{\partial H}{\partial z} + \frac{1}{\rho} \frac{\partial p}{\partial t}$$

where $H = h + \frac{w^2}{2}$ is the total enthalpy. The integrated result of equation (4) is obtained when all the unsteady terms are small, producing a quasi-steady flow. If the computed flow at the valve is at each time level essentially quasi-steady, Diwakar's technique works well. Note that when an insufficient number of points are used to specify a valve the internal pressure drops very rapidly on the intake stroke, the quasi-steady flow assumption is violated, and the calculation blows up. Reference [4] contains some excellent examples of this type of behavior.

The one-dimensional assumption by itself seems quite good. Allowing the tangential velocity components to float invariably produces poorer results than when they are fixed. Note that it would not be necessary to fix them to zero if inflow (still one-dimensional) at some angle were desired.

The treatment of flow at the exhaust valve follows a slightly different line of reasoning. Here the fluid is exhausting against the external back pressure of ambient conditions, rather than being drawn in from a constant-property reservior of infinite extent. It is important to note that unlike the pressure, the temperature at the valve should not be set to the ambient value, because after the heat release on the power stroke the internal fluid will be on a different isentrope than the external fluid. Equation (4) is thus inapplicable. The only scheme that makes physical sense is to specify constant pressure (ambient) at the valve, and then use equation (3) to solve for the temperature.

These conditions for intake and exhaust valve specifications seem to work well, and were used for most of the results given in this chapter. However, refinement is possible at the price of a slight increase in computer time and a modest increase in the level of complexity of the program. That is, one may view the intake flow more realistically as the endpoint of a ducted flow from the open air, rather than as just a boundary point of the internal flowfield. To implement such a model, the flow in the duct can be described by the quasi-one-dimensional inviscid flow equations of section 2.6. The setup is then as shown in Figure 24, with the large open end of the duct held at reservoir conditions. The valve point or points are then regular interior points of the engine flowfield calculation. The duct point closest to the valve is used by the engine calculation on the backward difference step; the valve point (or the average of the properties at all the valve points) is used on the forward difference step of the duct computation. The details involved in a one-dimensional calculation of this type are thoroughly covered in Reference [52].

Some experiments were run with the geometry of Figure 24 to compare the results of the scheme to the more usual method of this work. Such a comparison is given in Figure 25, where the pressure distribution at an early time (about ten percent of the total time required to reach a steady state) is given for a stationary-piston inflow case. The initial pressure and temperature were p = .8, T = .9382346. The data shown in Figure 25 was taken down the line of constant x and y, with varying z, from the valve to the piston. At this instant a travelling wave is in progress from the valve to the piston. Note that there is a significant difference in the two results, with smoother results and a smaller difference between the extremes for the ducted case. This and similar results obtained for intake flows with the engine turned on seem to indicate that use of the ducted intake provides a smoother, qualitatively more desirable result.

The problems, if any, associated with using a similar technique at the exhaust valve have not been investigated. This represents a worthwhile direction for future work.

5.3 Preliminary results for three-dimensional inviscid flows

It quickly became clear that there were more problems associated with obtaining even very simple three-dimensional results than had been the case for 2-D work. The primary test case was the same as has been repeatedly described; the engine was turned off (stationary piston) and a pressure and temperature differential established between the inside and outside of the chamber as an initial condition, with the intake valve open. Eventual equilibration to a steady state with a uniform pressure and temperature inside and out and all velocities of order 10^{-3} or smaller is expected, and occurs within roughly five hundred to a thousand time

steps in the usual 2-D computation. Such was not the case for the corresponding 3-D problem. A true steady state could not be reached.

The observed behavior was common to all test cases run. After approximately five hundred time steps, approximate equilibration would occur (pressure and temperature nearly unity everywhere, all velocities small) and then at this time, when the desired steady state had virtually been achieved, the calculation would diverge. The velocities in certain specific locations near the bottom of the cylinder would grow large, pressure and temperature would drop to an unrealistic level, and in general it became apparent that an equilibrated result would not be obtained.

Since the behavior of the three-dimensional algorithms was the same in both cartesian and cylindrical coordinates, coordinate singularity problems in the cylindrical system were ruled out as a possible cause of difficulty. There followed a long series of experiments with the rectangular engine model aimed at defining the cause of the behavior described above. In summary, it was found that a wide variety of alternate boundary condition formulations, both at the valve and the walls, did nothing to change the basic pattern. The same was true when the conservation forms of the equations were used instead of the usual non-conservation forms. Changing the size of the valve did not, within reasonable limits, affect the behavior, and even an exceptionally large valve would only blow up the calculation in a different fasion. An exceptionally small valve would cause the problem to appear in an exceptionally short time, but the same problem occurred.

A series of checks was devised to eliminate program errors as a possible cause of trouble. A two-dimensional program was obtained from

the existing three-dimensional version by not computing spatial derivatives in the y-direction and by eliminating the y-momentum equation. There could thus be no computed change in any quantity in the y-direction, so the calculation was confined to the valve plane. When this was done, the results agreed exactly with the previously obtained two-dimensional results of Diwakar [21]. The same thing was done in another way by dummying out the x-direction. Again the results were good. The test case described can be made two-dimensional by extending the valve width until it is a slit occupying all y-points at some constant x-value. When this was done, the results were again perfect. A further indication of program correctness was provided by the fact that until the calculation diverged, the computed temperatures and pressures agreed with the isentropic law to within one or two percent.

The results above seemed to indicate that the problem was of a more fundamental nature, so at this point the three-dimensional Navier-Stokes calculation of Chapter 4 was programmed. It was hoped that at least one truly three-dimensional problem could be found that could be solved adequately. Also, the 3-D viscous program was built up from the existing inviscid code by altering the wall and valve boundary conditions and adding the appropriate viscous terms to the governing equations. The correcting functioning of the resulting program was another indication that the difficulty did not lie in the original programming.

The success of the viscous code for a case where the inviscid algorithm had failed provided the clue that led to eventual resolution of the problem. The only difference that could be seen between the two cases was that the inviscid flow test did not have the damping of the Navier-Stokes solutions. This suggested that possibly the inviscid flow

equations for this three-dimensional problem required the addition of an artificial viscosity term to be stable. An opportunity was found to discuss the results outlined with R. W. MacCormack of NASA - Ames Research Center [53]. MacCormack claimed to have seen situations similar to that described above which had been shown to be due to the sign of the truncation error terms which produce the artificial viscosity that is implicit in the method. The situation is apparently analogous to that found in the behavior of the simple harmonic oscillator equation,

$$\frac{d^2\Phi}{dt^2} + \omega^2 \Phi = 0$$

where if the term ω^2 is positive, both solutions will be oscillatory, while if ω^2 is negative, one solution will be exponentially damped and the other will grow without bound. According to MacCormack, the remedy for this type of behavior is to add a term to the right-hand sides of the governing equations (component form) that is of the same order as the truncation error terms (thus leaving the overall accuracy of the method of the same order as before) but chosen so as to ensure that it would produce the correct net sign in these terms.

A form similar to that given by Lapidus [54] was suggested, and is given here for both cartesian and cylindrical systems:

$$\text{artificial viscosity} = c \left[\left|\frac{\partial u}{\partial x}\right| \frac{\partial^2 U_i}{\partial x^2} (\Delta x)^2 + \left|\frac{\partial v}{\partial y}\right| \frac{\partial^2 U_i}{\partial y^2} (\Delta y)^2 + \left|\frac{\partial w}{\partial z}\right| \frac{\partial^2 U_i}{\partial z^2} (\Delta z)^2 \right] \qquad (5\text{-}5a)$$

$$\text{artificial viscosity} = c\left[\left|\frac{\partial u}{\partial r}\right|\left(\frac{\partial^2 U_i}{\partial r^2}+\frac{1}{r}\frac{\partial U_i}{\partial r}\right)(\Delta r)^2+\right.$$

$$\left.\frac{1}{r}\left|\frac{\partial v}{\partial \phi}\right|\frac{\partial^2 U_i}{\partial \phi^2}(\Delta\phi)^2+\left|\frac{\partial w}{\partial z}\right|\frac{\partial^2 U_i}{\partial z^2}(\Delta z)^2\right] \qquad (5\text{-}5b)$$

where "c" is a positive constant of order (1/4) and U_i is used to indicate the i^{th} component of the U-vector being used. Thus, for the non-conservation forms of equations (2-27 to 2-31, the U-vector is

$$U = \begin{pmatrix} u \\ v \\ w \\ p \\ T \end{pmatrix}$$

and similarly for any other choice of dependent variables from Chapter 3.

The implementation of MacCormack's suggestion provided immediate success where other attempts had failed. Computations for a series of inflow cases with the rectangular engine were obtained in an attempt to determine the minimum acceptable damping coefficient; a value of .2 was settled upon.

Following the determination of the damping coefficient, a complete four-stroke rectangular engine test was run, with the combustion effect once again simulated by constant-volume heat addition at the top of the compression stroke. This is done more to stress the algorithm and observe the behavior than in any expectation that the results of doing so have any real relation to combustion phenomena. The rectangular engine test case provided a benchmark result, and proved useful in later comparisons with the corresponding cylindrical engine test, which was the primary case of interest. The test was run at 3000 RPM to facilitate comparison

with the majority of results obtained by Diwakar [4,21]. At this speed, the valve layout of Figure 19 was required to allow the engine to breathe properly on the intake stroke. This is not upsetting; the valves as shown in Figure 19 are of realistic size.

An attempt was made to duplicate the solutions of the above test case using the governing systems of equations expressed in the cartesian coordinate conservation form developed in Section 2.3.1. It was expected that such a solution would provide experience with the conservation forms that would be useful after switching to the cylindrical coordinate version. It was in that context that solutions of the equations in conservation form were expected to be most useful.

The simple inflow cases described above for the inviscid, non-conservation forms of the governing equations were reproduced without incident using equations (2-52 to 2-56), except that as mentioned above, the wall boundary condition scheme using the wave-reflection method was found to be inapplicable. Solution of the full-scale 3000 RPM engine test could not be obtained. The calculation blew up during the middle of the power stroke, but percursors to this behavior were apparent well beforehand, as indicated by Figure 26, which shows temperature distributions at approximately the same crank angle for the cartesian conservation formulation and the analogous non-conservation formulation. It is seen that oscillations develop in the conservation form results. These oscillations eventually grow to sufficient magnitude to cause the computation of negative temperatures. The author attributes this behavior to the same troubles (it is not known what they are) that arose when the wave-reflection boundary conditions were introduced into the conservation forms. As stated in Chapter 2, the results given here are not intended as a general

indictment of the use of the conservation form of the governing equations, or even their application to the present problem. It is most definitely true that the process of obtaining useful solutions in computational fluid dynamics calculations depends in a substantial measure upon the reservoir of experience that each investigator accumulates. This author has obtained most of his experience with the non-conservation forms. It may well be true that another investigator would be more familiar with the appropriate techniques for use with the conservation equations, and so would obtain better results. All that can be done here is to report the computational algorithms used and present the results obtained.

As a final note on this topic, it may be significant that the damping factor required to obtain useful solutions on even the simple inflow cases was fifty percent higher when using the conservation forms than when using the non-conservation forms. That is, roughly the same degree of quality in the results was obtained with a damping factor of .2 in the latter case as was obtained with a damping factor of .3 in the former case.

5.4 The centerline problem in cylindrical coordinates

When it was felt that the general problems which had previously affected the inviscid flow solutions in three dimensions were understood and corrected, attention was focused upon the engine model of greatest interest, the cylindrical model of Figures 21 and 22. There are some disadvantages to working in this system. Figure 22 indicates one obvious flaw; there is a bunching of coordinate points near the centerline and a lack of them near the walls in each plane of constant z. Since there is no a priori reason to expect more fluid dynamic action near the center, the extra points are not particularly helpful, and they penalize the

calculation by reducing the time step allowed by the CFL criterion of equation (3-6). Also, the valve shape allowed in a cylindrical coordinate model is possibly even more unrealistic than that for a rectangular engine model, although that may be debatable, since neither can be considered representative of the true geometry. However, it was felt that these disadvantages were balanced by the advantage of being able to correctly model the outer wall shape, thus eliminating the unrealistic corners and stagnation regions not present in the physical problem but a necessary part of a solution obtained with a rectangular model.

As stated in the preliminary remarks in this chapter, it was felt that the main difficulty would be due to the indeterminacy of the azimuthal angle at r = 0 in cylindrical coordinates, and the consequent multivalued nature of the flowfield representation in these coordinates at that point. It is to be emphasized that the flowfield is in no way special along the particular line specified by r = 0. It is simply the representation in a particular coordinate system that causes difficulty. This point is worth illustrating in more detail. Consider the example of Figure 27, which depicts the flow of a uniform stream in the +x direction. In this system, the expression defining the flow is the same for any arbitrary field point that may be chosen. It is

$$\underline{V} = U\,\hat{i}$$

for a stream of speed U. The same stream at the same field point in cylindrical coordinates has the representation

$$\underline{V} = \hat{r}\,U\cos\phi - \hat{\phi}\,U\sin\phi = u(r,\phi)\,\hat{r} + v(r,\phi)\,\hat{\phi}$$

which is clearly a function of the azimuthal coordinate ϕ. This particular flowfield will possess constant properties along any radial line

from the origin, but at the origin where the radial lines converge, the flowfield representation in cylindrical coordinates is necessarily multivalued. Another way to view the problem is that the unit vectors, $\hat{r}$ and $\hat{\phi}$, are themselves functions of the location of the field point, and it is in terms of the unit vectors that the individual velocity components u and v are defined.

The result of this behavior is that in a general cylindrical coordinate problem, one cannot obtain solutions along the singular line represented by the z-axis without developing a special procedure. Even if one does not consider the problem in the terms outlined above, equations (2-36 to 2-40) make it clear that r = 0 is a singular point, because of the (1/r) terms present. When the problem of interest is axisymmetric, so that the ϕ-derivatives are identically zero, the classical technique for either analytical or numerical work is to apply L'Hospital's rule as in section 2.5 to obtain a set of equations valid at the centerline. The case of interest here is not axisymmetric due to the influence of the valves, and so the full equations (2-36 to 2-40) must be used. If L'Hospital's rule is applied, equations (2-91 to 2-95) result, and it is not immediately clear what the limits in these equations should be. The entire problem becomes sufficiently annoying for Roache [50] to state that a convenient method for numerically handling the problem when values on the centerline are required has not yet been found. Roache suggests using an outer ring in cylindrical coordinates, a central region in cartesian coordinates, and an interpolation scheme to patch the two. Roache labels this approach as "clumsy".

The fact that the flowfield is physically well-behaved at r = 0 suggests that a technique be developed to communicate the necessary

information on conditions at the centerline to the numerical scheme for use on the backward difference step. It was on the problem of how best to do this that possibly the majority of effort on this project was expended. All of the approaches tried will be briefly mentioned in the hope that their lack of merit can save some future investigator the effort of trying them.

5.4.1 Averaging techniques at the centerline

The most obvious approach to specifying the flowfield values at $r = 0$ is to conjecture that conditions are represented by an average of those on the ring at $r = \Delta r$, the first ring at which normal computations may be performed. That is straightforward for pressure, temperature, and z-velocity (since its unit vector is independent of the location of the field point), but more thought is required to properly average the u and v components of velocity. The u and v components, corresponding to the radial and azimuthal velocity, do not in general lie in the same direction at any two field points. To average them, they must be converted into components in some reference system where they do have a common direction. It is convenient to use the cartesian coordinates to which the cylindrical system is conventionally referred to accomplish this. In the case of the cylindrical engine model used here, reference to Figure 21 will show that this forces the x-axis to be the symmetry plane. Since there can be no mass flow normal to this plane, it is necessary only to average those parts of the u and v components in cylindrical coordinates that contribute to flow along the x-axis in cartesian coordinates. Referring again to Figure 27, it is seen that

$$U = u(r,\phi,z) \cos \phi - v(r,\phi,z) \sin \phi \qquad (5\text{-}6)$$

gives the contribution to the x-directed flow from the velocity vector at any field point in a cylindrical system. Equation (6) is then used to obtain the contribution at each value of ϕ on the ring at $r = \Delta r$. These values are then averaged to obtain (in this approximate method) the representative flow velocity at the centerline. Letting this value be denoted by U_{avg}, the velocity representation in cylindrical coordinates along any line of constant ϕ and displaced slightly from the origin will appear to be

$$\lim_{r \to 0} u(\phi,z) = U_{avg}(z) \cos \phi \qquad (5\text{-}7)$$

$$\lim_{r \to 0} v(\phi,z) = -U_{avg}(z) \sin \phi \qquad (5\text{-}8)$$

It is emphasized that this is the form that u and v must have as r goes to zero; the only approximation lies in the determination of the value of U_{avg}, and of the w, p, and T averages as well. But if the flow velocity is to lie along the x-axis, as it must, then as seen from various angles around the point r = 0, the component velocities in cylindrical coordinates must be of the form given in equations (7) and (8).

This discussion has been somewhat protracted because it will be found necessary to return to this line of thinking later. For now it will suffice to note that no way was found in which such an averaging scheme could be made to work. Averaging of the simple variables (u,v, w,p,T) was attempted as outlined above. Mass averaging of the relevant variables was also tried, and both of these approaches were tried in a technique that involved taking the average values over the two adjacent

z-planes above and below the one where computation was being performed. The behavior of solutions for simple inflow cases as described several times previously was about the same in all such trials. The solutions would not blow up, but neither would they stabilize. Values at the centerline and on neighboring rings would oscillate in time, a clear indication that poor values of time derivatives (which of course depend on the poor values of spatial derivatives obtained) were being computed near the centerline and hence ruining the results obtained from the Taylor series applied to advance the flowfield values in time.

5.4.2 Other formulations of the governing equations

Because of the failures recounted above, the use of some of the other equivalent systems of governing equations discussed in Chapter 2 seemed to present the best hope for obtaining a solution. The cylindrical conservation form in particular appears to be perfect, because the U-vector,

$$U = r \begin{pmatrix} \rho \\ \rho u \\ \rho v \\ \rho w \\ \rho e_t \end{pmatrix}$$

is mathematically well-defined everywhere in the flowfield. This may be the case, but when one attempts to use equations (2-57 to 2-61) in a calculation such as that attempted here, the same behavior as for the averaging scheme in the non-conservation variables was observed. That is, the solutions oscillated badly in time and would not settle down, even for simple inflow cases.

The special non-conservation form of the governing equations that was derived in section 2.4 has the same property for its U-vector

$$U = r \begin{pmatrix} u \\ v \\ w \\ p \\ T \end{pmatrix}$$

as does that for the conservation equations; it therefore comes as no surprise to find that the solutions obtained with the dependent variable formulation of section 2.4 evidenced the same poor behavior as in the previous cases described.

The question of programming error is always important when no algorithm appears to be successful. To help demonstrate that the codes implementing the ideas described above were at least doing what they were intended to do, a series of checks was run for each program, in which the centerline treatment was altered to that for a wall boundary condition; i.e., a rigid bar of diameter $2\Delta r$ was inserted down the centerline of the cylinder. In all cases, the inflow tests carried out for this trial geometry produced results every bit as good as for the cartesian coordinate inflow cases. This seemed to absolve every portion of the program except that responsible for specifying conditions at the centerline.

It is interesting to note that if a large enough damping factor (.8) is used in the approaches described above, the large time-wise oscillations decrease to a relatively acceptable amplitude.

The author's explanation for the behavior of the above two special systems is simply that even though the particular formulations may yield mathematically acceptable values on the centerline, the real physical flow depends on such factors as pressure and temperature gradients, which cannot be adequately evaluated at $r = \Delta r$ unless values of the

primary variables can be found at r = 0. Very simply, no information can be communicated through the center region of width $2\Delta r$, because the dependent variables used in the systems described reduce all such information to the same value, zero. Yet proper description of the flowfield requires such information to be available. There seems to be an impasse.

5.4.3 Transformation of derivatives

There is another possible approach that allows one to ignore the question of what the actual values of the flowfield variables are on the centerline. Note that what is actually required is an expression for the backward difference in the r-direction for all points on the ring $r = \Delta r$ (see Figure 22), so that the corrector step may be correctly performed. Professor Everett Jones suggested obtaining this derivative through the transformation

$$\frac{\partial}{\partial r} = \frac{\partial x}{\partial r}\frac{\partial}{\partial x} + \frac{\partial y}{\partial r}\frac{\partial}{\partial y}$$

and since

$$x = r \cos \phi$$

$$y = r \sin \phi$$

the required derivatives $\frac{\partial x}{\partial r}$ and $\frac{\partial y}{\partial r}$ may be computed. Reference to Figure 22 will show that on the ring at $r = \Delta r$, there is always a point in the image field that allows the necessary backward y-difference to be obtained. Also, for $\phi < \frac{\pi}{2}$ there is a point in the range $\phi > \frac{\pi}{2}$ that allows the x-difference to be computed, and vice versa. The accuracy on these difference computations will not be exactly the same as for the overall scheme, but one would not expect it to be prohibitively poor. This is therefore a scheme that really should work; it does not. The author has no explanation.

5.4.4 The numerical use of L'Hospital's rule

Having outlined the approaches that failed, it is now appropriate to describe the one that succeeded. The application of L'Hospital's rule to the complete set of governing equations to obtain a set valid in the limit r = 0 has been given in section 2.5, with the result being equations (2-91 to 2-95). Considerable time was spent attempting to evaluate rigorously the limits found in those equations; i.e., attempting to show whether or not a term like $\frac{\partial^2 p}{\partial r \partial \phi}$ should be zero at the origin in the general case, and if not, then what? It was felt that this had to be done before a valid use of equations (2-91 to 2-95) could be made. Finally, since no argument could be constructed to show what the limits were, the following rationale was adopted:

1. There probably are no specific limits that should occur; the terms required will probably be both time and azimuth dependent.
2. It is not necessary to know <u>a priori</u> what the limiting terms in the L'Hospital equations should be. That is, there is no way in a finite difference solution to obtain any information about any quantity more accurately than is inherent in the grid resolution that is initially chosen. All derivatives are in fact expressions that result from taking a limit; this does not prevent the use of finite differences in approximating such limits for the purposes of obtaining a numerical solution. Therefore, such terms as $\lim_{r=0} \frac{\partial^2 p}{\partial r \partial \phi}$ can be appropriately treated by using the best finite difference that is available for them. As far as an accurate computation of such limits is concerned, the best that can be done is to resolve them to the limit of the grid spacing.

The argument advanced above is similar to that for the situation at a symmetry plane. One knows the values in the image region behind the plane of symmetry, hence finite differences in either the backward or forward direction may be constructed for the derivatives with respect to the normal coordinate. But as discussed in the previous sections on boundary conditions, one has the option of applying the knowledge that all quantities except the normal component of velocity are even functions with respect to the coordinate normal to the symmetry plane. Therefore, first derivatives of all such quantities on the symmetry plane are identically zero. This information comes from outside the finite-difference scheme, and may be used or not, as desired. It is felt that the process of obtaining the limits in the L'Hospital equations is analogous to the above case. The difference is that the option of applying analytical information does not exist; one is constrained to stay within the bounds of the finite-difference scheme.

It will be noted that the correct use of L'Hospital's rule depends on the existence of an indeterminate form, i.e., (0/0). It has not been established here that the governing equations (2-36 to 2-40) are actually indeterminate at the centerline. That is, the denominators of several terms approach zero as r does, but the numerators have not been considered. However, it must be true that the time derivatives on the left-hand sides remain finite at any point in the flowfield. If there is a solution for which this is not true, it is to be rejected anyway. Therefore, the numerators of the right-hand sides must approach zero at the centerline in a manner which generates an indeterminate form.

The above arguments merely allow a set of equations to be developed that would seem not to be inconsistent with the finite-difference

approximations inherent in the overall scheme. There is another fundamental objection to the use of L'Hospital's rule in situations where the ϕ-derivatives are not zero. If they are not zero, then at the centerline computations are being done at neighboring points in ϕ-space which are actually the same point in physical space, since $r = 0$. It would thus seem that equation (3-6) for the time step allowed by the CFL condition would mandate a limiting time step of zero, thus preventing the calculation from being advanced in time.

A further problem is that the region $r < 0$ does not exist, thus only forward differences can be used in the radial direction at the centerline. This will be shown to cause some difficulty which was eliminated by applying the one-sided second-order difference of equation (3-11).

Despite the above suspicions about limitations caused by the CFL criterion, it was decided to implement the L'Hospital equations for use on the centerline in the algorithm for the non-conservation form of the equations. It was felt that the centerline might be special in some way not anticipated that would invalidate the apparent time step limitation. It simply did not "feel right" that the equations should have such an artificial limitation imposed upon them. When programmed, the algorithm immediately gave excellent results on the inflow test cases, and so the next step was to attempt the full four-stroke engine calculation for the same speed (3000 RPM) as previously. This went well; results will be discussed in the following section. For now, since the scheme worked, it is appropriate to furnish some details of implementation that otherwise would be omitted.

The computations for the "ring" at r = 0 are handled much the same as those at any other place in the flowfield, with the exception that different governing equations are used after the spatial derivatives are obtained, and a few extra spatial cross-derivative terms are required. The method for obtaining the corresponding finite differences for such cross terms has been given in Chapter 3 and need not be repeated here. The values on the "ring" are physically stored in the same array as the U-vector for other locations, and prior to spatial differencing, a few conditions are imposed based on the physics of the flow at the center-line. First, it is important to recognize that the multivalued nature of the flowfield does not extend to the pressure, temperature, and z-component of velocity. Therefore, prior to each predictor or corrector step, these values are averaged on the "ring" that is stored for all values of ϕ at r = 0, and the entire ring then reset to the average value. Second, the true velocity vector through any point can have only one direction, and as discussed in section 5.4.1, this direction lies along the x-axis for the geometrical situation of this case, where the x-axis (lines of $\phi = 0$ and $\phi = \pi$) is in a plane of symmetry. Thus equations (7) and (8) above must hold exactly for the velocity distribution on the "ring" at r = 0. The only quantity left to be determined is the value of U_{avg}. Several sensible methods could be considered, but the only one used in this work was to simply take the average of all the x-resultants of velocity on the "ring" using equation (6) for each term in the average. It is felt that this is sufficiently accurate since the resetting process is performed before each predictor or corrector step. In a perfect computation, the average would not be needed; analysis of any one component on the ring would yield the value of U_{avg}. This

computation is not perfect, but it is not believed that the imperfections justify higher-order averaging techniques involving inward extrapolation along radial lines, etc.

This completes the special procedures involved in the handling of the values at the centerline. Note that the use of the method, while made more convenient by the presence of a plane of symmetry, is not restricted to cases where one exists. Even if the flow as a whole has no plane of symmetry, it is still true that the velocity "field" at the centerline must have the form of equations (7) and (8), with the exception that "ϕ" must be changed to "$\phi - \phi_o$", where ϕ_o denotes the angle (relative to the x-axis) of the line along which the velocity vector lies. This line is a line of symmetry for the "ring" at r = 0, and different z-planes will have different values of ϕ_o. The value of ϕ_o may be determined through the use of an equation giving the resultant velocity in the y-direction, as equation (6) yielded the x-resultant. The equation is

$$V = u(r,\phi,z) \sin \phi + v(r,\phi,z) \cos \phi \qquad (5\text{-}9)$$

which, as with equation (6), can be obtained from consideration of Figure 27. Recall that all velocity components must be zero along the line normal to the symmetry line. In general, the y-axis will not be such a line, and the value of y-directed velocity from equation (9) will therefore not be zero. The velocity vector is then along a line at some angle in the x-y plane. The angle along which it will lie follows from joint use of equations (6) and (9), from which

$$\phi_o = \tan^{-1} (V/U) \qquad (5\text{-}10)$$

Equation (10) is valid for each choice of ϕ giving values of U and V from equations (6) and (9). It would probably be best to average the result obtained from the entire "ring" at r = 0.

5.5 Results for the 3000 RPM cylindrical engine test

The complete four-stroke calculation requires the solution of whatever governing equations are used at approximately 16000 time steps and hence produces a tremendous volume of data. Most of this data can never be adequately reduced, so that results given here are either general remarks obtainable by merely scanning the data by eye, or remarks which address specific points to be made from plotted results. One example of a useful general remark is that pressures and temperatures are spatially constant to better than three significant digits on the compression stroke.

Figures 28-31 illustrate pressure and temperature behavior near the bottom of the intake stroke ($Z_p = 8.6$, with $1 < Z_p < 9$), both in the valve plane and normal to it, for the rectangular and cylindrical engine models. All are in the same z-plane ($z = 4\Delta z$). Figures 28 and 29 give pressure and temperature distributions for the cylindrical engine along three lines, defined by $\phi = 0$, $\phi = \pi/2$, and $\phi = \pi$. These results show immediately that even on the intake stroke, where 3-D effects are expected to be of greatest significance, the deviation from a purely axisymmetric distribution of results is minimal, not exceeding two percent in the worst case. Figure 30 shows the distribution of pressure and temperature in the valve plane (at $z = 4\Delta z$) for the rectangular engine. These results are in excellent qualitative agreement with the valve plane results for the cylindrical case, even though differing slightly

in overall level for the same crank angle. This is due to the difficulty of specifying valve areas which agree when dealing with two different shapes. Figure 31 displays pressure and temperature in the direction normal to the valve plane at two locations ($x = 2\Delta x$ and $x = 6\Delta x$) on the x-axis. Here the qualitative agreement with results from the cylindrical engine is not as good; there are slight standing waves which seem to be quite typical of intake pressure and temperature behavior normal to the valve plane, even for cases where the piston is stationary. Such behavior is not found in the cylindrical engine, which is to be expected, since waves cannot "stand" the same way for the two geometries. Whether such differences are important to account for in an engine model is a matter that cannot be answered by the present work.

Figure 32 is a velocity-vector plot, in the valve plane, for the cylindrical engine and is obtained for the same piston position on the intake stroke as the pressure and temperature plots discussed above. Some caution in interpreting the plot is necessary; the radial scale is stretched relative to the vertical scale in order to physically have room on the paper to produce the plot. The angles are not distorted by the stretching. The magnitudes are scaled so that the largest velocity found at that time receives a value of unity; any non-zero velocity smaller than .2 units is arbitrarily set to that value, since anything smaller is smaller than an arrowhead. In spite of these limitations, this plot and similar ones to follow provide a very vivid picture of the flow pattern in a way that other, more accurate data, cannot do. It should be noted that the pattern shown in Figure 32 is in excellent agreement with the two-dimensional results of Diwakar [4,21]. This is

a hoped-for result, and one which there is some reason to expect, since there can be no out-of-plane velocity component in the valve (symmetry) plane.

Figures 33-35 illustrate similar velocity-vector data taken at the top of the compression stroke, just before the heat addition which provided the simulated combustion. The data are from the cylindrical engine model and in three different planes; Figure 33 in the valve plane ($\Phi = \pi$ and $\phi = 0$), Figure 34 in the plane defined by $\phi = \pi/2$, normal to the valve plane, and Figure 35 in a plane of constant $z = 5\Delta z$. The data were taken at the top of the compression stroke to provide an indication of the type of mixing pattern that would occur and would be significant for studying the real combustion processes. In Figures 33 and 34, the vectors are again plotted in a transformed plane, this time with both the radial and vertical coordinates stretched, and by different amounts. The reason is that at the top of the compression stroke, very little space remains between the piston and the top of the cylinder, and data plotted on such a scale would be meaningless. This explains why the velocity vectors are so flat throughout much of the field, and why the turning points are so sharp where they occur. Figure 34 shows some interesting results, revealing a sort of donut-shaped swirl that is set up by the initial intake flow and persists thereafter. The data are plotted to the same scale as that of Figure 33 (and Figure 35 also), and show that the magnitude of the swirl in the cross-flow plane is considerably smaller than the overall magnitudes that can be seen in the valve plane. This is again a result that helps to indicate that flowfield modeling in the valve plane is a realistic approach for a 2-D calculation. Figure 35 shows that there is also a swirl established in the polar planes,

which also would seem to be due to the initial intake flow. Again, it is not in general of the magnitude of the flow in the valve plane.

Figures 36 and 37 are indicator diagrams taken at corresponding spots in the rectangular and cylindrical engines, respectively, and are more in the spirit of the type of data that comes from I.C. engine experiments than most of the results shown in the figures discussed so far. The rectangular engine pressure vs. specific volume history closely follows the isentropic curve, except during the heat addition process. This is excellent assurance that the calculation is working as hoped, because the governing equations imply isentropic flow (except for the damping due to the artificial viscosity term, which is of the order of the truncation error and thus small).

Figure 37 contains a wealth of interesting information. First, note that this calculation also follows the isentropic curve until after the heat addition is complete. At this point, it rapidly moves away from the isentrope which was computed based on values at the start of the power stroke (solid line) and moves down onto another isentrope. This process is essentially complete by the time the piston has moved from $Z_p = 1.0$ to $Z_p = 2.0$ (again, the maximum is 9.0). From the numerical data, the value of the isentropic constant, pv^γ, is 62.27 at the top of the compression stroke after heat addition, drops to 44.02 at $Z_p = 2$, to 43.66 at $Z_p = 3$, and 43.65 at $Z_p = 9$. This indicates that the heat addition process has not gone as smoothly as in the case of the rectangular engine model, where to all intents and purposes the pressure and temperature were spatially constant at any time during either the compression or power strokes. The loss of total pressure in the cylindrical engine model is a reflection of the existence of strong spatial

gradients established immediately after the heat addition at the top of the compression stroke. These spatial gradients are sufficiently large to allow the normally small damping terms to generate a significant increase in entropy and to reduce the gradients.

The time variation is relatively smooth as shown in Figure 38, where pressure and temperature vs. crank angle are plotted for both the rectangular and cylindrical engine models. The crank angles plotted span the last 45 degrees of the compression stroke and the first 45 degrees of the power stroke, thus covering the heat addition phase for both models. Again, it is shown that the rectangular engine follows a very smooth curve. While the curve for the cylindrical engine is slightly rougher, it is not nearly as rough as would have been indicated by the total pressure loss taking place at this time. This indicates that the gradients which must exist to produce the entropy increase are in the form of standing waves, rather than travelling waves which would show up on a time-dependent plot.

A plot of these standing waves at TDC on the compression stroke (following heat addition and the subsequent build-up of the wave) is given in Figure 39. Note that the pressure wave is almost exactly axisymmetric. This is to be expected, since the valves are closed, all velocities are relatively small, and all pressures and temperatures were nearly constant throughout the cylinder prior to the heat addition. The pattern of Figure 39 is repeated almost exactly for each z-plane in the cylinder. It is clear that if a pattern such as this is established, the strong gradients in conjunction with the normally insignificant artificial viscosity term will produce a total pressure loss shown on the indicator diagram for the cylindrical engine. The question is then

whether the standing waves are purely a numerical phenomenon, or whether they have some basis in reality. It was felt that an outright error was ruled out by the fact that when not stressed by the transient process of constant-volume heat addition, the results follow the isentropic curve as shown on the indicator diagram.

It is interesting to note that the shape of the computed distribution of pressure vs. radial coordinate depicted in Figure 39 can be shown to be qualitatively correct, under a set of assumptions which seem applicable to the physical situation at this point in the calculation. To a high degree of accuracy, the problem is axisymmetric at this time, for the reasons mentioned above (small velocities, valves closed), as well as for the obvious reason that the pressure and temperature distributions as computed before and after heat addition are very nearly axisymmetric. If a source of small-amplitude pressure waves is assumed (for the purpose here it is of no concern whether they are of physical or numerical origin) then the pressure field due to the original source of the waves will obey the time-dependent wave equation.

$$\nabla^2 \Psi = \frac{1}{a^2} \frac{\partial^2 \Psi}{\partial t^2}$$

$$a = (\gamma RT)^{1/2} = \text{sound velocity}$$

$$\Psi = \Psi(r,z,t) = \text{acoustic pressure field}$$

which is valid as long as non-linear effects are not important. This would seem reasonable near the top of the compression stroke, where both piston and flow velocities are small (of order 10^{-3} or less).

Application of the separation of variables technique requires

$$\Psi(r,z,t) = R(r)\ Z(z)\ \phi(t)$$

This well-known procedure [56] produces sinusoidal solutions for the time variation, sinusoidal or exponential behavior for the z-dependence, and a solution for the radial equation of

$$R(r) = A\ J_o(kr) + B\ Y_o(kr)$$

where

J_o = zeroth-order Bessel function, 1st kind

Y_o = zeroth-order Bessel function, 2nd kind

k = separation constant

The assumption of axisymmetry leads to the requirement

$$\frac{dp(r)}{dr}\Big|_{r=0} = 0$$

which yields the result $B = 0$, since

$$Y_o'(kr) = -k\ Y_1(kr)$$

and $Y_1(kr)$ is infinite at the origin [55]. Therefore,

$$R(r) = A\ J_o(kr) \qquad (5\text{-}11)$$

There is no need to evaluate the constant A. The point is that the radial pressure distribution of Figure 39 looks as much like the zeroth-order Bessel function of 1st kind as is possible, considering that only eight points are available to define the functional form. This radial pressure distribution persists until non-linear effects from the damping term and the increased magnitude of the piston velocity invalidate the original assumptions and the standing wave dissipates.

It is emphasized that no claim is made that the process described above is the correct process for this situation. The gradients which must initially exist to establish such a physically realizable flow should not be present if the results of the rectangular engine calculation are a guide. What is claimed is that the pressure distribution being computed in response to some disturbance is correct, and that if the initial disturbance is eliminated, accurate solutions should result.

It was felt that the most likely source of an initial numerical instability that would serve to establish the pressure distribution of Figure 39 was the first-order accuracy in the radial differencing scheme used at the centerline. To check this conjecture, the one-sided, second-order differencing formula of equation (3-11) was implemented at the centerline for all radial differencing, and the calculation re-started at the point of heat addition on the compression stroke. No sign of the standing wave pattern of Figure 39 was found even when the calculation was run well past the original point of its appearance. The computed isentrope stayed on the original isentrope established after heating (upper solid line of Figure 37), instead of settling on an isentrope corresponding to a lower total pressure. These results would seem to establish both the cause of the trouble and a cure for it.

The requirement to use second-order differencing at the centerline in the radial direction does impose an additional burden on the I.C. engine calculations presented here, because experience has shown that use of the one-sided second-order first derivative of equation (3-11) too near a valve severely degrades the calculation. The relatively coarse resolution used in this work is undoubtedly the cause. The valve points are simply too far from the centerline to be allowed to

give information describing the shape of the flowfield at r = 0. The same problem was found when using the one-sided difference equation (3-11) at a wall near a valve in the rectangular engine, so this difficulty is by no means related to the use of cylindrical coordinates. In any case, use of the scheme seems to require an additional ring of points between the valve and the centerline so as to better separate them.

The use of a second-order one-sided differencing scheme in the radial direction at the centerline may not be the only workable approach. Dwyer and Sanders [24] in their work on unsteady combustion phenomena point out that a problem similar to that above exists when the MacCormack scheme is used with shock fitting. Spatial differencing at the shock is reduced to first-order accuracy at the shock because the shock is a discontinuity in the flowfield. Details for avoiding the problem are not given, but the authors refer to the work of Salas [57] for information on more sophisticated techniques. These may well be applicable to the present case.

The results for the exhaust stroke are not as interesting as much of the material discussed above; they were found to be slightly rougher than the intake stroke results, a result reported by Diwakar [4,21]. This is thought to be due to the boundary condition which fixes a constand pressure at the exhaust valve. This hypothesis should be examined in future work, particularly in terms of the feasibility of attaching a one-dimensional duct to the exhaust valve, as discussed previously.

One interesting point is that Diwakar reported difficulty with the valve boundary condition unless the amount of heating applied during the compression and power strokes was kept sufficiently low to avoid supersonic flow. No such problem was experienced with the current work.

Heating was deliberately applied at a level sufficient to result in a greater-than-critical pressure difference at the exhaust valve when it opened. The flow velocities near the valve temporarily exceeded Mach one, then settled down as equilibration was approached, but with no sign of difficulty. Possibly the artificial viscosity term in the present calculation produces this benefit; this should be checked by adding such a term to the 2-D calculation. The corresponding test of removing the damping from the 3-D code cannot be performed, because the computation will fail for other reasons. The test would therefore prove nothing.

Chapter 6

CONCLUSIONS AND RECOMMENDATIONS

The main goal of the research for this dissertation was to explore the purely fluid mechanical problems associated with developing realistic computational fluid dynamic solutions for the flowfield in an internal combustion engine. A wide range of topics was explored, including both viscous and inviscid flows, two- and three-dimensional engine models in both cylindrical and cartesian systems, the effects of different dependent-variable formulations of the governing equations, the importance of valve and wall boundary conditions and the effects of various approaches to their treatments, the problems associated with coordinate system singularities and the worth of various approaches for dealing with them, and actual four-stoke I.C. engine calculations for the models considered, with attendent comparisons of these results. One main conclusion is that there is a virtually endless amount of work remaining to be done in a variety of interesting directions. The author has reached certain opinions regarding those things which should follow immediately and those things which are perhaps not ready for further work as yet. These conclusions are:

1. The use of inviscid flow, full-scale models such as dealt with here and in Reference [4] provide good results in simulating many aspects of I.C. engine flowfields and combustion phenomena. Much useful work can be and should be done with these models before proceeding to the relatively much more ponderous viscous flow calculations.

2. The three-dimensional solutions developed here uniformly suggest that three dimensions are not really necessary for current work. That is, the rectangular models differ slightly from both 2-D models and cylindrical models, but the results obtained in the valve plane for each of these seem similar, both in terms of gross phenomena such as the overall velocity vector patterns and in terms of more detailed results such as pressure and temperature distributions. This seems to indicate that results obtained in the valve plane, while not able to represent the entire flowfield, are reasonably useful. Thus the flowfield normal to the valve plane does not seem to be strongly coupled to the flow in that plane. A more sophisticated fluid dynamic model may change this conclusion, and for that reason it is desirable to have available a three-dimensional algorithm that can be used to check such possibilities.
Similarly, the axisymmetric calculations obtained by many investigators for the compression and power strokes (or even all four strokes with a centrally placed valve) appear to be reasonably valid when compared with the 3-D cylindrical solutions developed here. They could possibly be made even more so, with little additional complexity, by using initial conditions which include the type of velocity swirls that are produced by the effect of the open valve on the intake stroke as shown here and in Reference [4].
3. A technique believed to be the first of its kind has been developed for the treatment of general three-dimensional flows

in cylindrical coordinates. It produces qualitatively excellent results for many cases and verifiably exact (as on portions of the indicator diagram of Figure 37 and for stationary-piston intake flows) results for others. Special treatment of radial differences appears necessary at the centerline, but the method as a whole has great promise as a useful technique in computational fluid dynamics, and without doubt provides a capability not known to the author through the use of any other available method.

4. The "clumsy" suggestion of Roache [50] to the effect that cylindrical problems which lack axisymmetry can be treated by using a cartesian grid in the center, a cylindrical coordinate grid at the boundaries, and an interpolation scheme to patch the two, should be tried. It is recognized that this represents a substantial effort, but if successful it would provide useful comparisons with results from the present approach. Roache's suggestion may also make more efficient use of computer time because in cylindrical coordinates there are too many points near the center and too few near the walls. This keeps the CFL criterion below the level available in cartesian coordinates with comparable numbers of grid points.

Appendix

A. Program Listing for Cylindrical Engine Model

```
1*      C   THREE-DIMENSIONAL INVISCID FLOW MODEL OF THE FLUID DYNAMICS OF
2*      C   AN INTERNAL COMBUSTION ENGINE.  THE COMPUTATIONAL METHOD IS AN
3*      C   EXPLICIT FINITE DIFFERENCE SCHEME FOLLOWING THAT OF MACCORMACK.
4*      C   THIS VERSION CONTAINS 2ND ORDER DAMPING TERMS FOR STABILITY.
5*      C   THE COMPUTATION IS IN CYLINDRICAL COORDINATES (R,PHI,Z) WITH THE
6*      C   DEPENDENT VARIABLE VECTOR (U, V, W, P, T) AND WITH THE GOVERNING
7*      C   EQUATIONS IN NON-CONSERVATION FORM.  L'HOSPITAL'S RULE IS USED TO
8*      C   OBTAIN A SEPARATE SET OF GOVERNING EQUATIONS THAT APPLY AT R = 0,
9*      C   WHICH IS REPRESENTED IN THE STORAGE ARRAY BY U(I,1,K,L,IG), WHERE
10*     C   I = 1, 5 IS (U,V,W,P,T) INDEX; K = PHI-INDEX; L = Z-INDEX, AND
11*     C   IG = PREDICTOR / CORRECTOR STEP INDEX.
12*     C
13*     C   PROGRAMMER-  M. D. GRIFFIN, DEPT. OF AEROSPACE ENGINEERING, U. OF MD.
14*     C
15*           LOGICAL  HEADNG, VFLAG
16*           DIMENSION  U(5,10,15,10,2), TDU(5,10,15,10), SPH(15), CPH(15)
17*           DIMENSION  DELTA(3), IREMRK(20), TD(5), Q(5), QDDEL(5)
18*           DIMENSION  DDR(5), DDP(5), DDZ(5), D2R(5), D2P(5), D2Z(5), D2RP(5)
19*           EQUIVALENCE  (DELTA(1), DELR), (DELTA(2), DELP), (DELTA(3), DELZ)
20*           EQUIVALENCE  (Q(1),UU), (Q(2),VV), (Q(3),WW), (Q(4),P), (Q(5),T)
21*           EQUIVALENCE  (DDR(1),DUDR), (DDR(2),DVDR), (DDR(3),DWDR),
22*          *             (DDR(4),DPDR), (DDR(5),DTDR)
23*           EQUIVALENCE  (DDP(1),DUDP), (DDP(2),DVDP), (DDP(3),DWDP),
24*          *             (DDP(4),DPDP), (DDP(5),DTDP)
25*           EQUIVALENCE  (DDZ(1),DUDZ), (DDZ(2),DVDZ), (DDZ(3),DWDZ),
26*          *             (DDZ(4),DPDZ), (DDZ(5),DTDZ)
27*           EQUIVALENCE  (QDDEL(1),QDELU), (QDDEL(2),QDELV), (QDDEL(3),QDELW),
28*          *             (QDDEL(4),QDELP), (QDDEL(5),QDELT)
29*           DATA  PI/3.14159265/, TWOPI/6.2831853/, RTD/57.2957795/
30*           DATA  PREF,TREF,RGAS,CP/ 101325.,273.16,8314.3,1005./
31*           DATA  AMOLE/ 28.965/
32*           DATA  ISTOPY,JARR,KPHI,LZED/ 1HY,1HR,1HP,1HZ/
33*           DATA  DF/ .2/
```

```
34*       C
35*       C   READ RUN TIME COMMENTS (ONE CARD) FIRST.
36*       C
37*             READ(5,5000) IREMRK
38*        5000 FORMAT(20A4)
39*       C
40*       C   READ PROBLEM DATA AND INITIAL CONDITIONS (NON-DIMENSIONAL) FOR THIS RUN.
41*       C
42*             READ(5,5005) INIT,MAXIT,NWRITE,CFL,TIME,ETIME,DELZ,MAXR,
43*            1 MAXP,MAXZ,IVIR,IVER,PAMB,TAMB,RMAX,ZMAX,RL,GAP,ERPM
44*        5005 FORMAT(3I10,E10.4/3E15.7/5I5,2E10.4/5E10.4)
45*             READ(5,5010) (((U(I,J,K,L,1),I=1,5),J=1,MAXR),K=1,MAXP),L=1,MAXZ)
46*        5010 FORMAT(5E14.7)
47*       C
48*       C   SECTION BELOW SETS PARAMETERS WHICH DETERMINE VALVE LOCATION AND
49*       C   SIZE FROM THE PARAMETERS IVIR AND IVER WHICH ARE READ IN.
50*       C   *** POINTS WITH RADIAL INDEX < 4 MAY NOT BE USED AS VALVE POINTS. ***
51*       C
52*       C
53*                JMINIV = IVIR - 1
54*                JMINEV = IVER - 1
55*                JMAXIV = IVIR + 2
56*                JMAXEV = IVER + 2
57*                KMINIV = MAXP - 2
58*                KMAXEV = 3
59*       C
60*       C   SOME USEFUL CONSTANTS.  NOTE VREF IS REFERENCE SPEED OF SOUND.
61*       C
62*                MPM1 = MAXP - 1
63*                ZM = MAXZ - 1
64*                AMP = .5 * (ZMAX-GAP) / RL
65*                CENTER = .5 * (ZMAX+GAP) / RL
66*                IF(INIT.EQ.1) DELZ = (GAP/RL)/ZM
67*                DELR = RMAX / ((MAXR-1)*RL)
68*                DELP = PI / MPM1
69*                RAIR = RGAS / AMOLE
70*                IWRITE = 0
71*                GAMMA = CP / (CP-RAIR)
72*                GAMM1 = GAMMA - 1.0
73*                GOGM1 = GAMMA / GAMM1
74*                GM1OG = 1. / GOGM1
75*                VREF = SQRT(GAMMA*RAIR*TREF)
```

```
      TIREF = RL / VREF
      RTIME = TIME * TIREF
C
C   INITIALIZE PISTON MOTION PARAMETERS.
C
      SPR = 0.
      VPIST = 0.
      OMEGA = 0.
      IF(ERPM.LE.0.) GO TO 1000
      SPR = 60. / (ERPM*TIREF)
      OMEGA = TWOPI / SPR
 1000 SPR2 = 2. * SPR
C
C   COMPUTE TABLE OF SINES AND COSINES FOR CENTERLINE SCHEME.
C
      DO 1010 K = 1, MAXP
      DEL = (K-1) * DELP
      SPH(K) = SIN(DEL)
      CPH(K) = COS(DEL)
 1010 CONTINUE
      SPH(1) = 0.
      CPH(1) = 1.
      SPH(MAXP) = 0.
      CPH(MAXP) = -1.
C
C   WRITE OUT DOCUMENTATION FOR THIS RUN.
C
      WRITE(7,9000) IREMRK
 9000 FORMAT(////5X,'3-D I. C. ENGINE INVISCID FLOWFIELD CALCULATION IN
     *CYLINDRICAL'/5X,'COORDINATES WITH PRIME VECTOR U = (U, V, W, P, T)
     *, AND GOVERNING'/5X'EQUATIONS IN NON-CONSERVATION FORM.  THIS VERS
     *ION CONTAINS 2ND-'/5X,'AND 4TH ORDER DAMPING TERMS FOR STABILITY, AND US
     *ES L'HOSPITAL'S RULE'/5X'TO OBTAIN A SET OF EQUATIONS AT R = 0.'
     *///5X'COMMENTS ON THIS RUN:  ',20A4)
      WRITE(7,9005) INIT,TIME,RTIME,NWRITE,CFL,ZMAX,RMAX,MAXR,MAXP,
     1 MAXZ,ERPM,GAP,IVIR,MAXP,IVER,PAMB,TAMB,DELTA,RL,VREF,TIREF,
     2 PREF,TREF,RAIR,GAMMA
```

```
 9005 FORMAT(///12X'PARAMETERS FOR THIS RUN'//9X'STARTING ITERATION-',
     * 2X,I9/9X'NON-DIMENSIONAL TIME-',G12.6/9X'REAL TIME-',11X,G12.6,
     *  ' SECONDS'/9X'DATA PRINT INTERVAL-  ',I9/9X'CFL FUDGE FACTOR-',4X,
     * G12.6/9X'CYLINDER HEIGHT-',5XG12.6,' METERS'/9X'CYLINDER RADIUS-'
     * ,5XG12.6,' METERS'/9X,'# OF R POINTS-',7X,I9/9X,'# OF PHI POINTS-'
     * ,5X,I9/9X'# OF Z POINTS-',7X,I9/9X,'ENGINE SPEED-',8X,G12.6,
     *  ' RPM'/9X,'PISTON CLEARANCE-',4X,G12.6,' METERS'/9X,
     *  'INTAKE VALVE CENTER-  (',I2,',',I2,', 1)'/9X'EXHAUST VALVE CENT
     *ER-  (',I2,', 1, 1)'/9X'AMBIENT PRESSURE-',4X,G12.6/9X,
     *  'AMBIENT TEMPERATURE-  ',G12.6/9X,'DELTA R-',13X,G12.6/9X,
     *  'DELTA PHI-',11X,G12.6/9X'CURRENT DELTA Z-',5X,G12.6/9X,
     *  'REFERENCE LENGTH-',4X,G12.6,' METERS'/9X'REFERENCE VELOCITY-  ',
     *  G12.6,' M/SEC'/9X'REFERENCE TIME-',6X,G12.6,' SECONDS'/9X,
     *  'REFERENCE PRESSURE-  ',G12.6,' NT/M**2'/9X'REFERENCE TEMP.-',5X,
     *  G12.6,' DEGREES K'/9X'SPECIFIC GAS CONST.-  ',G12.6,' M**2/SEC**2/
     *DEG. K'/9X'VALUE OF GAMMA-',6X,G12.6)
C
C  BEGIN THE TIME LOOP.  FIRST CHECK TO SEE IF TIME TO QUIT, THEN
C  IF NOT BEGIN NEXT STEP BY COMPUTING DELTAT FROM CFL CRITERION.
C
      DO 1800 IT = INIT, MAXIT
      IF(NWRITE.GT.IWRITE) GO TO 102C
      IWRITE = 0
      WRITE(6,9065) IT
 9065 FORMAT(/1X'STARTING ON ITERATION #',I7,'.  DO YOU WISH TO STOP?')
      READ(5,5015) IPRINT
 5015 FORMAT(A1)
      IF(IPRINT.EQ.ISTOPY) GO TO 181C
 1020 DELTAT = 100.
      DEL = DELR * DELP
      IF(DELR.LT.DEL) DEL = DELR
      IF(DELZ.LT.DEL) DEL = DELZ
      DO 1030 J = 1, MAXR
      DO 1030 K = 1, MAXP
      DO 1030 L = 1, MAXZ
      QMAG = SQRT(U(1,J,K,L,1)**2 + U(2,J,K,L,1)**2 + U(3,J,K,L,1)**2)
      DT = DEL / (QMAG + SQRT(U(5,J,K,L,1)))
      IF(DT.LT.DELTAT) DELTAT = DT
 1030 CONTINUE
```

```
152*            DELTAT = CFL * DELTAT
153*      C
154*      C   START PREDICTOR/CORRECTOR LOOP (IG = 1 OR IG = 2).
155*      C
156*            DO 179C IG = 1, 2
157*            NG = 3 - IG
158*      C
159*      C   DETERMINE PISTON POSITION AND VELOCITY AND CURRENT VALUE OF DELZ.
160*      C
161*            IF(ERPM.GT.0.) GO TO 104C
162*            CRANK = 0.
163*            GO TO 1050
164*       1040 IF(IG.EQ.2) ETIME = ETIME + DELTAT
165*            IF(ETIME.GT.SPR2) ETIME = ETIME - SPR2
166*            CRANK = OMEGA * ETIME
167*            HCYL = -AMP * COS(CRANK) + CENTER
168*            VPIST = AMP * OMEGA * SIN(CRANK)
169*            DELZ = HCYL / ZM
170*            CRANK = RTD * CRANK
171*      C
172*      C   PREPARE TO SET THE INTAKE AND/OR EXHAUST VALVE BOUNDARY CONDITIONS.
173*      C   NOTE THAT THE VALVE COORDINATES AS READ IN DENOTE ONLY THE CENTERS.
174*      C
175*      C        0.0  < CRANK <  PI      ------  INTAKE STROKE
176*      C          PI < CRANK <  2*PI    ------  COMPRESSION STROKE
177*      C       2*PI  < CRANK <  3*PI    ------  POWER STROKE
178*      C       3*PI  < CRANK <  4*PI    ------  EXHAUST STROKE
179*      C
180*      C   INTAKE STROKE ---- CONSTANT ENTROPY AND TOTAL ENTHALPY, PLUS THE
181*      C   CONSTRAINT THAT VELOCITY IS IN THE Z-DIRECTION AT VALVE POINTS.
182*      C
183*       1050 IF(CRANK.GT.18C.) GO TO 1090
184*            DO 1060 J = JMINIV, JMAXIV
185*            DO 1060 K = KMINIV, MAXP
186*            WW = U(3,J,K,1,IG)
187*            T = TAMB - .5 * GAMM1 * WW**2
188*            P = PAMB * (T/TAMB)**GOGM1
189*            U(1,J,K,1,IG) = 0.
190*            U(2,J,K,1,IG) = 0.
191*            U(4,J,K,1,IG) = P
192*            U(5,J,K,1,IG) = T
193*       1060 CONTINUE
```

```
194*      C
195*      C  SET THE CLOSED-VALVE CONDITIONS ON EXHAUST VALVE.
196*      C
197*       1070 DO 1080 J = JMINEV, JMAXEV
198*            DO 1080 K = 1, KMAXEV
199*            WW = U(3,J,K,1,IG)
200*            T = U(5,J,K,1,IG)
201*            T = (SQRT(T) - .5*GAMM1*WW)**2
202*            U(3,J,K,1,IG) = 0.
203*            U(4,J,K,1,IG) = U(4,J,K,1,IG) * (T/U(5,J,K,1,IG))**GOGM1
204*            U(5,J,K,1,IG) = T
205*        1080 CONTINUE
206*            GO TO 1120
207*      C
208*      C  SET THE CLOSED-VALVE CONDITIONS AT THE INTAKE PORT.
209*      C
210*       1090 DO 1100 J = JMINIV, JMAXIV
211*            DO 1100 K = KMINIV, MAXP
212*            WW = U(3,J,K,1,IG)
213*            T = U(5,J,K,1,IG)
214*            T = (SQRT(T) - .5*GAMM1*WW)**2
215*            U(3,J,K,1,IG) = 0.
216*            U(4,J,K,1,IG) = U(4,J,K,1,IG) * (T/U(5,J,K,1,IG))**GOGM1
217*            U(5,J,K,1,IG) = T
218*        1100 CONTINUE
219*            IF(CRANK.LE.540.) GO TO 1070
220*      C
221*      C  EXHAUST STROKE B.C. IMPOSES CONSTANT PRESSURE AT VALVE AND SETS
222*      C  THE TEMPERATURE TO THE CORRESPONDING ISENTROPIC VALUE.  NOTE THAT
223*      C  THERE IS NO CONSTRAINT ON THE FLUID VELOCITY DIRECTION IMPOSED HERE.
224*      C
225*            DO 1110 J = JMINEV, JMAXEV
226*            DO 1110 K = 1, KMAXEV
227*            P = U(4,J,K,1,IG)
228*            T = U(5,J,K,1,IG)
229*            U(4,J,K,1,IG) = PAMB
230*            U(5,J,K,1,IG) = T * (U(4,J,K,1,IG)/P)**GM1OG
231*        1110 CONTINUE
```

```
232*      C
233*      C   APPLY THE SYMMETRY CONDITION THAT VV = 0 ON PHI = 0 CR PI.
234*      C
235*       1120 DO 1130 J = 1, MAXR
236*            DO 1130 L = 1, MAXZ
237*            VV = U(2,J,1,L,IG)
238*            T = U(5,J,1,L,IG)
239*            T = (SQRT(T) - .5*GAMM1*VV)**2
240*            U(2,J,1,L,IG) = 0.
241*            U(4,J,1,L,IG) = U(4,J,1,L,IG) * (T/U(5,J,1,L,IG))**GOGM1
242*            U(5,J,1,L,IG) = T
243*            VV = U(2,J,MAXP,L,IG)
244*            T = U(5,J,MAXP,L,IG)
245*            T = (SQRT(T) + .5*GAMM1*VV)**2
246*            U(2,J,MAXP,L,IG) = 0.
247*            U(4,J,MAXP,L,IG) = U(4,J,MAXP,L,IG) * (T/U(5,J,MAXP,L,IG))**GOGM1
248*            U(5,J,MAXP,L,IG) = T
249*       1130 CONTINUE
250*      C
251*      C   APPLY BOUNDARY CONDITION ON SIDEWALL OF CYLINDER.
252*      C
253*            DO 1140 K = 1, MAXP
254*            DO 1140 L = 1, MAXZ
255*            UU = U(1,MAXR,K,L,IG)
256*            T = U(5,MAXR,K,L,IG)
257*            T = (SQRT(T) + .5*GAMM1*UU)**2
258*            U(1,MAXR,K,L,IG) = 0.
259*            U(4,MAXR,K,L,IG) = U(4,MAXR,K,L,IG) * (T/U(5,MAXR,K,L,IG))**GOGM1
260*            U(5,MAXR,K,L,IG) = T
261*       1140 CONTINUE
262*      C
263*      C   APPLY THE BOUNDARY CONDITION AT Z = ZMAX; I.E., WW = VPIST, AND THE
264*      C   BOUNDARY CONDITION WW = 0 AT Z = 0 (EXCEPT AT VALVE LOCATIONS, WHICH
265*      C   ARE TAKEN CARE OF ABOVE).
266*      C
```

```
267*            DO 1150 J = 1, MAXR
268*            VFLAG = .FALSE.
269*            IF((J.GE.JMINIV).AND.(J.LE.JMAXIV)) VFLAG = .TRUE.
270*            IF((J.GE.JMINEV).AND.(J.LE.JMAXEV)) VFLAG = .TRUE.
271*            DO 1150 K = 1, MAXP
272*            WW = U(3,J,K,MAXZ,IG) - VPIST
273*            T = U(5,J,K,MAXZ,IG)
274*            T = (SQRT(T) + .5*GAMM1*WW)**2
275*            U(3,J,K,MAXZ,IG) = VPIST
276*            U(4,J,K,MAXZ,IG) = U(4,J,K,MAXZ,IG) * (T/U(5,J,K,MAXZ,IG))**GOGM1
277*            U(5,J,K,MAXZ,IG) = T
278*            IF(((K.LE.KMAXEV).OR.(K.GE.KMINIV)).AND.VFLAG) GO TO 1150
279*            WW = U(3,J,K,1,IG)
280*            T = U(5,J,K,1,IG)
281*            T = (SQRT(T) - .5*GAMM1*WW)**2
282*            U(3,J,K,1,IG) = 0.
283*            U(4,J,K,1,IG) = U(4,J,K,1,IG) * (T/U(5,J,K,1,IG))**GOGM1
284*            U(5,J,K,1,IG) = T
285*         1150 CONTINUE
286*       C
287*       C   OBTAIN AVERAGE VALUES ON INNER RING WHERE L'HOSPITAL'S RULE IS USED,
288*       C   THEN SET THE INNER RING UP FOR THE NEXT STEP.
289*       C
290*               DO 1170 L = 1, MAXZ
291*               UU = U(1,1,1,L,IG) - U(1,1,MAXP,L,IG)
292*               WW = U(3,1,1,L,IG) + U(3,1,MAXP,L,IG)
293*               P = U(4,1,1,L,IG) + U(4,1,MAXP,L,IG)
294*               T = U(5,1,1,L,IG) + U(5,1,MAXP,L,IG)
295*               DO 1160 K = 2, MPM1
296*               UU = UU + 2.*(U(1,1,K,L,IG)*CPH(K) - U(2,1,K,L,IG)*SPH(K))
297*               WW = WW + 2.*U(3,1,K,L,IG)
298*               P = P + 2.*U(4,1,K,L,IG)
299*               T = T + 2.*U(5,1,K,L,IG)
300*            1160 CONTINUE
301*               UU = UU / (2*MPM1)
302*               WW = WW / (2*MPM1)
303*               P = P / (2*MPM1)
304*               T = T / (2*MPM1)
305*               DO 1170 K = 1, MAXP
306*               U(1,1,K,L,IG) = UU * CPH(K)
307*               U(2,1,K,L,IG) = -UU * SPH(K)
308*               U(3,1,K,L,IG) = WW
309*               U(4,1,K,L,IG) = P
310*               U(5,1,K,L,IG) = T
311*            1170 CONTINUE
```

```
C
C  TIME TO PRINT?
C
      IF(IG.EQ.2) GO TO 1340
      IWRITE = IWRITE + 1
      IF(NWRITE.GT.IWRITE) GO TO 1340
      HEADNG = .FALSE.
      WRITE(6,9025) IT
 9025 FORMAT(/1X'ITERATION # ',I6,'.  DO YOU WANT TO PRINT EVERYTHING?')
      READ(5,5015) IPRINT
      IF(IPRINT.NE.ISTOPY) GO TO 1200
      HEADNG = .TRUE.
C
C  PRINT ALL GRID VALUES AT THIS TIME STEP.
C
      WRITE(7,9030) IT, RTIME, TIME, HCYL, CRANK, VPIST
 9030 FORMAT(////1X'TIME STEP #',12X,I9/1X'REAL TIME -',12X,G12.6,
     1' SECONDS'/1X'NON-DIMENSIONAL TIME - ',G12.6/1X'PISTON POSITION -'
     2 ,6X,G12.6/1X'CRANKSHAFT ANGLE -',5X,G12.6,' DEGREES'/1X
     3 'PISTON VELOCITY -',6X,G12.6/)
      WRITE(7,9015)
 9015 FORMAT(/1X'(IR,IP,IZ)',7X'(U)',9X'(V)',9X'(W)',9X'(P)',9X'(T)')
      DO 1190 L = 1, MAXZ
      DO 1190 K = 1, MAXP
      DO 1190 J = 1, MAXR
      DO 1180 I = 1, 5
      Q(I) = U(I,J,K,L,1)
 1180 CONTINUE
      WRITE(7,9020) J, K, L, UU, VV, WW, P, T
 9020 FORMAT(1X'(',I2,',',I2,',',I2,')',5G12.6)
 1190 CONTINUE
C
C  SEE IF DATA IN A PARTICULAR "PLANE" IS DESIRED.
C
 1200 WRITE(6,9050)
 9050 FORMAT(/1X'DO YOU WANT DATA IN A PARTICULAR "PLANE"?')
      READ(5,5015) IPRINT
      IF(IPRINT.NE.ISTOPY) GO TO 1340
      IF(HEADNG) GO TO 1210
      HEADNG = .TRUE.
      WRITE(7,9030) IT, RTIME, TIME, HCYL, CRANK, VPIST
 1210 WRITE(6,9055)
 9055 FORMAT(/1X'WHICH COORDINATE HELD CONSTANT?')
      READ(5,5015) IPRINT
```

```
C
C  IF SO, WHICH "PLANE"?
C
      IF(IPRINT.NE.JARK) GO TO 1220
      KEY = -1
      GO TO 1240
 1220 IF(IPRINT.NE.KPHI) GO TO 1230
      KEY = 0
      GO TO 1240
 1230 IF(IPRINT.NE.LZED) GO TO 1200
      KEY = 1
 1240 WRITE(6,9060)
 9060 FORMAT(/1X'ENTER THE CONSTANT VALUE')
      READ(5,5020) ICOORD
 5020 FORMAT()
      WRITE(7,9015)
      IF(KEY) 1250, 1280, 1310
 1250 DO 1270 L = 1, MAXZ
      DO 1270 K = 1, MAXP
      DO 1260 I = 1, 5
      Q(I) = U(I,ICOORD,K,L,1)
 1260 CONTINUE
      WRITE(7,9020) ICOORD, K, L, UU, VV, WW, P, T
 1270 CONTINUE
      GO TO 1200
 1280 DO 1300 L = 1, MAXZ
      DO 1300 J = 1, MAXR
      DO 1290 I = 1, 5
      Q(I) = U(I,J,ICOORD,L,1)
 1290 CONTINUE
      WRITE(7,9020) J, ICOORD, L, UU, VV, WW, P, T
 1300 CONTINUE
      GO TO 1200
 1310 DO 1330 K = 1, MAXP
      DO 1330 J = 1, MAXR
      DO 1320 I = 1, 5
      Q(I) = U(I,J,K,ICOORD,1)
 1320 CONTINUE
      WRITE(7,9020) J, K, ICOORD, UU, VV, WW, P, T
 1330 CONTINUE
      GO TO 1200
```

```
C
C  BEGIN LOOP THROUGH THE FLOW-FIELD COORDINATES, TO COMPUTE THE SPATIAL
C  DERIVATIVES AND SOLVE THE EQUATIONS OF MOTION.
C
 1340 DO 1790 IZ = 1, MAXZ
      ZVPIST = IZ - 1
      ZVPIST = VPIST * (ZVPIST/ZM)
      DO 1790 IR = 1, MAXR
      R = (IR-1) * DELR
      DO 1790 IP = 1, MAXP
C
C  GET DDR USING FORWARD/BACKWARD DIFFERENCES FOR PREDICTOR/CORRECTOR
C  STEP, EXCEPT AT IR = 1 OR MAXR, WHERE THEY'RE THE SAME EACH TIME.
C  NOTE THAT IR = 1 IS ACTUALLY RING OF ZERO RADIUS, WHERE L'HOSPITAL'S
C  RULE IS USED TO OBTAIN EQUATIONS TO ADVANCE IN TIME AT R = 0.  ALL
C  RADIAL DIFFERENCING AT THE CENTERLINE IS DONE WITH SECOND-ORDER
C  ACCURATE 3-POINT ONE-SIDED DIFFERENCES.  NOTE THAT WE ALSO COMPUTE
C  2ND-DERIVATIVES FOR USE IN DAMPING TERMS, EXCEPT AT WALL & Z-AXIS.
C
      IF(IR.EQ.1) GO TO 1400
      IF((IG.EQ.2).OR.(IR.EQ.MAXR)) GO TO 1360
      DO 1350 I = 1, 5
      DDR(I) = (U(I,IR+1,IP,IZ,IG) - U(I,IR,IP,IZ,IG)) / DELR
 1350 CONTINUE
      GO TO 1380
 1360 DO 1370 I = 1, 5
      DDR(I) = (U(I,IR,IP,IZ,IG) - U(I,IR-1,IP,IZ,IG)) / DELR
 1370 CONTINUE
 1380 IF(IR.EQ.MAXR) GO TO 1400
      DO 1390 I = 1, 5
      D2R(I) = (U(I,IR+1,IP,IZ,IG) - 2.*U(I,IR,IP,IZ,IG) +
     * U(I,IR-1,IP,IZ,IG)) / DELR**2
 1390 CONTINUE
      GO TO 1430
 1400 DO 1410 I = 1, 5
      D2R(I) = 0.
 1410 CONTINUE
      IF(IR.NE.1) GO TO 1430
      DO 1420 I = 1, 5
      DDR(I) = (-3.*U(I,1,IP,IZ,IG) + 4.*U(I,2,IP,IZ,IG) -
     * U(I,3,IP,IZ,IG)) / (2.*DELR)
 1420 CONTINUE
```

```
C
C   COMPUTE DDP.  NOTE EFFECT OF SYMMETRY CONDITION AT PHI = 0 OR PI.
C   ALSO GET 2ND DERIVATIVES IN PHI-DIRECTION.
C
 1430 IF(IP.EQ.1) GO TO 1470
      IF(IP.EQ.MAXP) GO TO 1490
      IF(IG.EQ.2) GO TO 1450
      DO 1440 I = 1, 5
      DDP(I) = (U(I,IR,IP+1,IZ,IG) - U(I,IR,IP,IZ,IG)) / DELP
 1440 CONTINUE
      GO TO 1510
 1450 DO 1460 I = 1, 5
      DDP(I) = (U(I,IR,IP,IZ,IG) - U(I,IR,IP-1,IZ,IG)) / DELP
 1460 CONTINUE
      GO TO 1510
 1470 DO 1480 I = 1, 5
      DDP(I) = 0.
      D2P(I) = 2.*(U(I,IR,IP+1,IZ,IG) - U(I,IR,IP,IZ,IG)) / DELP**2
 1480 CONTINUE
      DDP(2) = U(2,IR,2,IZ,IG) / DELP
      D2P(2) = 0.
      GO TO 1530
 1490 DO 1500 I = 1, 5
      DDP(I) = 0.
      D2P(I) = 2.*(U(I,IR,MPM1,IZ,IG) - U(I,IR,MAXP,IZ,IG)) / DELP**2
 1500 CONTINUE
      DDP(2) = -U(2,IR,MPM1,IZ,IG) / DELP
      D2P(2) = 0.
      GO TO 1530
 1510 DO 1520 I = 1, 5
      D2P(I) = (U(I,IR,IP+1,IZ,IG) - 2.*U(I,IR,IP,IZ,IG) +
     * U(I,IR,IP-1,IZ,IG)) / DELP**2
 1520 CONTINUE
C
C   FOR IR = 1 (R = 0) SOME SPECIAL CROSS DERIVATIVES ARE NEEDED.
C
```

```
      1530 IF(IR.NE.1) GO TO 1600
           IF((IP.EQ.1).OR.(IP.EQ.MAXP)) GO TO 1570
           IF(IG.EQ.2) GO TO 1550
           DO 1540 I = 1, 5
           D2RP(I) = (-(U(I,3,IP+1,IZ,IG)-U(I,3,IP,IZ,IG))/DELP + 4.*
          * (U(I,2,IP+1,IZ,IG)-U(I,2,IP,IZ,IG))/DELP - 3.*DDF(I))/(2.*DELR)
      1540 CONTINUE
           GO TO 1600
      1550 DO 1560 I = 1, 5
           D2RP(I) = (-(U(I,3,IP,IZ,IG)-U(I,3,IP-1,IZ,IG))/DELP + 4.*
          * (U(I,2,IP,IZ,IG)-U(I,2,IP-1,IZ,IG))/DELP - 3.*DDF(I))/(2.*DELR)
      1560 CONTINUE
           GO TO 1600
      1570 DO 1580 I = 1, 5
           D2RP(I) = 0.
      1580 CONTINUE
           IF(IP.EQ.MAXP) GO TO 1590
           D2RP(2)= (-U(2,3,2,IZ,IG)+4.*U(2,2,2,IZ,IG)-3.*U(2,1,2,IZ,IG))
          * / (2.*DELR*DELP)
           GO TO 1600
      1590 D2RP(2)= (-U(2,3,MPM1,IZ,IG)+4.*U(2,2,MPM1,IZ,IG)-3.*
          * U(2,1,MPM1,IZ,IG))/(2.*DELR*DELP)
      C
      C  COMPUTE DDZ AND D2Z.
      C
      1600 IF(IZ.EQ.1) GO TO 1610
           IF((IG.EQ.2).OR.(IZ.EQ.MAXZ)) GO TO 1630
      1610 DO 1620 I = 1, 5
           DDZ(I) = (U(I,IR,IP,IZ+1,IG) - U(I,IR,IP,IZ,IG)) / DELZ
      1620 CONTINUE
           GO TO 1650
      1630 DO 1640 I = 1, 5
           DDZ(I) = (U(I,IR,IP,IZ,IG) - U(I,IR,IP,IZ-1,IG)) / DELZ
      1640 CONTINUE
      1650 IF((IZ.EQ.1).OR.(IZ.EQ.MAXZ)) GO TO 1670
           DO 1660 I = 1, 5
           D2Z(I) = (U(I,IR,IP,IZ+1,IG) - 2.*U(I,IR,IP,IZ,IG) +
          * U(I,IR,IP,IZ-1,IG)) / DELZ**2
      1660 CONTINUE
           GO TO 1690
      1670 DO 1680 I = 1, 5
           D2Z(I) = 0.
      1680 CONTINUE
```

```
518*      C
519*      C  REQUIRED SPATIAL DERIVATIVES NOW COMPUTED. SET UP SOME TEMPORARY
520*      C  VECTORS PRIOR TO SOLVING EQUATIONS OF MOTION FOR THIS STEP.
521*      C
522*       1690 DO 1700 I = 1, 5
523*            Q(I) = U(I,IR,IP,IZ,IG)
524*       1700 CONTINUE
525*            ADWDZ = ABS(DWDZ)
526*            TOGP = T / (GAMMA*P)
527*            IF(IR.EQ.1) GO TO 1730
528*            DO 1710 I = 1, 5
529*            QDDEL(I) = UU * DDR(I) + (VV/R) * DDP(I) + WW * DDZ(I)
530*       1710 CONTINUE
531*            DELDOQ = DUDR + UU/R + DVDP/R + DWDZ
532*      C
533*      C  FORM TIME DERIVATIVES FROM GOVERNING EQUATIONS.
534*      C
535*            TD(1) = ZVPIST*DUDZ - QDELU - TOGP*DPDR + VV**2/R
536*            TD(2) = ZVPIST*DVDZ - QDELV - TOGP*DPDP/R - UU*VV/R
537*            TD(3) = ZVPIST*DWDZ - QDELW - TOGP*DPDZ
538*            TD(4) = ZVPIST*DPDZ - QDELP - GAMMA*P*DELDOQ
539*            TD(5) = ZVPIST*DTDZ - QDELT - GAMM1*T*DELDOQ
540*      C
541*      C  ADD DAMPING TERMS TO CURRENT TIME DERIVATIVE CALCULATION.
542*      C
543*            ADUDR = ABS(DUDR)
544*            ADVDP = ABS(DVDP)
545*            DO 1720 I = 1, 5
546*            TD(I) = TD(I) + DF * (ADUDR*(D2R(I)+DDR(I)/R)*DELR**2 + (ADVDP/R)*
547*           * D2P(I)*DELP**2 + ADWDZ*D2Z(I)*DELZ**2)
548*       1720 CONTINUE
549*            GO TO 1760
550*      C
551*      C  SECTION BELOW HANDLES SPECIAL CASE OF IR = 1 (R = 0).
552*      C
553*       1730 DELDOQ = 2.*DUDR + D2RP(2) + DWDZ
554*            DO 1740 I = 1, 5
555*            QDDEL(I) = UU*DDR(I) + VV*D2RP(I) + DVDR*DDP(I) + WW*DDZ(I)
556*       1740 CONTINUE
557*            TD(1) = ZVPIST*DUDZ - QDELU - TOGP*DPDR + 2.*VV*DVDR
558*            TD(2) = ZVPIST*DVDZ - QDELV - TOGP*D2RP(4) - UU*DVDR - VV*DUDR
559*            TD(3) = ZVPIST*DWDZ - QDELW - TOGP*DPDZ
560*            TD(4) = ZVPIST*DPDZ - QDELP - GAMMA*P*DELDOQ
561*            TD(5) = ZVPIST*DTDZ - QDELT - GAMM1*T*DELDOQ
```

```
562*      C
563*      C   FORM DAMPING TERMS.
564*      C
565*            D2VDRP = ABS(D2RP(2))
566*            DO 1750 I = 1, 5
567*            TD(I) = TD(I) + DF*(D2VDRP*D2P(I)*DELP**2 + ADWDZ*D2Z(I)*DELZ**2)
568*       1750 CONTINUE
569*      C
570*      C   IF CORRECTOR STEP, COMPUTE AVERAGE TIME DERIVATIVE.
571*      C
572*       1760 IF(IG.EQ.1) GO TO 1780
573*            DO 1770 I = 1, 5
574*            TD(I) = (TD(I) + TDU(I,IR,IP,IZ)) / 2.
575*       1770 CONTINUE
576*      C
577*      C   USE TAYLOR SERIES TO ADVANCE IN TIME.
578*      C
579*       1780 DO 1790 I = 1, 5
580*            U(I,IR,IP,IZ,NG) = U(I,IR,IP,IZ,1) + DELTAT * TD(I)
581*            TDU(I,IR,IP,IZ) = TD(I)
582*       1790 CONTINUE
583*            TIME = TIME + DELTAT
584*            RTIME = TIME * TIREF
585*       1800 CONTINUE
586*            IT = MAXIT
587*            MAXIT = MAXIT + (MAXIT-INIT) + 1
588*            INIT = IT + 1
589*            GO TO 1820
590*      C
591*      C   IF NORMAL EXIT, WRITE OUTPUT ON RESTART FILE FOR NEXT TIME.
592*      C
593*       1810 MAXIT = MAXIT + (IT-INIT)
594*            INIT = IT
595*       1820 WRITE(9,5000) IREMRK
596*            WRITE(9,5005) INIT,MAXIT,NWRITE,CFL,TIME,ETIME,DELZ,MAXR,
597*           1 MAXP,MAXZ,IVIR,IVER,PAME,TAMB,RMAX,ZMAX,FL,GAP,EPPM
598*            DO 1840 L = 1, MAXZ
599*            DO 1840 K = 1, MAXP
600*            DO 1840 J = 1, MAXR
601*            DO 1830 I = 1, 5
602*            Q(I) = U(I,J,K,L,1)
603*       1830 CONTINUE
604*            WRITE(9,5010) Q
605*       1840 CONTINUE
606*            STOP
607*            END
```

B. Sample Input Data Set

```
12345678901234567890123456789012345678901234567890123456789012345678901234567890 (column counter)
3000 RPM TEST RUN FOR CYLINDRICAL ENGINE PROGRAM.
         1        1000         250   .7000+00
   .0000000       .0000000       .0000000
     9     9    10     5     5   .1000+01   .1000+01
 .4000-01  .5000-01  .1000-01  .1000-01  .3000+04
  .0000000       .0000000       .0000000       1.000000+00   1.0000000+00
  .0000000       .0000000       .0000000       1.000000+00   1.0000000+00
                                .
                                .

                        810 identical lines
                                .
                                .
   .0000000       .0000000       .0000000       1.000000+00   1.0000000+00
   .0000000       .0000000       .0000000       1.000000+00   1.0000000+00
   .0000000       .0000000       .0000000       1.000000+00   1.0000000+00
12345678901234567890123456789012345678901234567890123456789012345678901234567890 (column counter)
```

C. Portion of Sample Output for Input Data of Section B

```
3-D I. C. ENGINE INVISCID FLOWFIELD CALCULATION IN CYLINDRICAL
COORDINATES WITH PRIME VECTOR U = (U, V, W, P, T), AND GOVERNING
EQUATIONS IN NON-CONSERVATION FORM.  THIS VERSION CONTAINS 2ND-
ORDER DAMPING TERMS FOR STABILITY, AND USES L'HOSPITAL'S RULE
TO OBTAIN A SET OF EQUATIONS AT R = 0.

COMMENTS ON THIS RUN:  3000 RPM TEST RUN FOR CYLINDRICAL ENGINE PROGRAM.
```

PARAMETERS FOR THIS RUN

STARTING ITERATION-	1	
NON-DIMENSIONAL TIME-	.000000	
REAL TIME-	.000000	SECONDS
DATA PRINT INTERVAL-	250	
CFL FUDGE FACTOR-	.700000	
CYLINDER HEIGHT-	.900000-01	METERS
CYLINDER RADIUS-	.400000-01	METERS
# OF R POINTS-	9	
# OF PHI POINTS-	9	
# OF Z POINTS-	10	
ENGINE SPEED-	3000.00	RPM
PISTON CLEARANCE-	.100000-01	METERS
INTAKE VALVE CENTER-	(5, 9, 1)	
EXHAUST VALVE CENTER-	(5, 1, 1)	
AMBIENT PRESSURE-	1.00000	
AMBIENT TEMPERATURE-	1.00000	
DELTA R-	.500000	
DELTA PHI-	.392699	
CURRENT DELTA Z-	.111111	
REFERENCE LENGTH-	.100000-01	METERS
REFERENCE VELOCITY-	331.299	M/SEC
REFERENCE TIME-	.301843-04	SECONDS
REFERENCE PRESSURE-	101325.	NT/M**2
REFERENCE TEMP.-	273.160	DEGREES K
SPECIFIC GAS CONST.-	287.046	M**2/SEC**2/DEG. K
VALUE OF GAMMA-	1.39981	

```
TIME STEP #                          250
REAL TIME -                    .579650-03  SECONDS
NON-DIMENSIONAL TIME -         19.2037
PISTON POSITION -              1.06614
CRANKSHAFT ANGLE -             10.4337     DEGREES
PISTON VELOCITY -              .686915-02
```

(IR,IP,IZ)	(U)	(V)	(W)	(P)	(T)
(1, 9, 1)	-.372497-01	.000000	.000000	.990019	.997142
(2, 9, 1)	-.356085-01	.000000	.000000	.997774	.999377
(3, 9, 1)	-.253411-01	.000000	.000000	.991378	.997573
(4, 9, 1)	.000000	.000000	.364646-01	.999070	.999734
(5, 9, 1)	.000000	.000000	.458290-01	.998531	.999580
(6, 9, 1)	.000000	.000000	.334047-01	.999219	.999777
(7, 9, 1)	.000000	.000000	.227982-01	.999636	.999896
(8, 9, 1)	.427697-02	.000000	.000000	.994498	.998462
(9, 9, 1)	.000000	.000000	.000000	.998532	.999585
(1, 9, 2)	-.389291-01	.000000	.573078-03	.990309	.997224
(2, 9, 2)	-.390685-01	.000000	-.102517-02	.998262	.999513
(3, 9, 2)	-.337341-01	.000000	-.155693-02	.992052	.997760
(4, 9, 2)	-.250352-01	.000000	.351388-01	.999208	.999771
(5, 9, 2)	-.198279-02	.000000	.428171-01	.997567	.999312
(6, 9, 2)	.101316-02	.000000	.323624-01	.998863	.999676
(7, 9, 2)	.117059-01	.000000	.210730-01	.998829	.999674
(8, 9, 2)	.990485-02	.000000	.690401-04	.995862	.998818
(9, 9, 2)	.000000	.000000	.678546-03	.999928	.999986
(1, 9, 3)	-.380793-01	.000000	.138543-02	.990185	.997190
(2, 9, 3)	-.394244-01	.000000	-.906843-03	.998142	.999473
(3, 9, 3)	-.417289-01	.000000	.497224-04	.991877	.997684
(4, 9, 3)	-.346847-01	.000000	.322627-01	.999772	.999950
(5, 9, 3)	-.988404-02	.000000	.398559-01	.996471	.999017
(6, 9, 3)	.205344-02	.000000	.293750-01	.998533	.999583
(7, 9, 3)	.150575-01	.000000	.194041-01	.998117	.999488
(8, 9, 3)	.982226-02	.000000	.144124-02	.995627	.998753
(9, 9, 3)	.000000	.000000	.255019-02	.999319	.999809
(1, 9, 4)	-.367699-01	.000000	.222141-02	.990284	.997217
(2, 9, 4)	-.402619-01	.000000	.724784-03	.997853	.999392
(3, 9, 4)	-.418862-01	.000000	.154873-02	.991864	.997678
(4, 9, 4)	-.376129-01	.000000	.286755-01	1.00032	1.00012
(5, 9, 4)	-.112284-01	.000000	.344296-01	.996913	.999138
(6, 9, 4)	.206575-02	.000000	.253990-01	.998560	.999591
(7, 9, 4)	.140685-01	.000000	.174468-01	.998120	.999490
(8, 9, 4)	.846916-02	.000000	.259647-02	.995762	.998791
(9, 9, 4)	.000000	.000000	.379916-02	.999319	.999809

D. Running Time for Sample Case

The execution time for the sample case given above, with 810 grid points used to specify the geometry, is about 16.5 minutes per thousand time steps. This figure is for the UNIVAC 1100/40, with a printing interval of 250 time steps. Approximately 16000 time steps (using a CFL multiplier of approximately .7) are required for a full four-stroke solution. The UNIVAC 1100/40 is about twice as fast as the UNIVAC 1108.

REFERENCES

1. Obert, E. F., Internal Combustion Engine Processes and Air Pollution, Intext Education Publishers, New York, 1973.

2. Lichty, L. C., Internal Combustion Engines, McGaw-Hill, New York, 1939.

3. Roache, P. J., "Report of the Numerical Fluid Dynamics Panel," Workshop on the Numerical Simulation of Combustion for Application to Spark and Compression Ignition Engines," A. A. Boni, (ed.), sponsored by the National Science Foundation, La Jolla, California, 23-25 April 1975.

4. Diwakar, R., "Interaction of Combustion with the Aerodynamic Flowfield in an Internal Combustion Reciprocating Engine - A Two--Dimensional Solution," Ph.D. thesis, Department of Aerospace Engineering, University of Maryland, College Park, Maryland, 1977.

5. Lavoie, George A., Heywood, John B., and Keck, James C., "Experimental and Theoretical Study of Nitric Oxide Formation in Internal Combustion Engines," Combustion Science and Technology, Volume 1, pps. 313-326, 1970.

6. Sirignano, W. A., "One-Dimensional Analysis of Combustion in a Spark-Ignition Engine," Combustion Science and Technology, Volume 7, pps. 99-108, 1973.

7. Bracco, F. V. and Sirignano, W. A., "Theoretical Analysis of Wonkel Engine Combustion," Combustion Science and Technology, Volume 7, pps. 109-123, 1973.

8. Bellan, Josette R. and Sirignano, W. A., "A Theory of Turbulent Flame-Front Development and Nitric Oxide Formation in Stratified

Charge Internal Combustion Engines," Combustion Science and Technology, Volume 8, pps. 51-68, 1973.

9. Bellan, Josette R., and Sirignano, W. A., "Combustion and NO Formation in a Stratified Charge Engine: A Two Turbulent Equation Model," Combustion Sci. and Tech., Vol. 12, pps. 75-104, 1976.

10. Libby, P. A., and Chen, K. K., "Remarks on Quasi-Linearization Applied in Boundary Layer Calculations," AIAA Journal, Volume 4, pps. 937--939, 1966.

11. Lee, E. S., Quasilinearization and Invarient Imbedding, Academic Press, New York, 1968.

12. Bracco, F. V., "Theoretical Analysis of Stratified Two-Phase Wankel Engine Combustion," Combustion Science and Technology, Volume 8, pps. 69-84, 1973.

13. Bracco, F. V., "Introducing a New Generation of More Detailed and Informative Combustion Models," SAE Paper #741174, International Stratified Charge Engine Conference, Troy, Michigan, October 30 - November 1, 1974.

14. Boni, A. A., Chapman, M. and Schneyer, G. P., "A One-Dimensional Variable Area Computer Simulation of Combustion in a Divided Chamber Stratified Charge Engine." ASME Paper #75-WA/DGP-1, 1975.

15. Boni, A. A., Chapman, M., Cook, J. L., and Schneyer, G. P., "Computer Simulation of Combustion in a Stratified Charge Engine," presented at the Sixteenth International Symposium on Combustion, Massachusetts Institute of Technology, Cambridge, Mass., August 15-21, 1976.

16. Hirt, C. W., and Amsden, A. A., and Cook. J. L., "An Arbitrary Lagrangian-Eulerian Computing Method for All Flow Speeds," Journal of Computational Physics, Volume 14, pps. 227-253, March, 1974.

17. Bracco, F. V., Gupta, H. C., Krishnamurthy, L., Sontavicca, D. A., Steinberger, R. L., Warshaw, V., "Two-Phase, Two-Dimensional, Unsteady Combustion in Internal Combustion Engines; Preliminary Theoretical Results." SAE Paper #760114, Automotive Engineering Congress and Exposition, Detroit, Michigan, February 23-27, 1976.

18. Bracco, F. V., "Modelling of Two-Phase, Two-Dimensional Unsteady Combustion for Internal Combustion Engines," paper presented at the Institution of Mechanical Engineers Conference on Stratified Charge Engines, London, England, November 23-25, 1976.

19. Rivard, W. C., Farmer, C. A., and Butler, T. D., "RICE - A Computer Program for Multicomponent Chemically Reactive Flows at All Speeds," Los Alamos Scientific Laboratory Report LA-5812, November 1974.

20. Griffin, M. D., Anderson, J. D., Jr., and Diwakar, R., "Navier-Stokes Solutions for the Flowfield in an Internal Combustion Engine," AIAA Paper #76-403, 9th AIAA Fluid and Plasmadynamics Meeting, San Diego, California, July 14-16, 1976. Also, AIAA Journal, Volume 14, #12, pps. 1665-1666, December 1976.

21. Diwakar, R., Anderson, J. D., Jr., Griffin, M. D., and Jones, E., "Inviscid Solutions for the Flowfield in an Internal Combustion Engine," AIAA Journal, Volume 14, #12, pps. 1667-1668, December 1976.

22. Gosman, A. D., and Watkins, A. P., "A Computer Prediction Method for Turbulent Flow and Heat Transfer in Piston/Cylinder Assemblies," paper presented at the Symposium on Turbulent Shear Flows, University Park, Pennsylvania, April 1977.

23. Dwyer, H. A., and Sanders, B. R., "Unsteady Flow and Flame Propagation in a Prechamber of a Stratified Charge Engine," paper presented at the Institution of Mechanical Engineers International Conference on Stratified Charge Engines, London, England, November 23-25, 1976.

24. Dwyer, H. A. and Sanders, B. R., "Modeling of Unsteady Combustion Phenomena," AIAA Paper #77-136, AIAA 15th Aerospace Sciences Meeting, Los Angeles, California, January 24-26, 1977.

25. Pouring, A. A., Blaser, R. F., Keating, E. L., and Rankin, B. H., "The Influence of Combustion with Pressure Exchange on the Performance of Heat Balanced Internal Combustion Engines," SAE Paper #770120, International Automotive Engineering Congress and Exposition, Detroit, Michigan, February 28 - March 4, 1977.

26. Dwyer, H., Allen, R., Ward, M, Karnopp, D., and Margolis, D., "Shock Capturing Finite Difference Methods for Unsteady Gas Transfer," AIAA Paper #74-521, Palo Alto, California, 1974.

27. Rizzi, A. W. and Bailey, H. E., "A Generalized Hyperbolic Marching Method for Chemically Reacting 3-D Supersonic Flow Using a Splitting Technique," AIAA Second Computational Fluid Dynamics Conference Proceedings, June 19-20, 1975.

28. Witze, P. O., "Measurements of the Spatial Distribution and Engine Speed Dependence of Turbulent Air Motion in an I.C. Engine," SAE Paper #770220, International Automotive Engineering Congress and Exposition," Detroit, Michigan, February 28 - March 4, 1977.

29. Witze, P. O., "Hot Wire Measurements of the Turbulence Structure in a Motored Spark-Ignition Engine," Sandia Laboratories Report #SAND77-8233, Livermore, California, May 1977.

30. Schlichting, H., Boundary Layer Theory, (6th ed.), McGraw-Hill, New York, 1968.

31. White, Frank Mangrem, Viscous Fluid Flow, McGraw-Hill, New York 1974.

32. Marion, Jerry B., Classical Dynamics of Particles and Systems (2nd ed.), Academic Press, New York, 1973.

33. Moretti, Gino and Abbett, Michael, "A Time-Dependent Computational Method for Blunt-Body Flows," AIAA Journal, Volume 4, #12, pps. 2136-2141, 1966.

34. Moretti, Gino and Bleich, G., "Three-Dimensional Flow Around Blunt Bodies," AIAA Journal, Volume 5, p. 1557, 1967.

35. Moretti, G. and Salas, M., " Computation of Three-Dimensional Flows About Aircraft Configurations," Computers and Fluids, Volume 1, #2, June 1973.

36. Kutler, P. and Lomax, H., "A Systematic Development of the Supersonic Flowfields Over and Behind Wings and Wing-Body Configurations Using a Shock-Capturing Finite-Difference Approach," AIAA Paper #71-99, AIAA 9th Aerospace Sciences Meeting, New York, January 25-27, 1971.

37. Kutler, P., Lomax, H., and Warming, R. F., "Computation of Space Shuttle Flowfields Using Non-Centered Finite-Difference Techniques," AIAA Journal, Volume 11, #2, pps. 196-204, February 1973.

38. MacCormack, R. W., "Numerical Solution of the Interaction of a Shock Wave With a Laminar Boundary Layer," Lecture Notes in Physics, Volume 8, Springer-Verlag, New York, 1971.

39. MacCormack, R. W. and Paullay, A. J., "Computational Efficiency Achieved by Time-Splitting of Finite-Difference Operators," AIAA Paper #72-154, 1972.

40. Kutler, Paul, "Computation of Three-Dimensional Inviscid Supersonic Flows," Lecture Notes in Physics, Springer-Verlag, New York, 1974.

41. Anderson, J. D., Jr., Gas Dynamic Lasers - An Introduction, Academic Press, New York, 1976.

42. Anderson, J. D., Jr., "Time Dependent Solutions of Non-Equilibrium Nozzle Flows - A Sequel," AIAA Journal, Volume 8, pps. 2280-2282, 1970.

43. Anderson, J. D., Jr., "Time Dependent Analysis of Population Inversions in an Expanding Gas," Physics of Fluids, Volume 13, pps. 1983-1989, 1970.

44. Owczarek, Jerzy A., Fundamentals of Gas Dynamics, International Textbook Company, Scranton, PA., 1964.

45. MacCormack, R. W., "The Effect of Viscosity on Hypervelocity Impact Cratering," AIAA Paper #69-354, AIAA Hypervelocity Impact Conference, Cincinnati, Ohio, April 30 - May 2, 1969.

46. MacCormack, R. W., "A Numerical Method for Solving the Navier-Stokes Equations with Application to Shock-Boundary Layer Interactions," AIAA Paper #75-1, 13th AIAA Aerospace Sciences Meeting, Pasadena, California, January 20-22, 1975.

47. Kothari, A. P., and Anderson, J. D., Jr., "Navier-Stokes Solutions for Chemical Laser Flows: Cold Flows," AIAA Journal, Volume 14, pps. 702-703, 1976.

48. Abbett, Michael J., "Boundary Condition Computational Procedures for Inviscid Supersonic Flowfields," Proceedings, AIAA Computational Fluid Dynamics Conference, 1973.

49. Rudinger, George, Wave Diagrams for Nonsteady Duct Flow, Van Nostrand, New York, 1955. Also available as a Dover edition.

50. Roache, Patrick J., Computational Fluid Dynamics, Hermosa Publishers, Albuquerque, N.M., 1972.

51. Taylor, Thomas D., "Numerical Methods for Predicting Subsonic, Supersonic, and Transonic Flows," AGARDograph No. 187, 1974.

52. Griffin, Michael D., and Anderson, John D., Jr., "On the Application of Boundary Conditions to Time-Dependent Computations for Quasi--One-Dimensional Fluid Flows," to be published in Computers and Fluids.

53. MacCormack, R. W., personal communication, NASA - Ames Research Center, May 3, 1977.

54. Lapidus, Arnold, "A Detached Shock Calculation by Second-Order Finite Differences," Journal of Computational Physics, Volume 2, pps. 154-177, 1967.

55. Abramowitz, M., and Stegun, I. A., Handbook of Mathematical Formulas with Functions, Tables, and Graphs, National Bureau of Standards Applied Mathematics Series 55, U. S. Government Printing Office, Ninth Printing, 1970.

56. Tolstoy, T., and Clay, C. S., Ocean Acoustics: Theory and Experiment in Underwater Sound, McGraw-Hill, New York 1966.

57. Salas, M. D., "The Anatomy of Floating Shock Fitting," Proceedings of the AIAA Second Computational Fluid Dynamics Conference, Hartford, Connecticut, June 1975.

GEOMETRICAL MODEL AND GRID
LAYOUT FOR 2-D ENGINE
WITHOUT EXTERNAL MANIFOLD

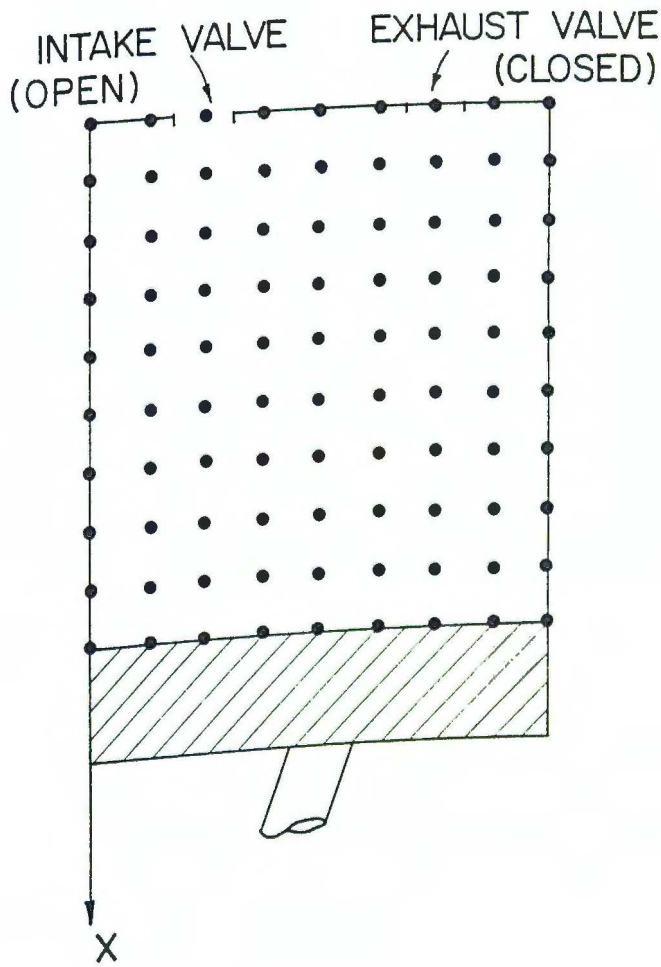

FIGURE 1

GEOMETRY OF 2-D ENGINE MODEL
WITH EXTERNAL MANIFOLD

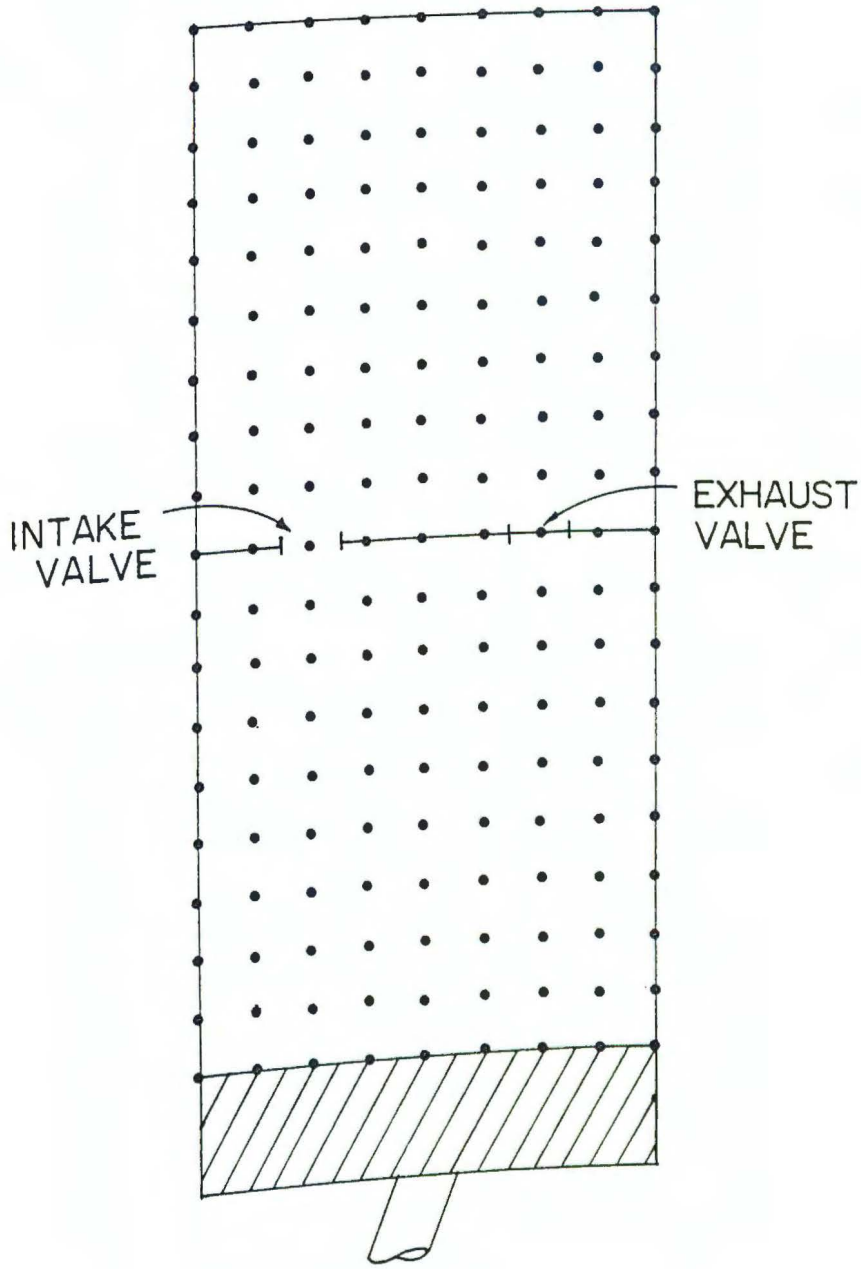

FIGURE 2

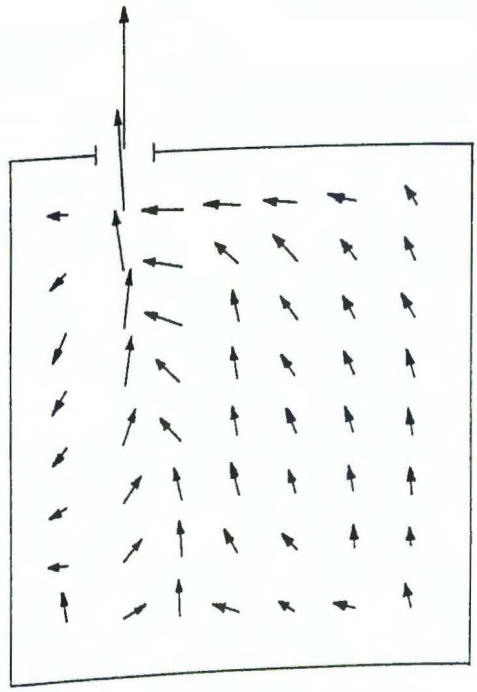

$P_{o\,INT}$ = 0.05 ATM.

P_{EXT} = 0.01 ATM.

T = 273.16°K

t = 500 Δt = 0.04 MSEC

EXHAUST TEST WITH
STATIONARY PISTON

FIGURE 3

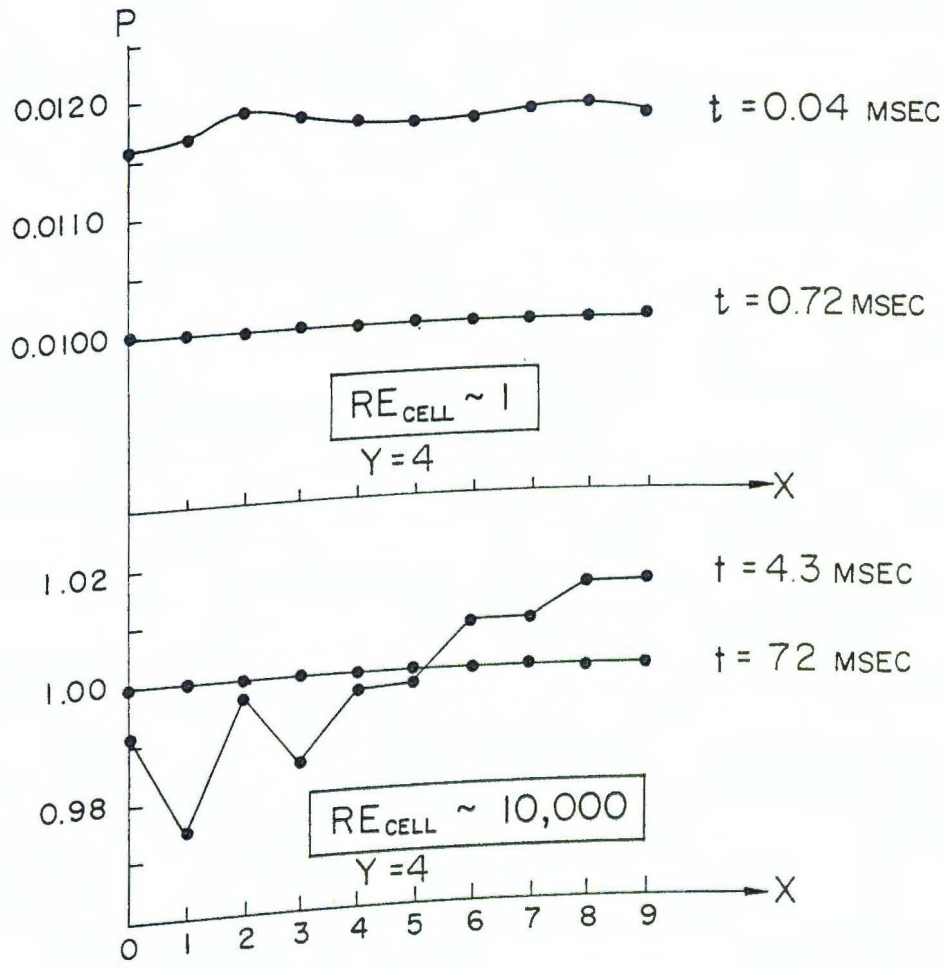

PRESSURE DISTRIBUTIONS FOR LOW AND HIGH CELL-RE EXHAUST TESTS

FIGURE 4

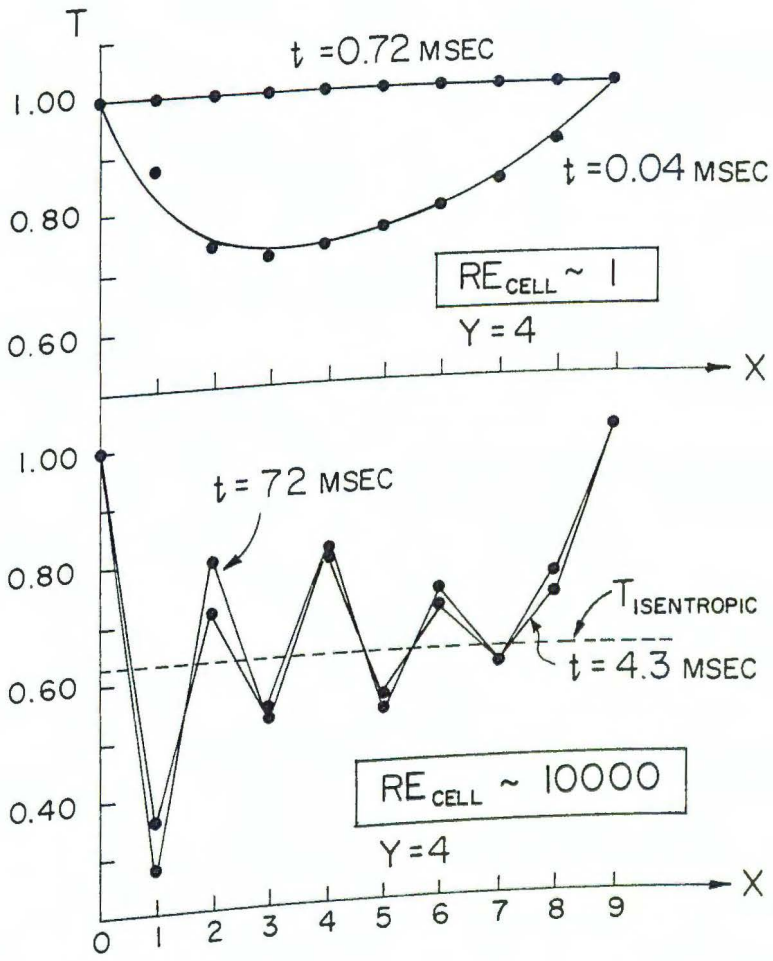

TEMPERATURE DISTRIBUTIONS FOR LOW AND HIGH CELL-RE EXHAUST TESTS

FIGURE 5

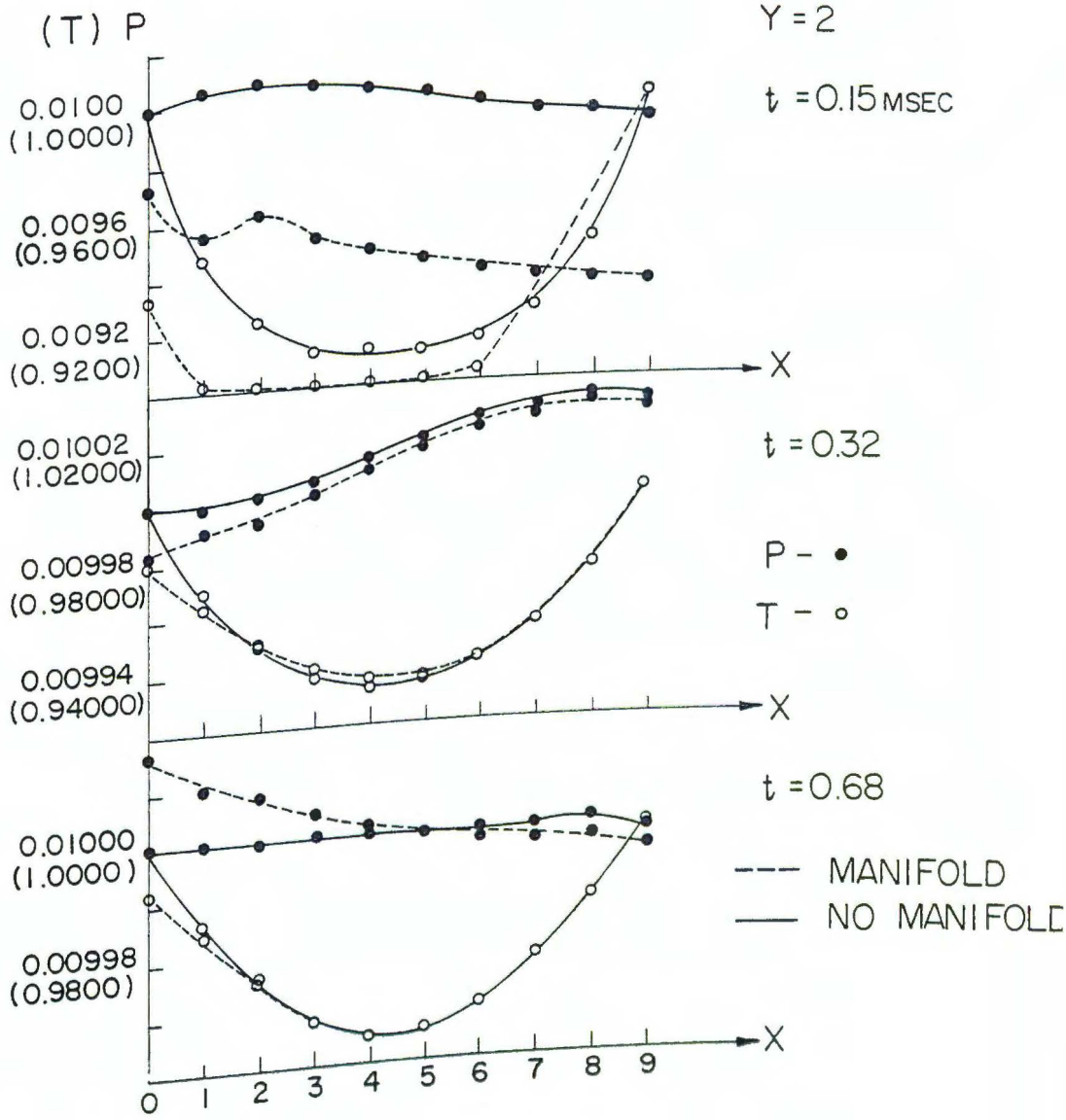

TIME HISTORY FOR PRESSURE AND TEMPERATURE ON EXHAUST WITH AND W/O MANIFOLD

FIGURE 6

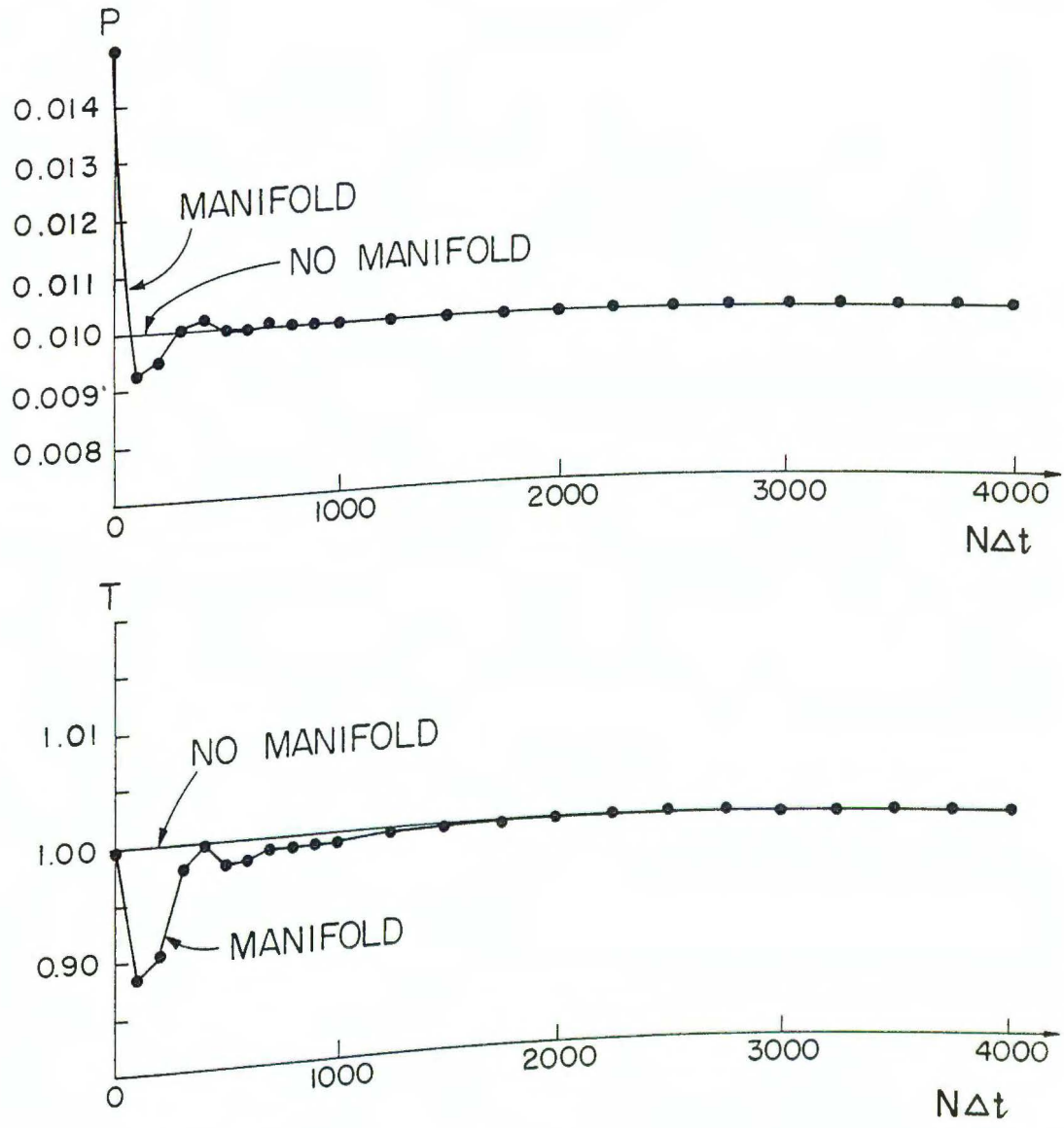

TIME HISTORY OF PRESSURE AND TEMPERATURE AT VALVE WITH AND W/O MANIFOLD

FIGURE 7.

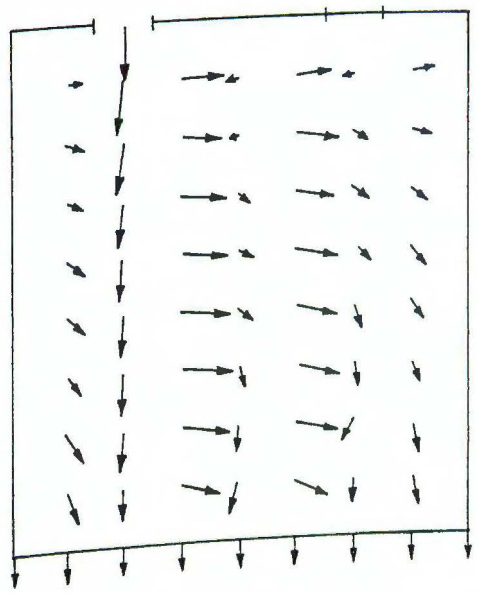

$t = 0.5$ MSEC $= 5000\Delta t$

$X_p = 1.77$

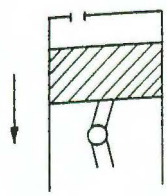

VELOCITY DISTRIBUTION
ON INTAKE STROKE

FIGURE 8

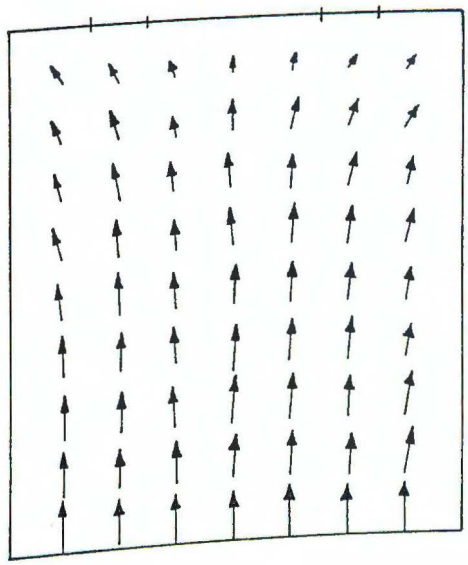

$t = 2.7$ MSEC $= 10500\Delta t$

$X_p = 8.87$

VELOCITY DISTRIBUTION
ON COMPRESSION STROKE

FIGURE 9

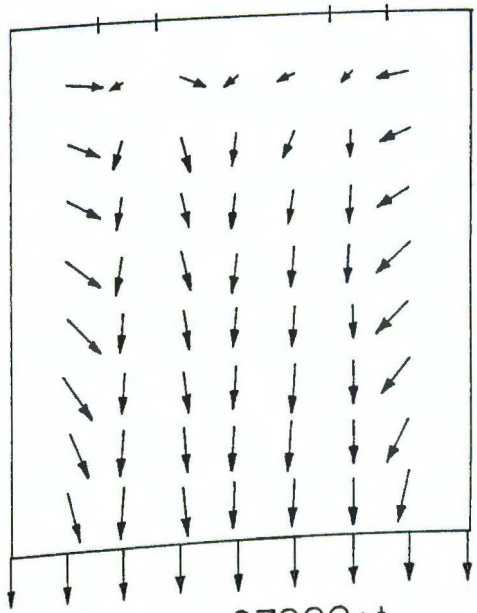

$t = 5.5$ MSEC $= 27000\Delta t$

$X_p = 1.71$

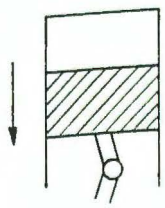

VELOCITY DISTRIBUTION
ON POWER STROKE

FIGURE 10

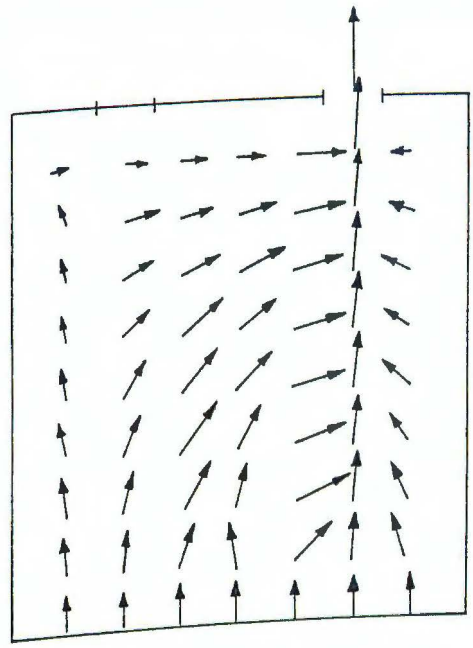

$t = 8.78$ MSEC $= 34500\Delta t$

$X_p = 4.83$

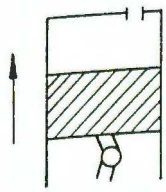

VELOCITY DISTRIBUTION
ON EXHAUST STROKE

FIGURE 11

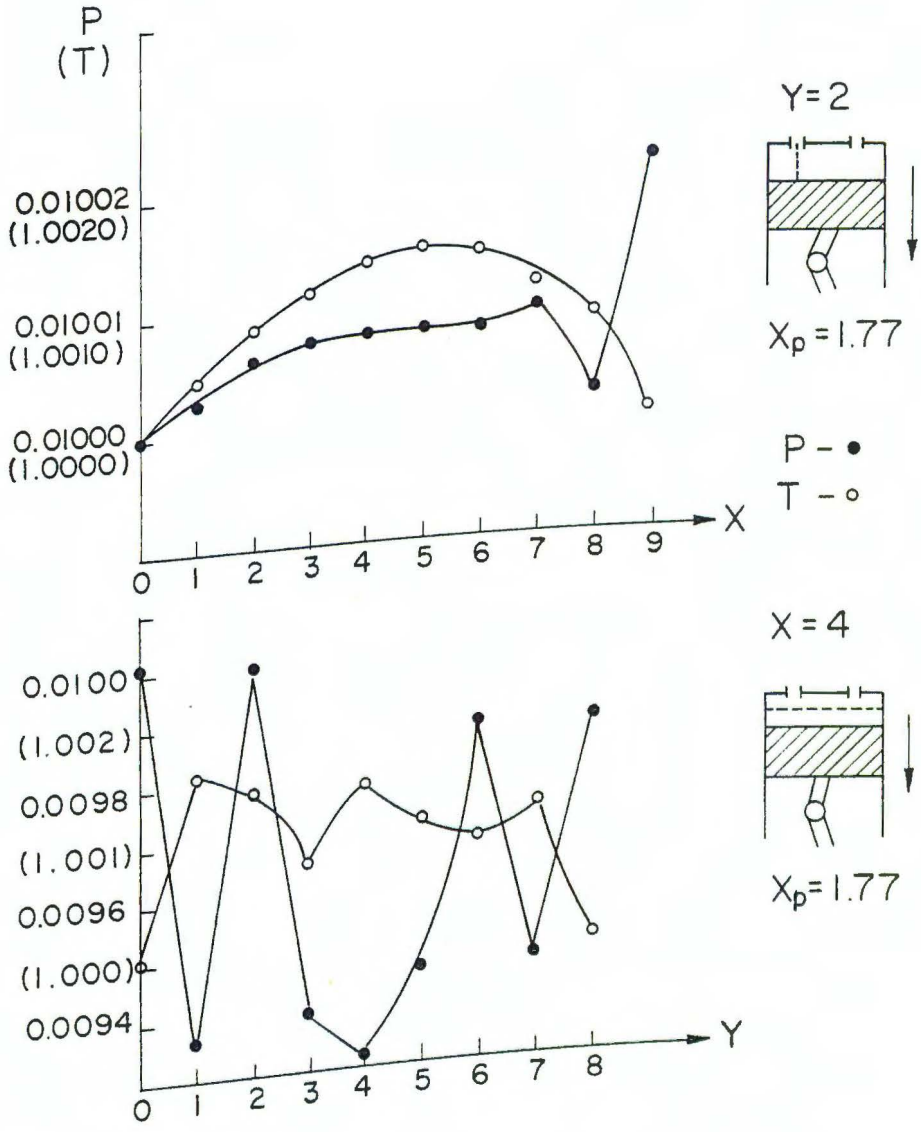

PRESSURE AND TEMPERATURE DISTRIBUTIONS - INTAKE

FIGURE 12

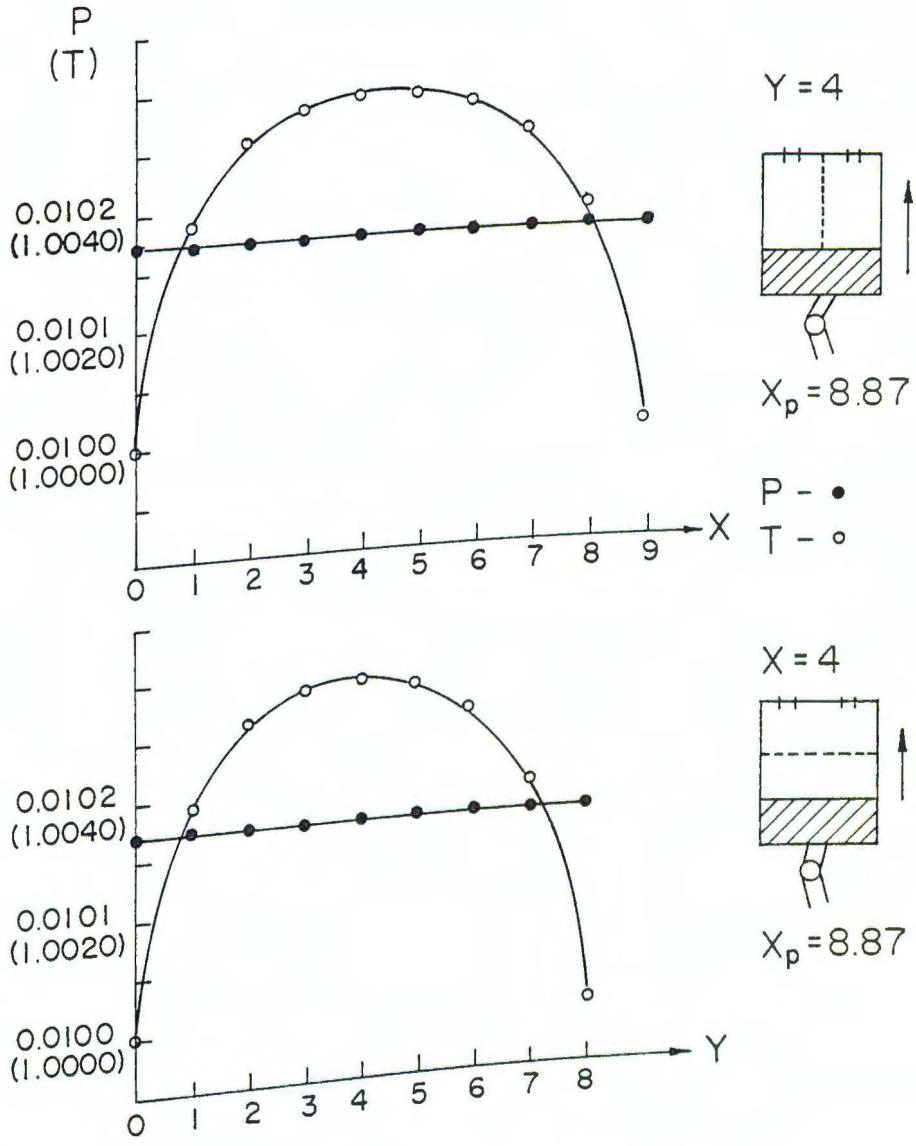

PRESSURE AND TEMPERATURE DISTRIBUTIONS - COMPRESSION

FIGURE 13

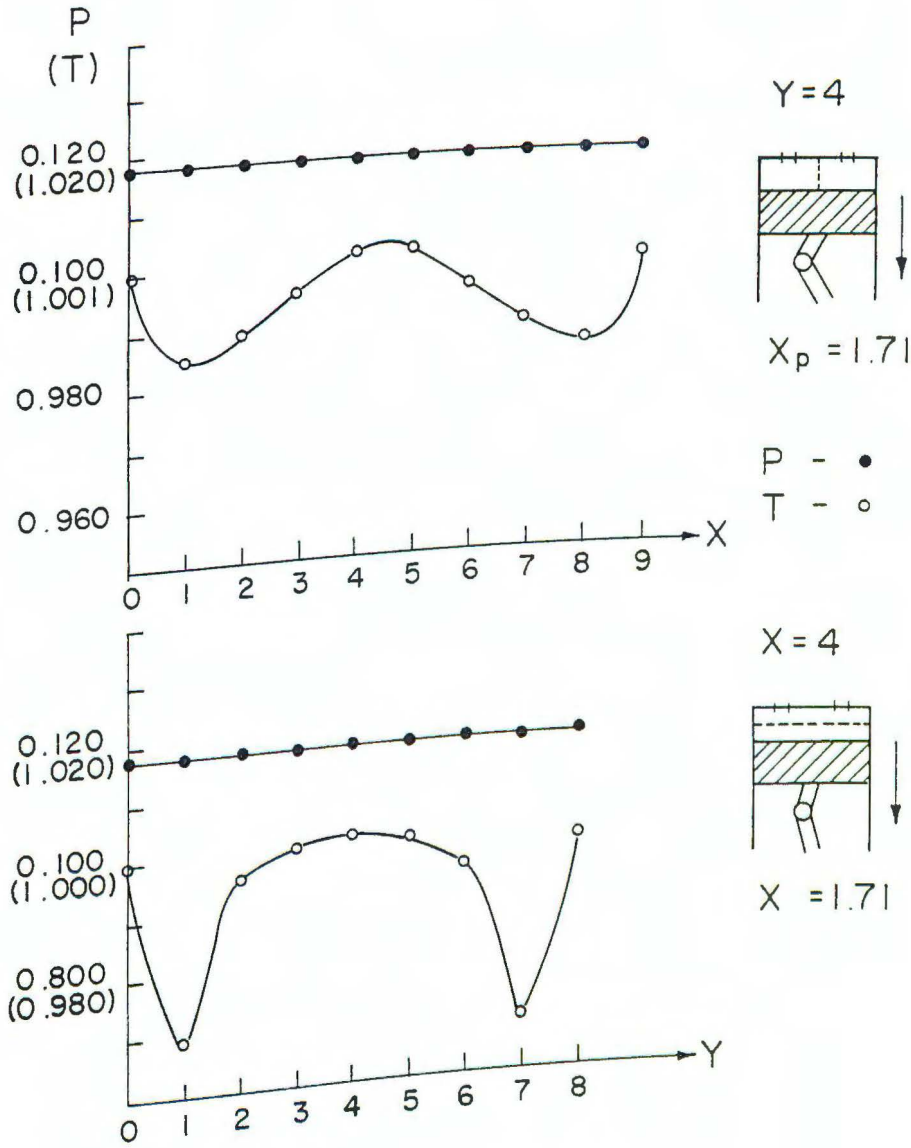

PRESSURE AND TEMPERATURE DISTRIBUTIONS - POWER

FIGURE 14

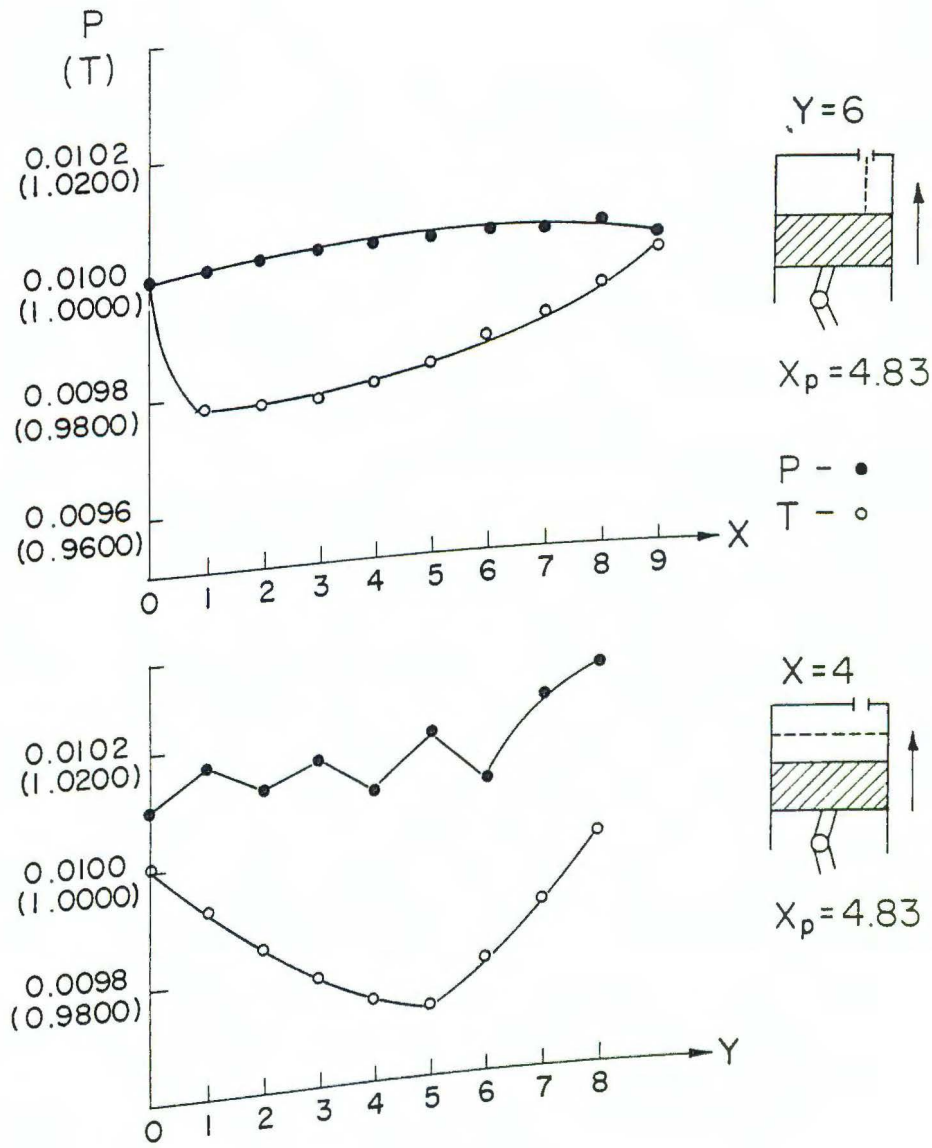

PRESSURE AND TEMPERATURE DISTRIBUTIONS - EXHAUST

FIGURE 15

FIGURE 16

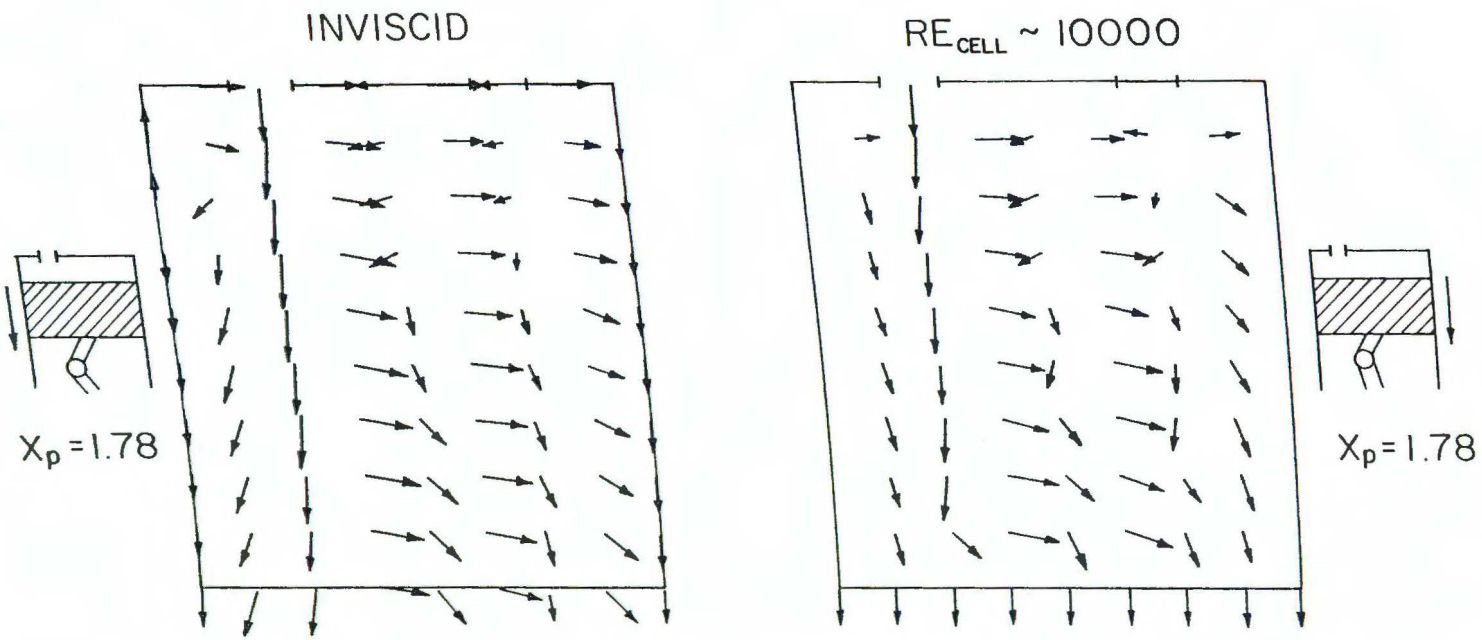

VELOCITY DISTRIBUTIONS - INTAKE:
INVISCID AND HIGH CELL RE CASES

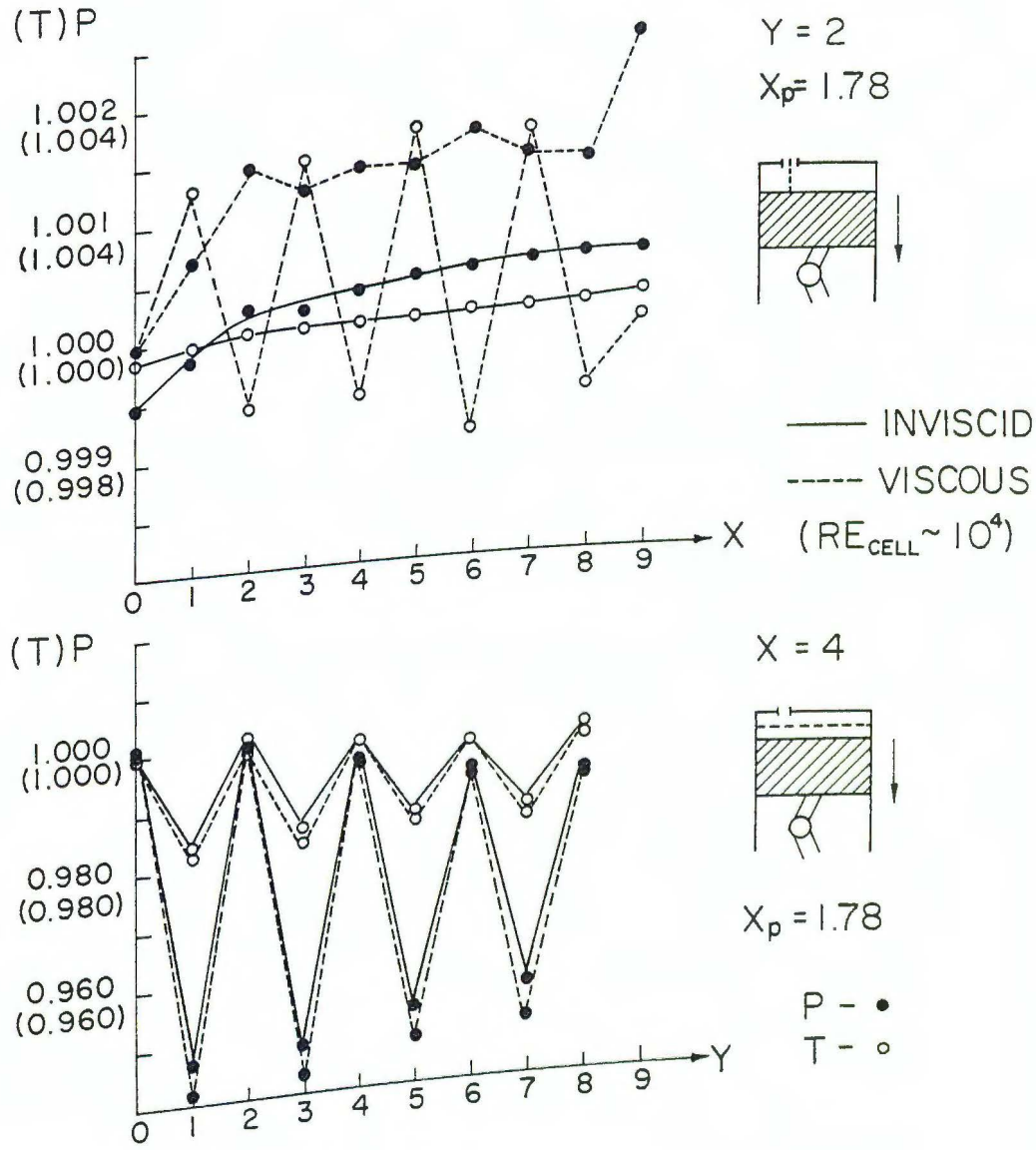

PRESSURE AND TEMPERATURE ON INTAKE STROKE FOR INVISCID AND HIGH CELL RE

FIGURE 17

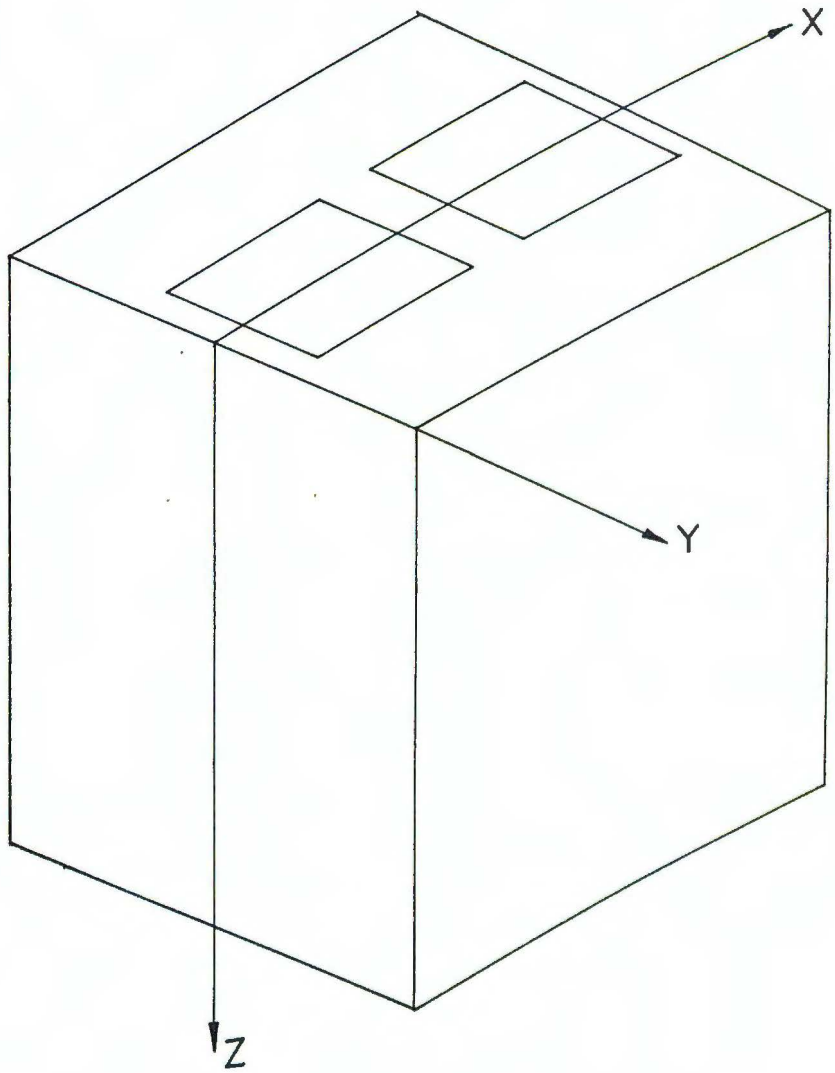

3-D RECTANGULAR ENGINE MODEL

FIGURE 18

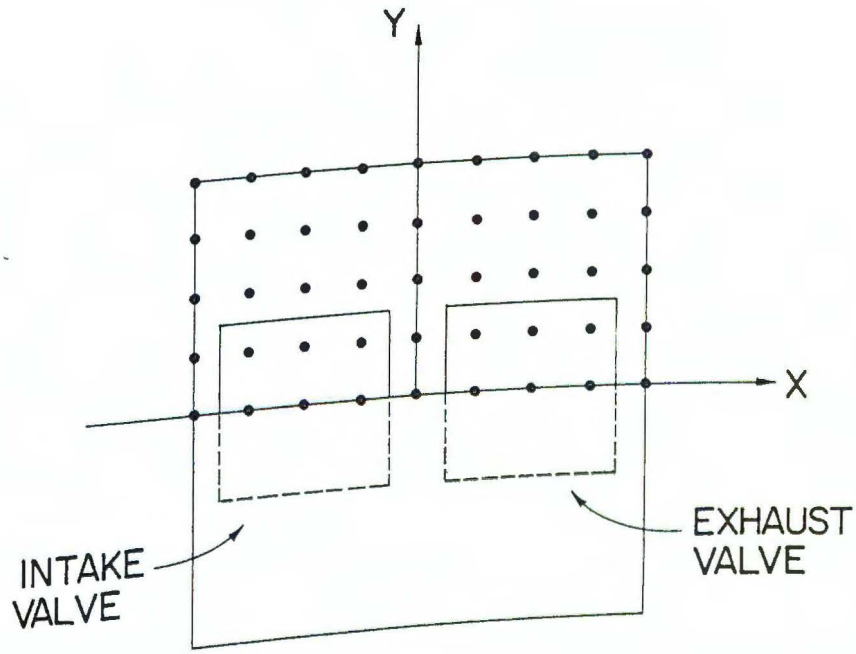

TOP SURFACE OF RECTANGULAR ENGINE AS SEEN FROM INSIDE AND LOOKING UP, SHOWING GRID LAYOUT

FIGURE 19

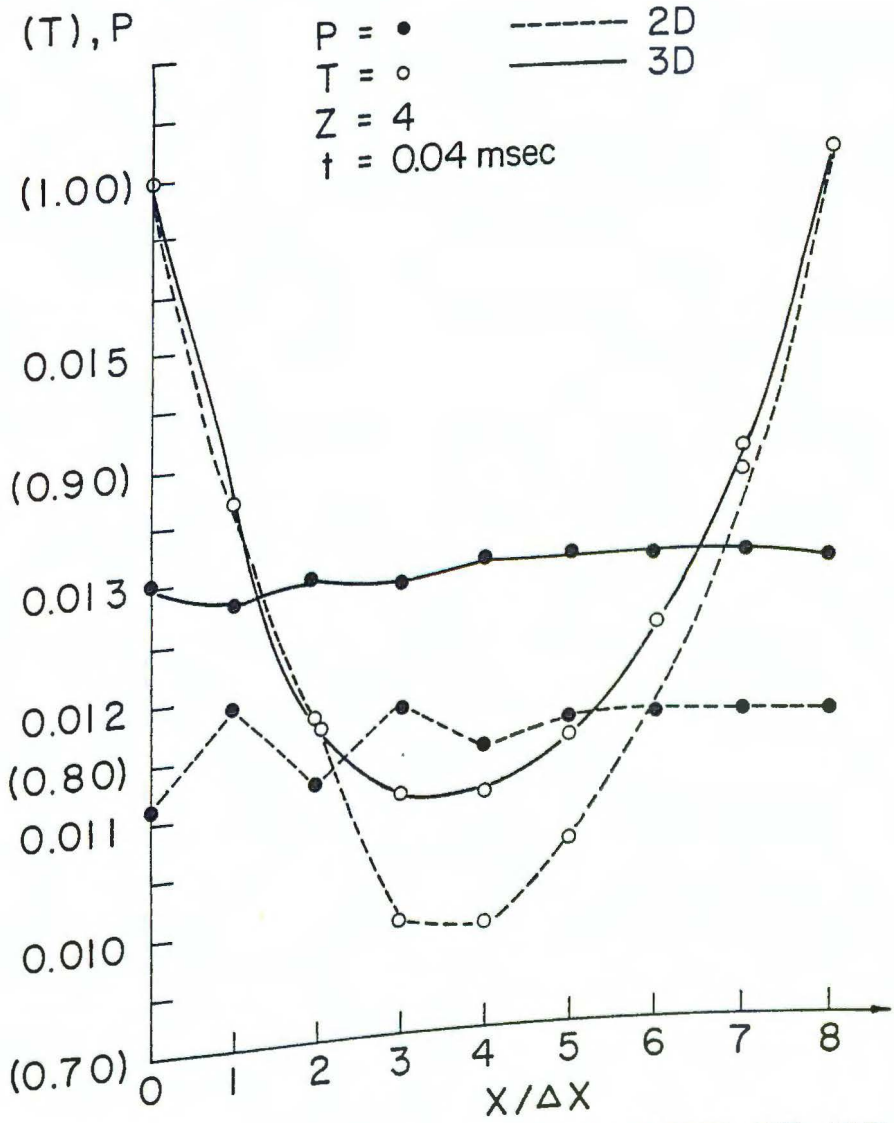

COMPARISON OF 2-D AND 3-D PRESSURE AND TEMPERATURE DISTRIBUTIONS FOR STATIONARY PISTON EXHAUST TEST (VISCOUS)

FIGURE 20

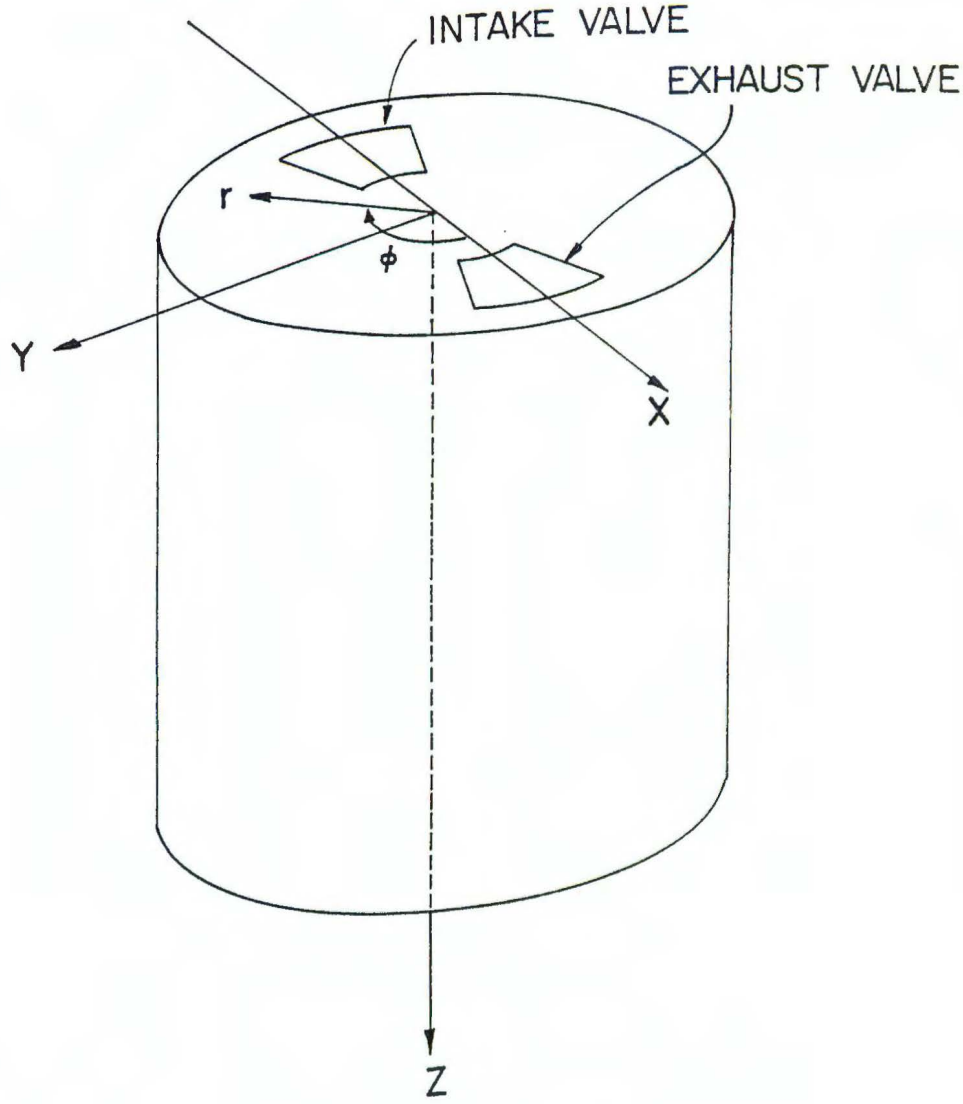

CYLINDRICAL ENGINE MODEL
SHOWING COORDINATE SYSTEM

FIGURE 21

FIGURE 22

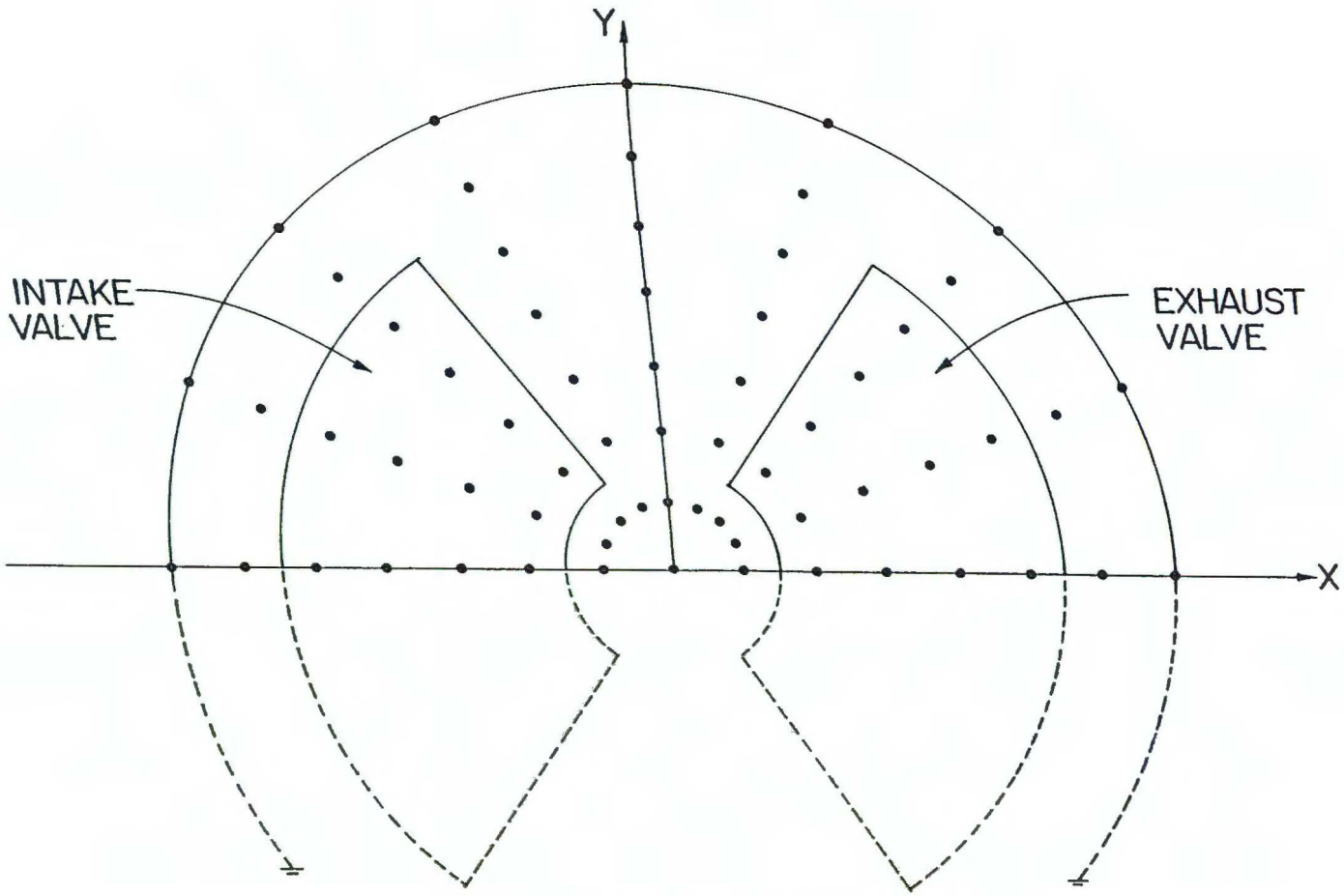

TOP OF CYLINDER
AS SEEN FROM INSIDE
AND SHOWING GRID LAYOUT

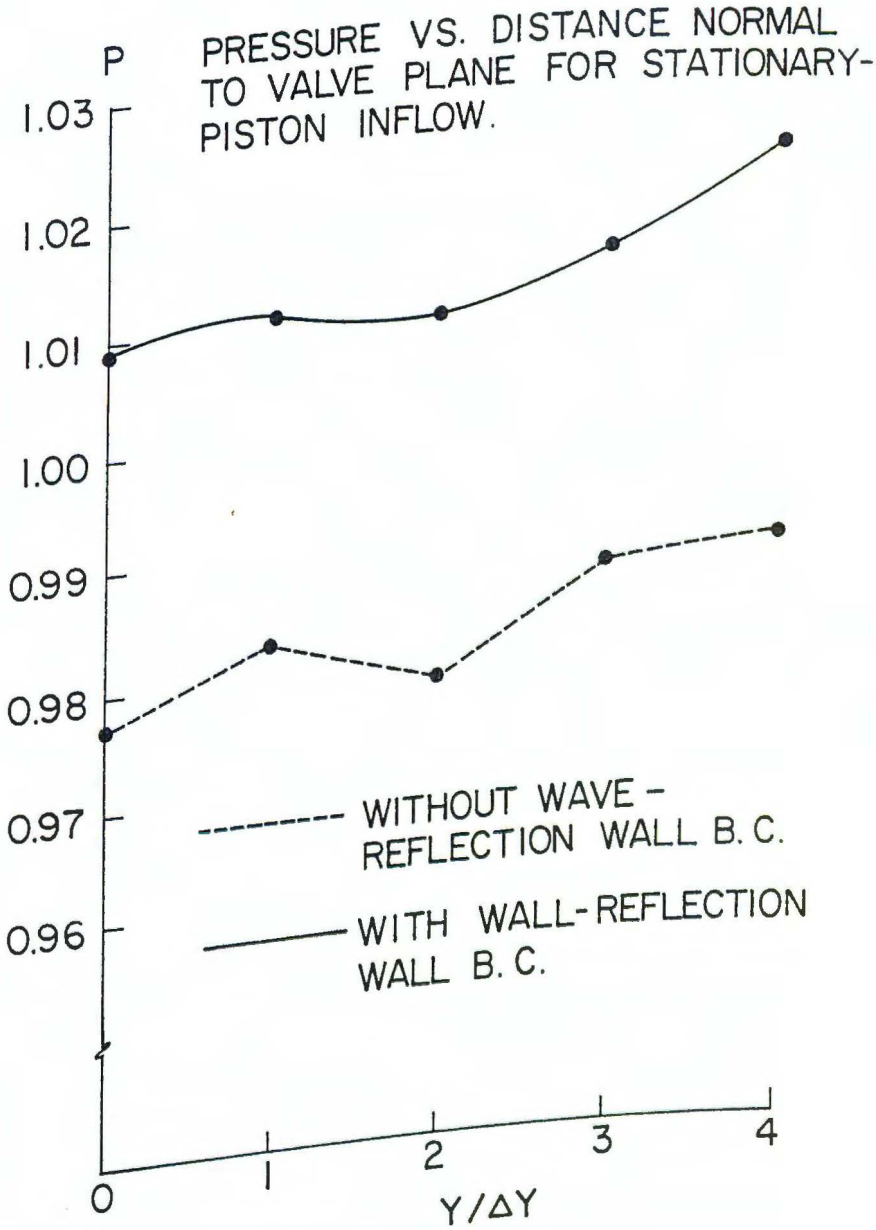
P
PRESSURE VS. DISTANCE NORMAL TO VALVE PLANE FOR STATIONARY-PISTON INFLOW.
1.03
1.02
1.01
1.00
0.99
0.98
0.97
0.96
WITHOUT WAVE - REFLECTION WALL B. C.
WITH WALL-REFLECTION WALL B. C.
0
1
2
3
4
Y/ΔY

FIGURE 23

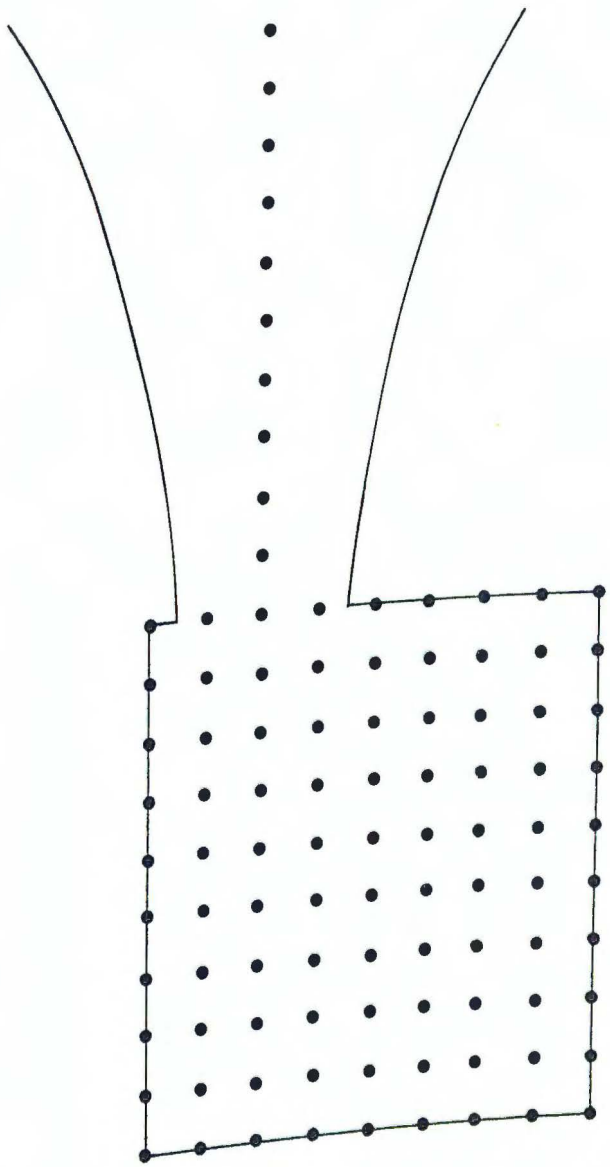

EXAMPLE OF RECTANGULAR ENGINE WITH DUCTED INTAKE MANIFOLD ATTACHED

FIGURE 24

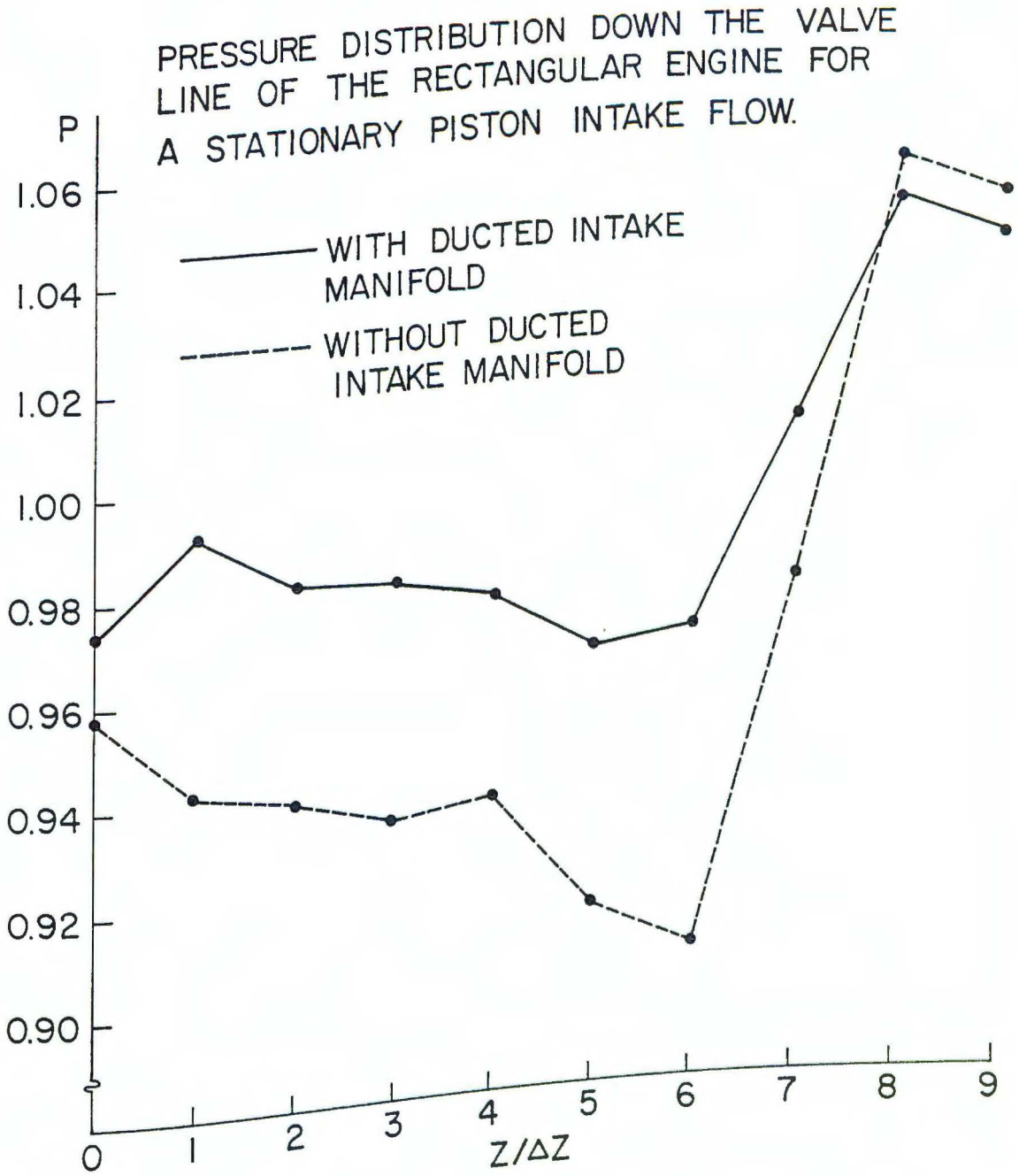
PRESSURE DISTRIBUTION DOWN THE VALVE LINE OF THE RECTANGULAR ENGINE FOR A STATIONARY PISTON INTAKE FLOW.
P
1.06
1.04
1.02
1.00
0.98
0.96
0.94
0.92
0.90
WITH DUCTED INTAKE MANIFOLD
WITHOUT DUCTED INTAKE MANIFOLD
0
1
2
3
4
5
6
7
8
9
Z/ΔZ

FIGURE 25

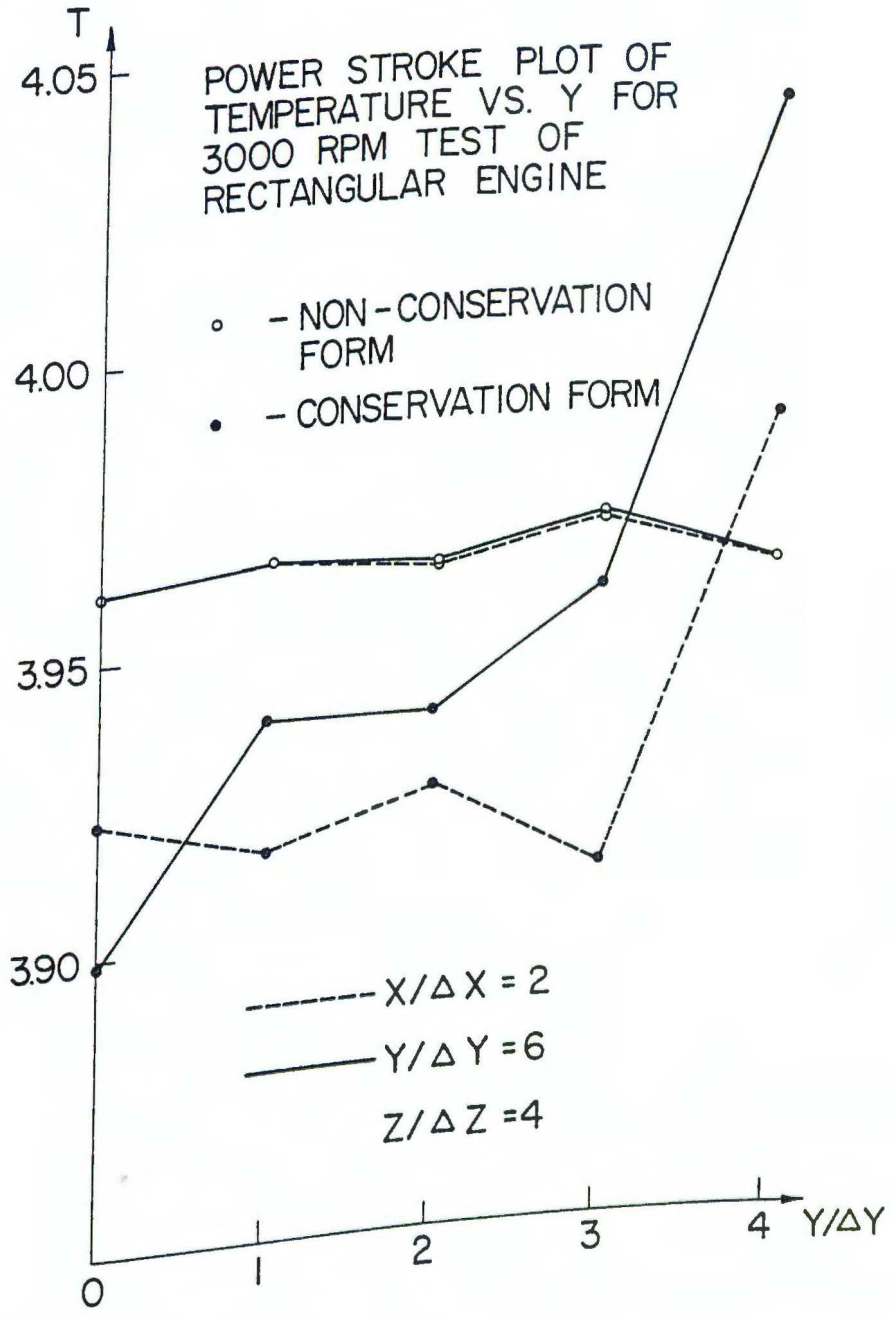
T
4.05
4.00
3.95
3.90
POWER STROKE PLOT OF TEMPERATURE VS. Y FOR 3000 RPM TEST OF RECTANGULAR ENGINE
- NON-CONSERVATION FORM
- CONSERVATION FORM
X/ΔX = 2
Y/ΔY = 6
Z/ΔZ = 4
0
1
2
3
4
Y/ΔY

FIGURE 26

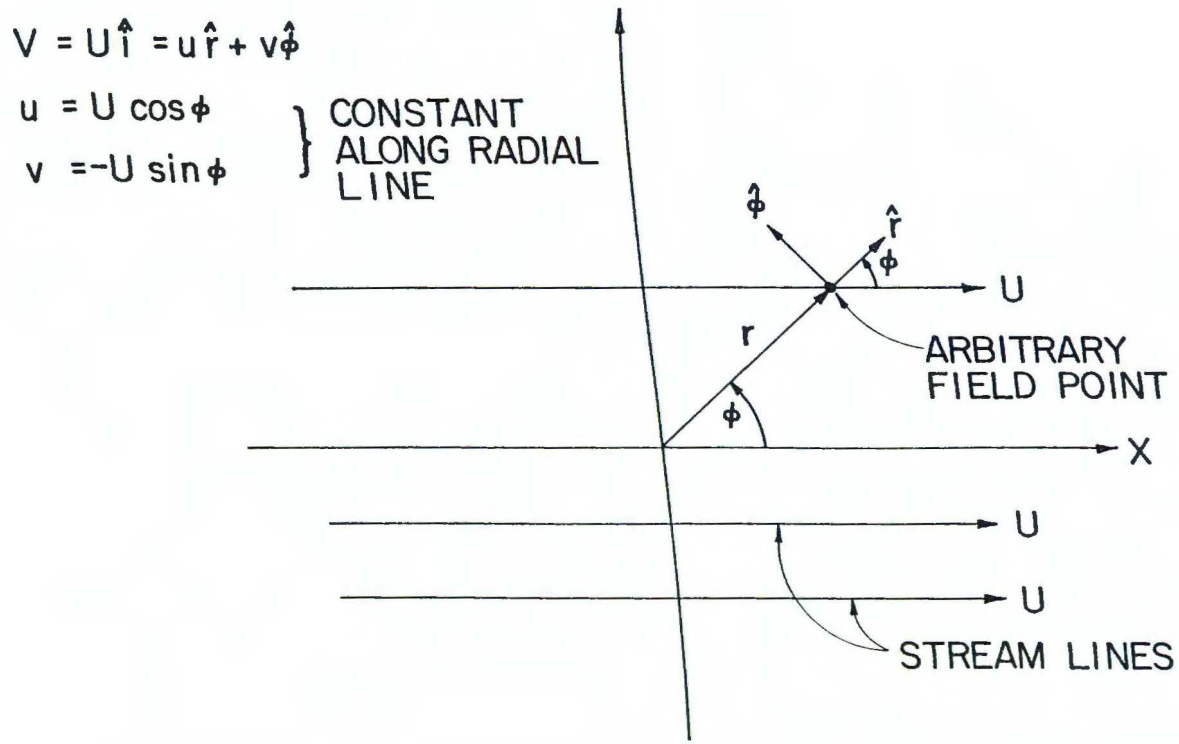

ILLUSTRATING HOW A UNIFORM STREAM FLOW IS MULTIVALUED AT r=0 IN CYLINDERICAL SYSTEM

FIGURE 27

INTAKE STROKE PLOT OF PRESSURE VS. RADIAL COORDINATE FOR CRANK ANGLE OF 154° AT Z = 4ΔZ

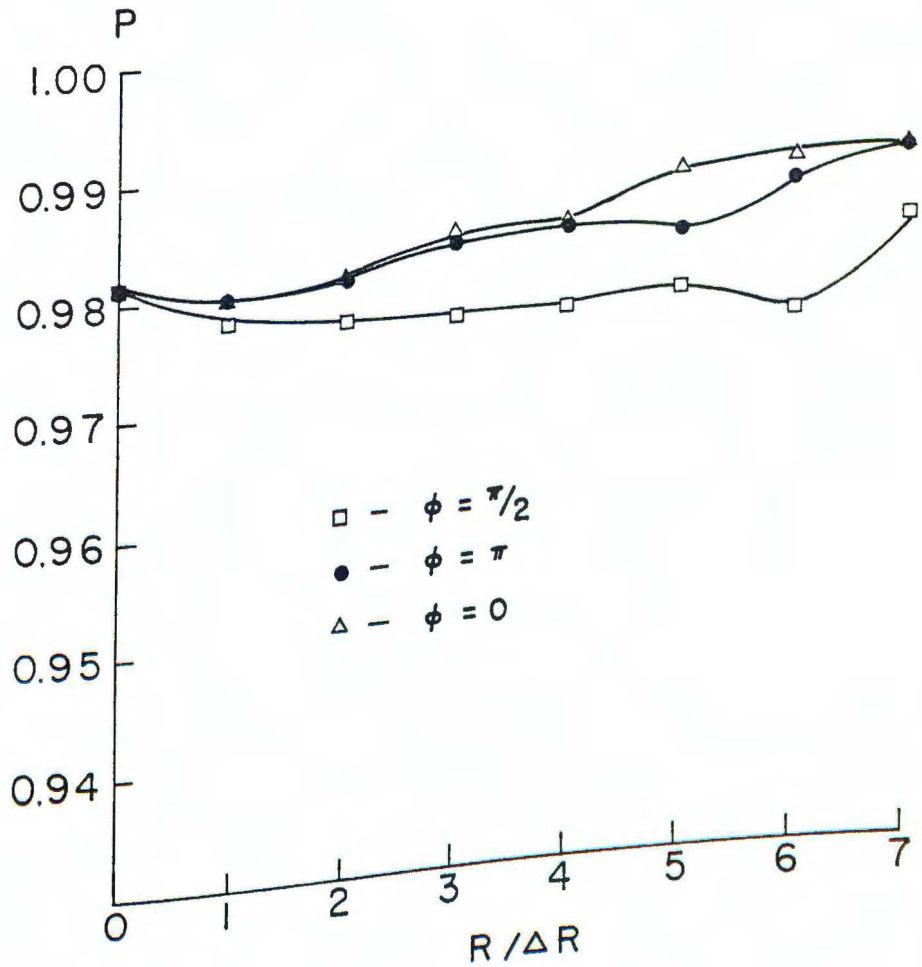

FIGURE 28

INTAKE STROKE PLOT OF TEMPERATURE VS. RADIAL COORDINATE FOR CRANK ANGLE OF 154° AT Z = 4ΔZ

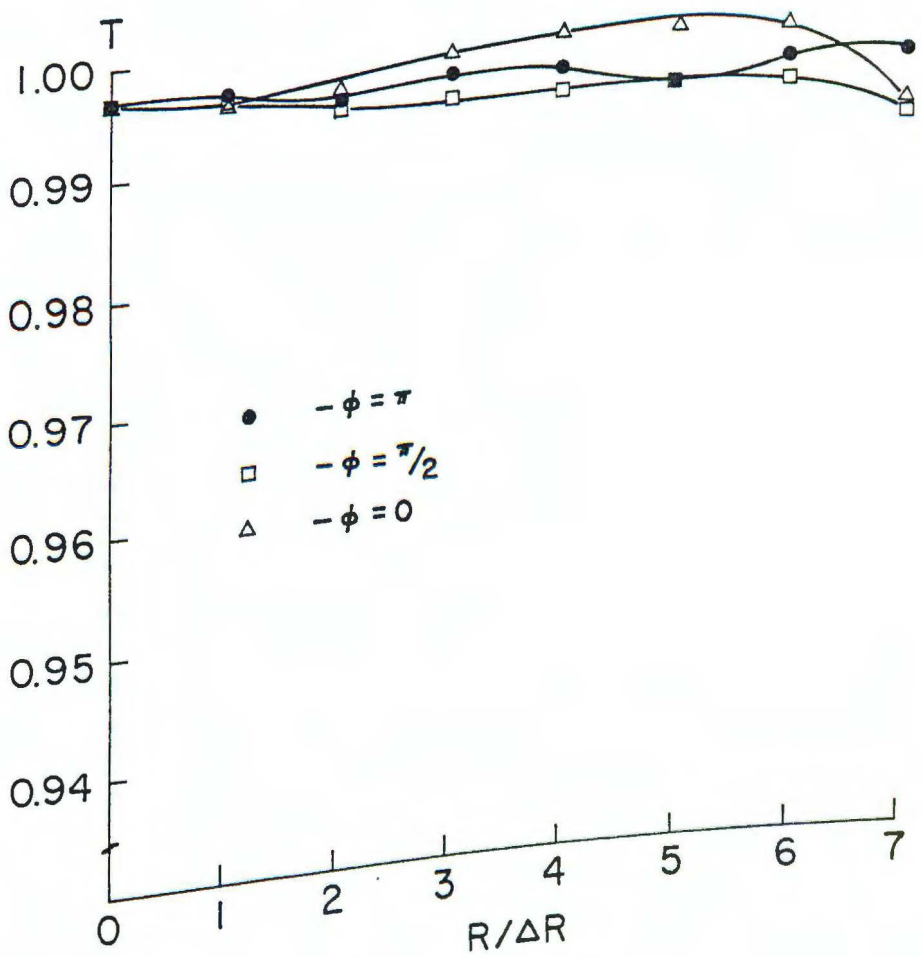

FIGURE 29

FIGURE 30

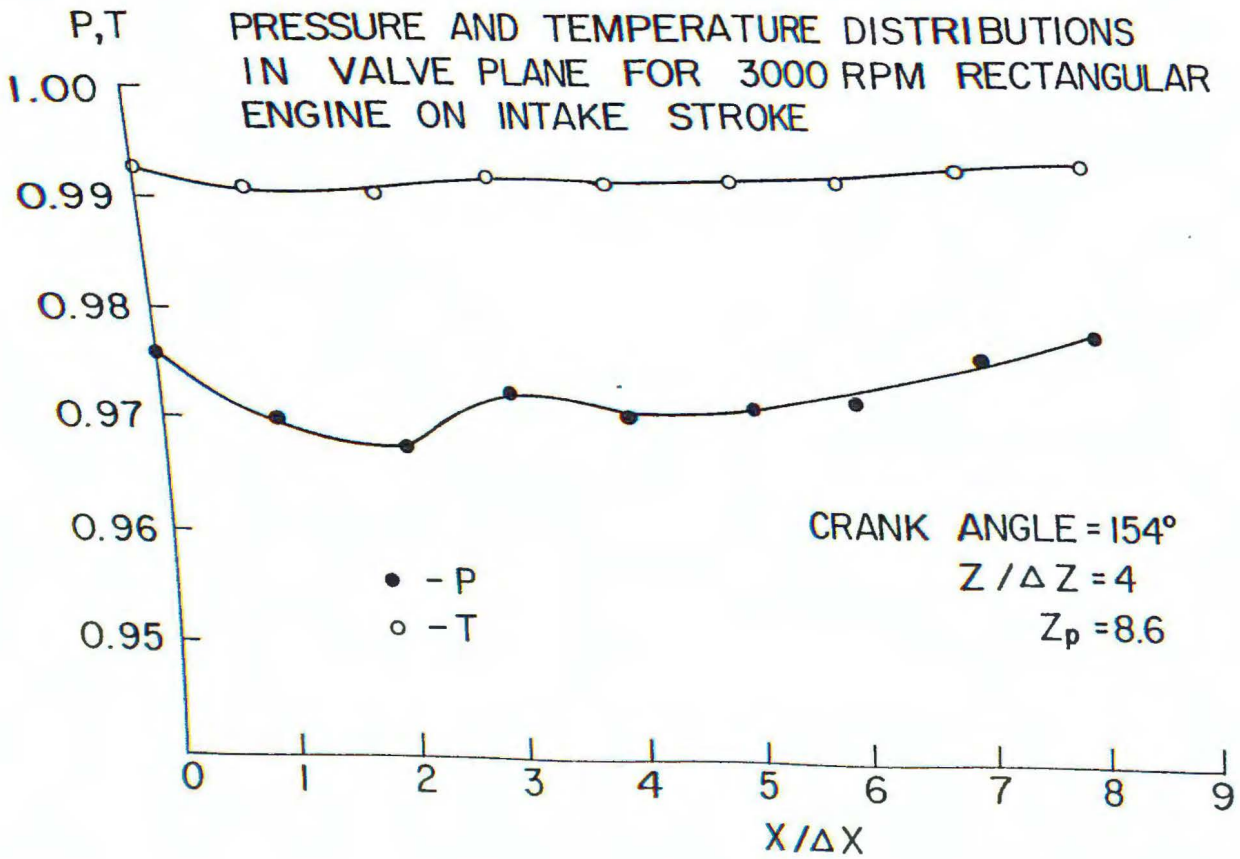
P,T
PRESSURE AND TEMPERATURE DISTRIBUTIONS IN VALVE PLANE FOR 3000 RPM RECTANGULAR ENGINE ON INTAKE STROKE
1.00
0.99
0.98
0.97
0.96
0.95
• - P
○ - T
CRANK ANGLE = 154°
Z / Δ Z = 4
Z_p = 8.6
0
1
2
3
4
5
6
7
8
9
X/ΔX

PRESSURE AND TEMPERATURE RESULTS VS. Y FOR 3000 RPM RECTANGULAR ENGINE TEST ON INTAKE STROKE

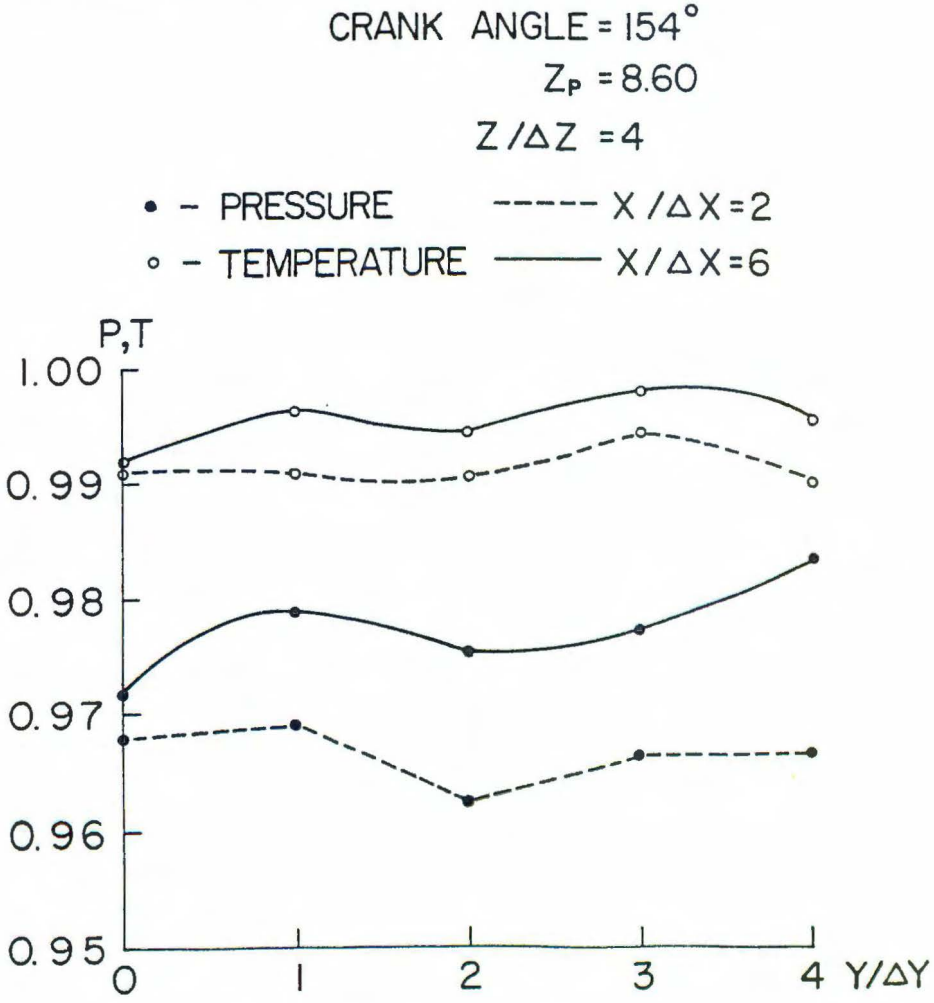

FIGURE 31

FIGURE 32

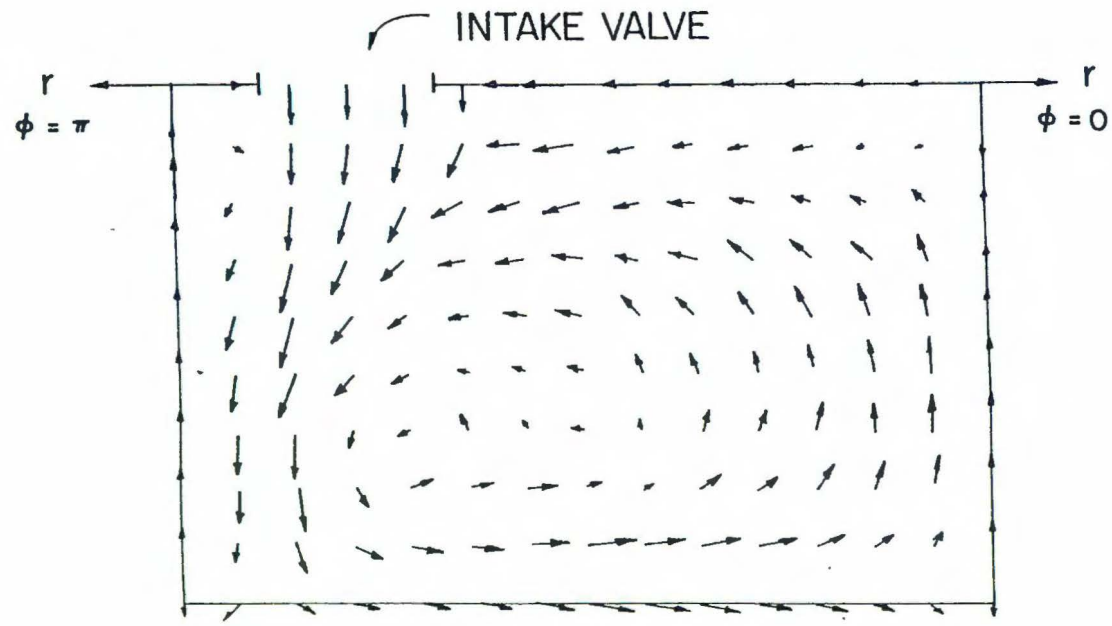

VELOCITY PATTERN NEAR BDC ON INTAKE STROKE, CRANK ANGLE = 154°, Z_p = 8.60, 3000 RPM, CYLINDRICAL ENGINE

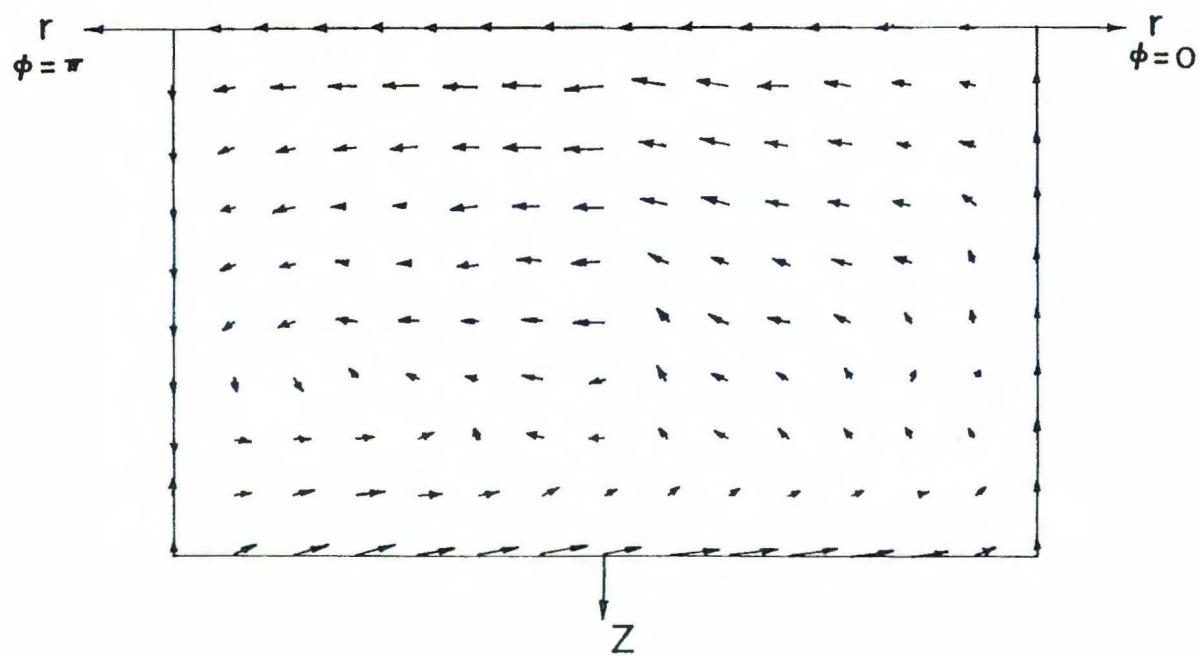

VELOCITY PATTERN NEAR TDC - COMPRESSION
CRANK ANGLE = 348° , Z_p = 1.09
3000 RPM , CYLINDRICAL GEOMETRY

VELOCITY PATTERN NEAR TDC-
COMPRESSION CRANK ANGLE = 348°
$Z_p = 1.09$, 3000RPM, IN PLANE
NORMAL TO VALVE PLANE,
CYLINDRICAL ENGINE

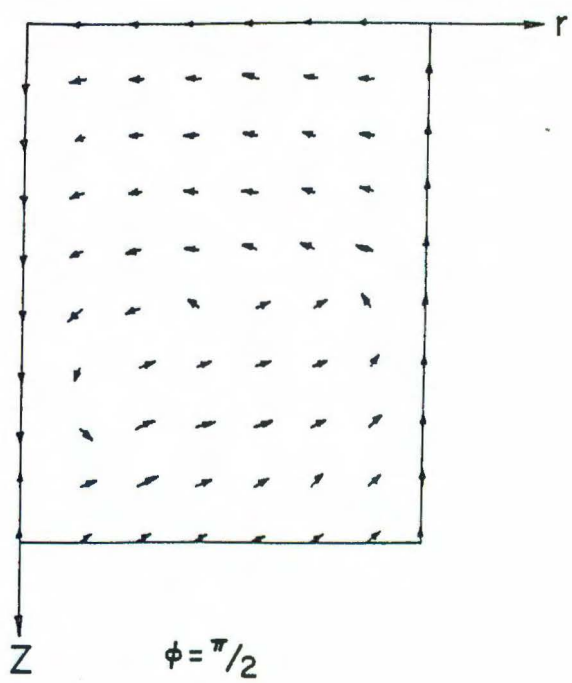

FIGURE 34

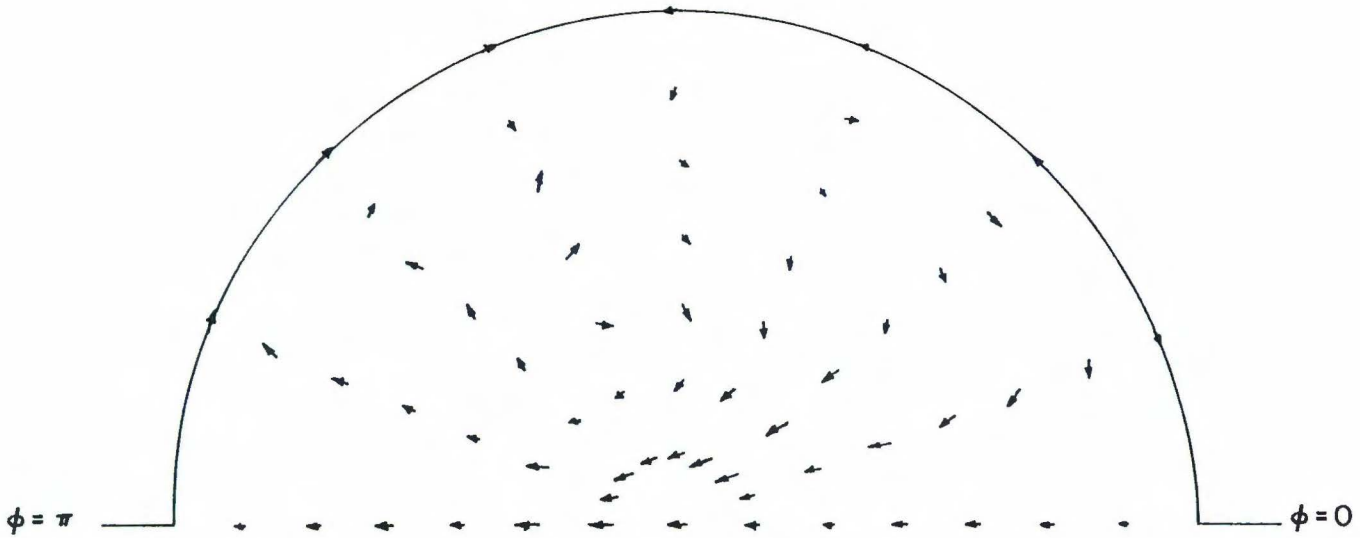

VELOCITY PATTERN NEAR TDC - COMPRESSION
CRANK ANGLE = 348° , Z_p = 1.09, 3000 RPM ,
$Z/\Delta Z$ = 5 , CYLINDRICAL ENGINE

FIGURE 35

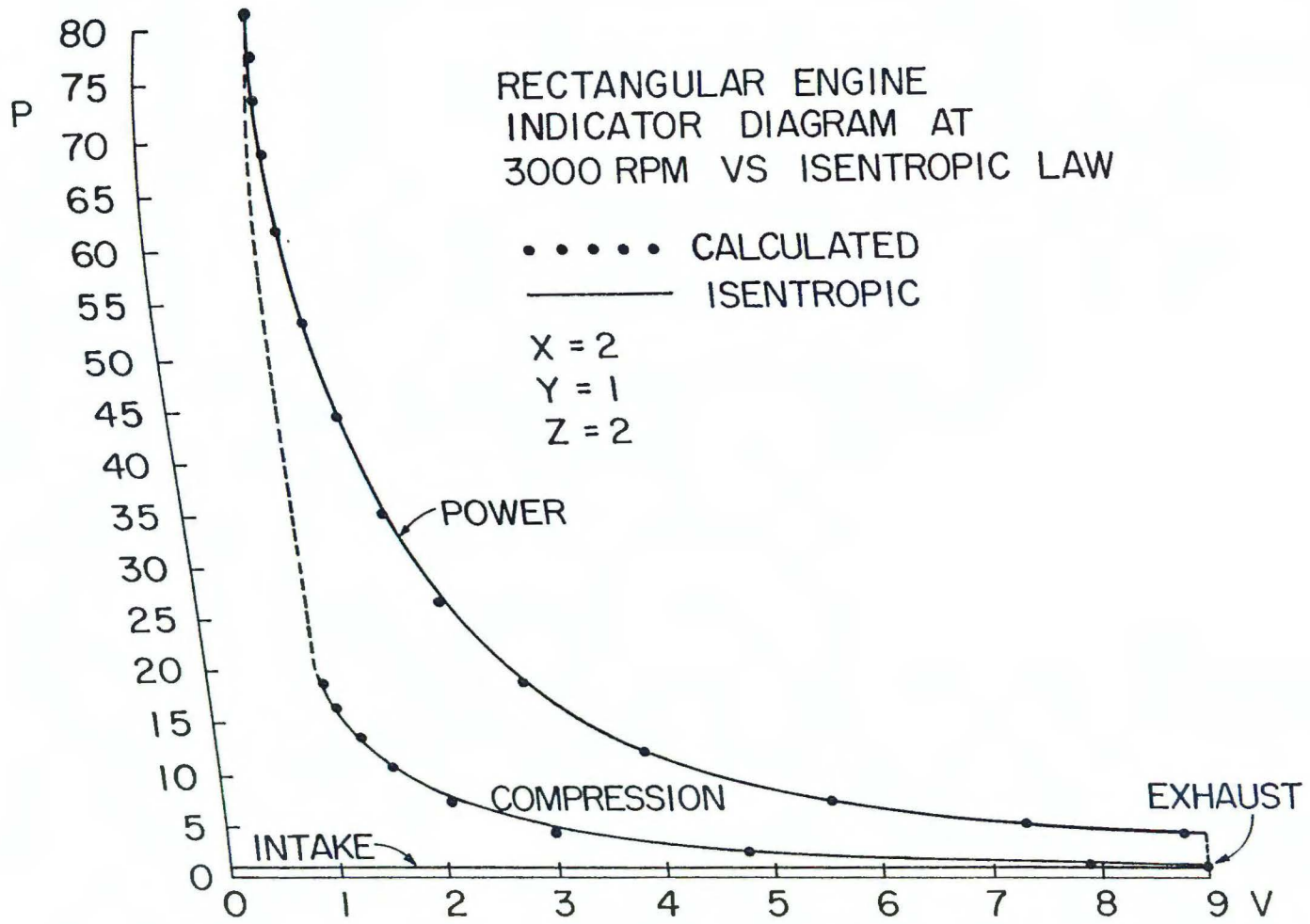
RECTANGULAR ENGINE
INDICATOR DIAGRAM AT
3000 RPM VS ISENTROPIC LAW
• • • • • CALCULATED
——— ISENTROPIC
X = 2
Y = 1
Z = 2
P
V
POWER
COMPRESSION
EXHAUST
INTAKE
80
75
70
65
60
55
50
45
40
35
30
25
20
15
10
5
0
0
1
2
3
4
5
6
7
8
9

FIGURE 36

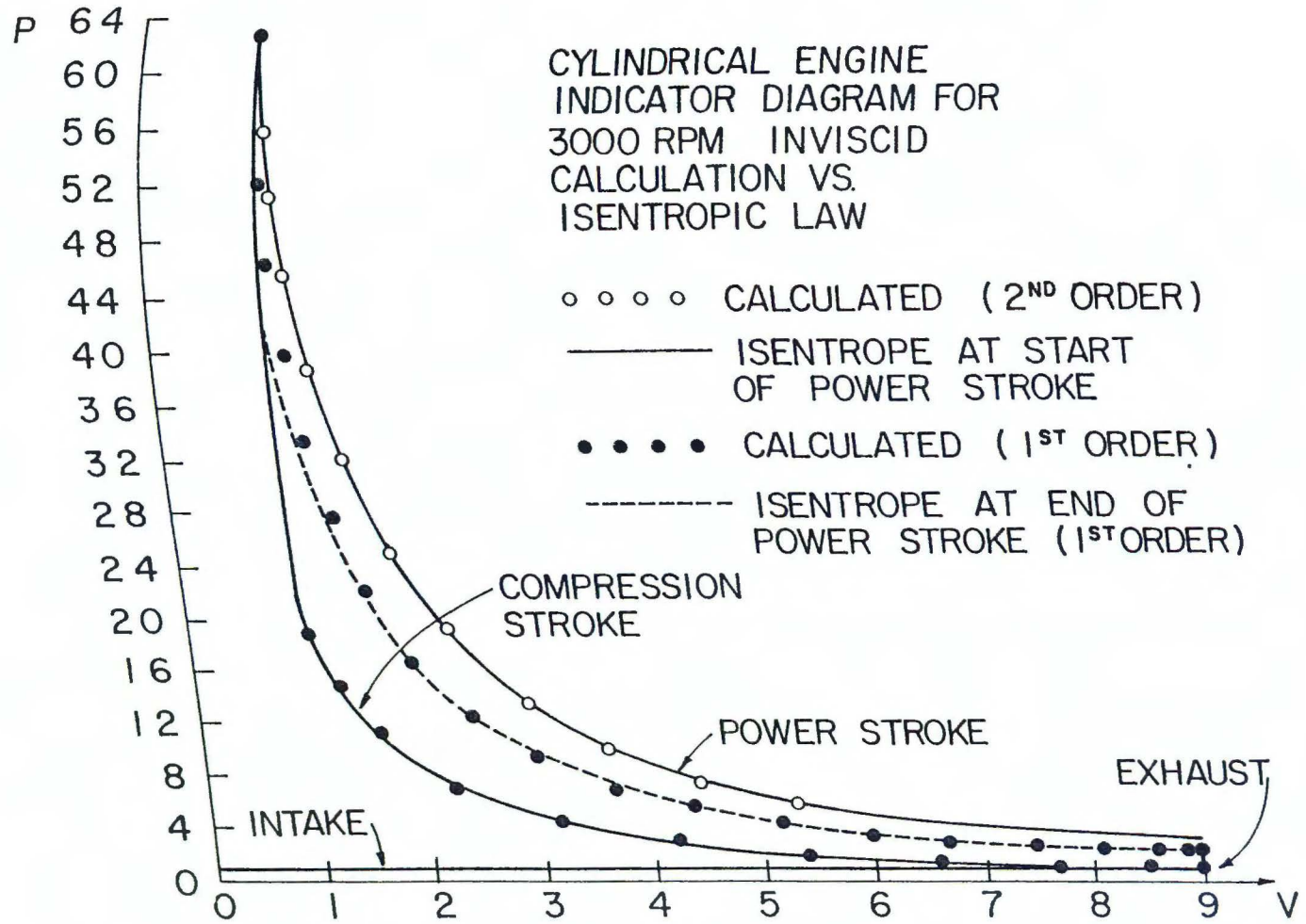
P
64
60
56
52
48
44
40
36
32
28
24
20
16
12
8
4
0
0
1
2
3
4
5
6
7
8
9
V
CYLINDRICAL ENGINE
INDICATOR DIAGRAM FOR
3000 RPM INVISCID
CALCULATION VS.
ISENTROPIC LAW
CALCULATED (2ND ORDER)
ISENTROPE AT START
OF POWER STROKE
CALCULATED (1ST ORDER)
ISENTROPE AT END OF
POWER STROKE (1STORDER)
COMPRESSION
STROKE
POWER STROKE
EXHAUST
INTAKE

FIGURE 37

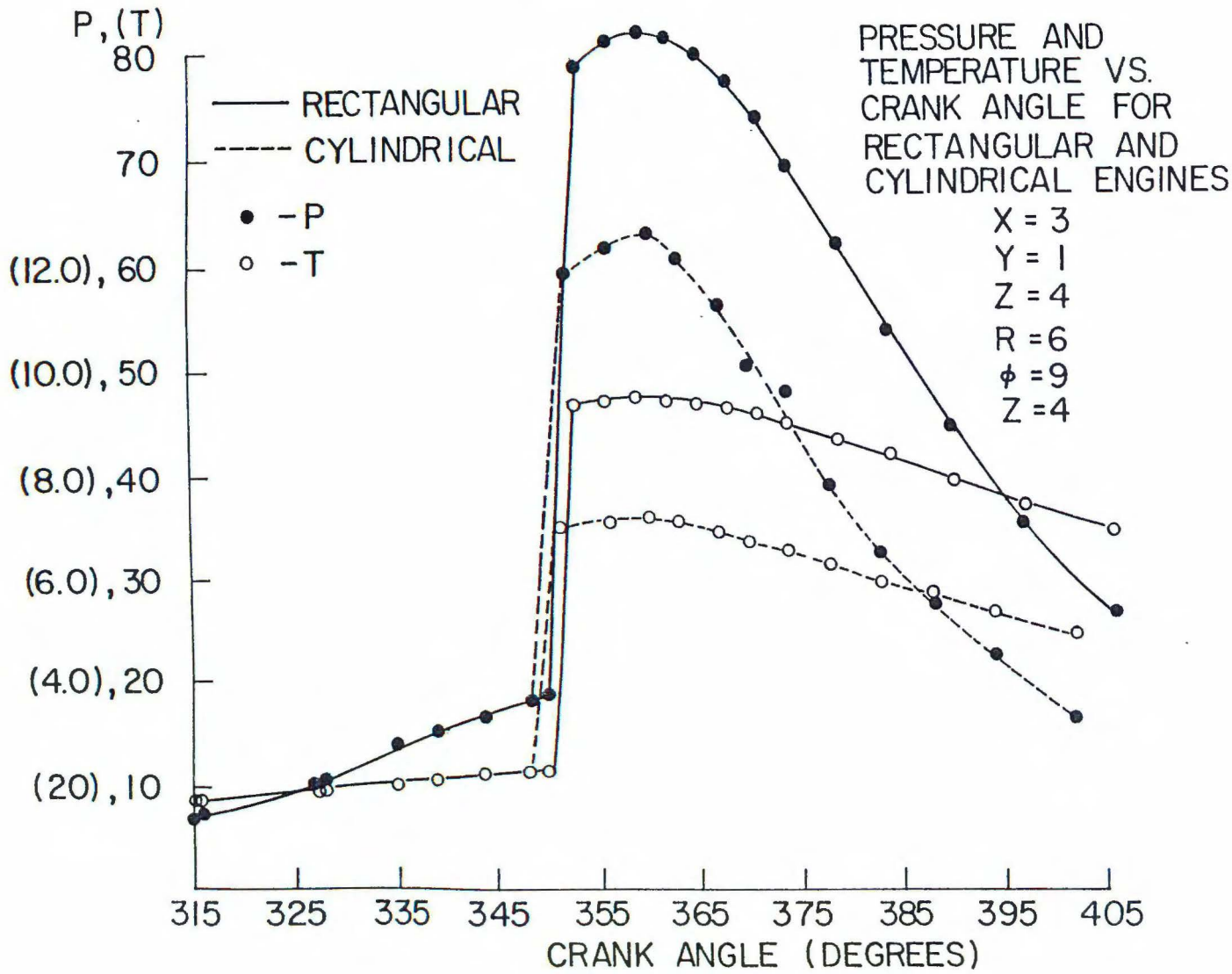
P,(T)
80
70
(12.0), 60
(10.0), 50
(8.0), 40
(6.0), 30
(4.0), 20
(20), 10
RECTANGULAR
CYLINDRICAL
-P
-T
PRESSURE AND TEMPERATURE VS. CRANK ANGLE FOR RECTANGULAR AND CYLINDRICAL ENGINES
X = 3
Y = 1
Z = 4
R = 6
φ = 9
Z = 4
315
325
335
345
355
365
375
385
395
405
CRANK ANGLE (DEGREES)

FIGURE 38

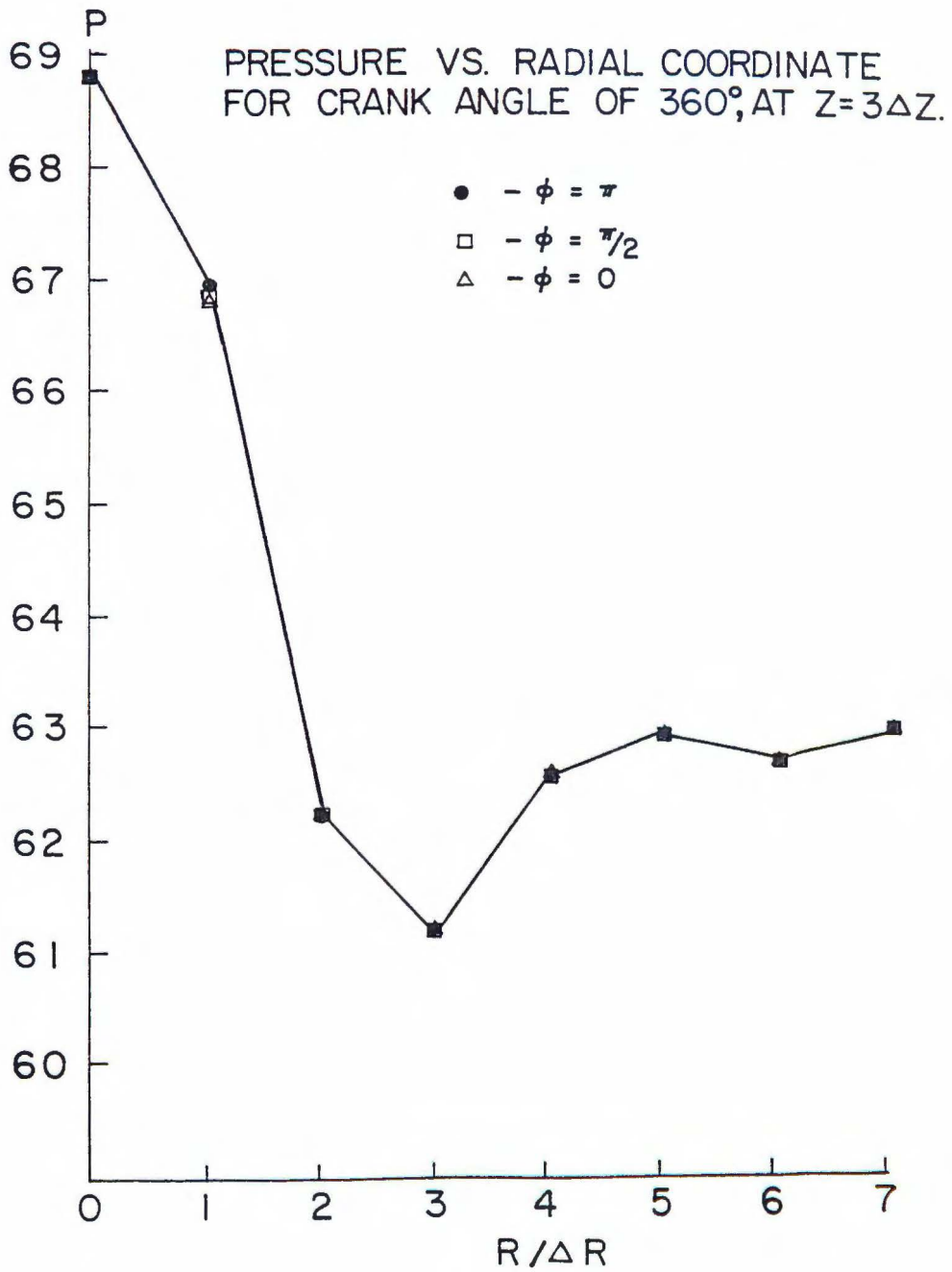
P
69
68
67
66
65
64
63
62
61
60
PRESSURE VS. RADIAL COORDINATE
FOR CRANK ANGLE OF 360°, AT Z=3ΔZ.
● − φ = π
□ − φ = π/2
△ − φ = 0
0
1
2
3
4
5
6
7
R/ΔR

FIGURE 39